

**Competitive Biosorption of Ag(I) and Cu (II) by Tripolyphosphate Crosslinked  
Chitosan Beads**

by

© Chunxia Mao

A thesis submitted to the

School of Graduate Studies

in partial fulfillment of the requirements for the degree of

**Master of Engineering**

**Faculty of Engineering and Applied Science**

Memorial University of Newfoundland

**October 2015**

St. John's

Newfoundland and Labrador

## ABSTRACT

In this study, alkalization of chitosan before crosslinking was applied in to enhance the adsorption capacity of the modified chitosan. Competitive adsorption of Ag (I) and Cu (II) from bimetallic solutions was studied using the newly synthesized tripolyphosphate crosslinked chitosan beads. Results indicated that alkalization before crosslinking helps to protect free-amine groups from crosslinking and hence increases the uptake capacity and selectively of the synthesized beads towards Ag (I). The maximum uptakes of Ag (I) and Cu (II) were 82.9 and 15.5 mg/g respectively at room temperature with an initial concentration of each metal being 2.0 mmol/L and the sorbent dosage of 1.0 g L<sup>-1</sup>. Langmuir isotherm and pseudo-second order kinetic model provide better descriptions of adsorption isotherm and kinetics of metal ions on sorbent surfaces. Analyses from FT-IR and XPS confirmed that free amine, hydroxyl and P<sub>3</sub>O<sub>10</sub><sup>5-</sup> groups are involved in metal binding with amine and hydroxyl groups more selective to Ag (I).

Then, continuous adsorption with the newly synthesized chitosan beads was simulated using the lumped kinetic model. According to the parameters obtained in the batch adsorption, the overall mass-transfer coefficient ( $K_f$ ), and axial dispersion coefficient ( $D_L$ ) were determined using the empirical correlations. The value of  $K_f$  for Ag (I) is in the range of  $5.028 \times 10^{-5}$  s<sup>-1</sup> to  $8.389 \times 10^{-5}$  s<sup>-1</sup>, the value of  $K_f$  for Cu (II) was in the range of  $8.000 \times 10^{-5}$  s<sup>-1</sup> to  $1.283 \times 10^{-4}$  s<sup>-1</sup>; The range of axial dispersion coefficient for Ag (I) and Cu (II) were both varying from  $1.806 \times 10^{-4}$  cm<sup>2</sup>/s to  $1.778 \times 10^{-4}$  cm<sup>2</sup>/s. Results from the breakthrough and elution profiles indicated that decreasing the flow rate, sample

concentration and injection time, or increasing the bed length could enhance the separation of the two metal ions. Besides, it was found that concentration overload by increasing the sample concentration is more effective to improve the separation of two metal ions in fixed-bed column than volume overload by increasing the injection time.

In conclusion, the newly synthesized chitosan-based biosorbents showed great selective adsorption for Ag (I) in bimetallic solutions, and the simulation studies provided good potential in industrial applications to recover precious metal ions from water or wastewater.

## **ACKNOWLEDGEMENTS**

Professor Yan Zhang, my supervisor, contributes her extraordinary, valuable and selfless directions throughout the research work. It is hard to imagine the accomplishment of the study without her continuous support and encouragement. First of all, I would like to give my deepest thanks to her.

Jingjing Cai, Nan Zhang, Yan Li, and all my good friends and lab-mates gives me unforgettable memory of enjoying the lab time and the life together during the journey.

RDC and Memorial University of Newfoundland provide me the financial support and assistance for this study, which makes all of above possible. I would like to express my acknowledgment for their continuous support.

With deepest and endless love, Qianfeng Xue and my family shares with me all the joy and suffering always. Any laudatory and appreciation words are not excessive to express my gratitude to them.

## Table of Contents

ABSTRACT-----	i
ACKNOWLEDGEMENTS-----	iii
Table of Contents-----	iv
List of Tables-----	vii
List of Figures-----	viii
List of Symbols, Nomenclature or Abbreviations-----	x
Chapter 1 Introduction	
1.1 Background-----	1
1.2 Objective and scope of study-----	3
1.3 Thesis Outline-----	5
Chapter 2 Literature Review	
2.1 Importance of metal recovery in industry-----	6
2.2 Biosorption and biosorbents-----	7
2.2.1 Available raw materials-----	7
2.2.2 Chitosan based biosorbents-----	8
2.3 Adsorption mechanism-----	19
2.3.1 Physical adsorption-----	20
2.3.2 Chemical reduction-----	22
2.4 Column test and mathematic modeling-----	23
2.4.1 Breakthrough curve and elution curve-----	23
2.4.2 Mathematical model-----	25
2.4.2.1 General rate model-----	26
2.4.2.2 Lumped kinetic model-----	28

2.4.2.3 Equilibrium-Dispersive model-----	29
2.4.2.4 Ideal model-----	30
2.4.3 Mass transfer effect on column test-----	30
 Chapter 3 Competitive Adsorption of Ag(I) and Cu(II) on Chitosan Beads Cross-linked with Sodium Tripolyphosphate	
3.1 Introduction-----	32
3.2 Materials and Methods-----	35
3.2.1 Material and chemicals-----	35
3.2.2 Preparation of cross-linked chitosan beads-----	35
3.2.3 Swelling rate test-----	37
3.2.4 Batch sorption tests-----	38
3.2.5 ICP-OES-----	40
3.2.6 ATR-FTIR-----	40
3.2.7 XPS-----	41
3.2.8 XRD-----	41
3.3 Results and Discussion-----	42
3.3.1 Sorbent screening and characterization-----	42
3.3.2 Swelling properties-----	46
3.3.3 Adsorption isotherm-----	47
3.3.4 Adsorption kinetics-----	50
3.3.5 Sorption Mechanism-----	56
3.3.5.1 FTIR-----	56
3.3.5.2 XPS-----	58
3.3.5.3 XRD-----	64
3.3.6 Desorption of metal ions-----	68
3.4 Conclusion-----	70
 Chapter 4 Simulation of the Fixed Bed Adsorption of Ag (I) and Cu (II) onto TCAC sorbents	
4.1 Introduction-----	72

4.2 Mathematical Model-----	74
4.3 Methodology to determine model parameters-----	77
4.3.1 Column parameters-----	77
4.3.2 Empirical correlations of axial dispersion coefficient ( $D_L$ )-----	78
4.3.3 Determination of the overall mass transfer coefficient ( $K_f$ )-----	80
4.4 Results and Discussion-----	82
4.4.1 Model parameters-----	82
4.4.1.1 Axial dispersion coefficient ( $D_L$ )-----	82
4.4.1.2 The overall mass transfer coefficient ( $K_f$ )-----	83
4.4.2 Elution and breakthrough of Ag(I) and Cu (II) from the fixed-bed column---	85
4.4.2.1 Effect of flow rate-----	85
4.4.2.2 Effect of bed length-----	89
4.4.2.3 Effect of sample concentration and injection time ( $t$ )-----	93
4.5 Conclusion-----	97
Chapter 5 Conclusion and Recommendation	
5.1 Conclusion-----	99
5.2 Recommendation-----	101
References	
Appendix	

## List of Tables

- Table 3.1 Adsorption studies of two types of TPP-crosslinking beads
- Table 3.2 Swelling percentage of two types of TPP beads in different pH
- Table 3.3 Isotherm parameters of the adsorption of Ag(I) and Cu(II) on TCAC at T=25°C
- Table 3.4 Kinetic parameters for Ag(I) and Cu(II) adsorption on TCAC
- Table 3.5 Desorption study of Ag(I) and Cu(II) on TCAC
- Table 4.1 Transformation from PDE to ODE
- Table 4.2 Physical parameters of TCAB beads and fixed-bed columns
- Table 4.3 Empirical axial dispersion correlations
- Table 4.4 Empirical correlations for Sherwood number ( $Sh$ ) and its applied ranges
- Table 4.5  $D_L$  (cm<sup>2</sup>/s) values for Ag<sup>+</sup> and Cu<sup>2+</sup> calculated from various correlations
- Table 4.6 The values of  $k_f$  (cm/s) for Ag<sup>+</sup> and Cu<sup>2+</sup> calculated from various correlations
- Table 4.7 The values of mass transfer Biot number ( $Bi_m$ ) at different flow rates
- Table 4.8  $Pe$  values at different bed lengths

## List of Figures

- Scheme 1 Alkalization and cross-linking of chitosan with sodium tripolyphosphate
- Figure 3.1 Dried TCAC
- Figure 3.2 ATR-IR of chitosan powder, TPP-crosslinked chitosan beads with and without alkalization before crosslinking
- Figure 3.3 Crosslinking mechanism of TPP chitosan beads: coacervation (a, left); ionic-crosslinking (b, right)
- Figure 3.4 Non-linear Langmuir and Freundlich isotherm for the adsorption of Ag(I) and Cu(II) ions onto TCAC in a binary metal solution
- Figure 3.5 Comparison of different kinetic models (a. First-order, b. Second-order, c. Intrapartical diffution (ID), d. Elovich's equation(EE)) for the sorption of Ag(I) and Cu(II) ions onto TCAC
- Figure 3.6 ATR-IR of TCAC before and after adsorption in  $\text{AgNO}_3$  and  $\text{Cu}(\text{NO}_3)_2$  Solution
- Figure 3.7 XPS spectra of TCAC before and after silver and copper sorption
- Figure 3.8 before and after sorption XPS N1s (a), O1s (b), P2p (c), Ag 3d (d) and Cu 2p (e) spectra of TCAC
- Figure 3.9 XRD patterns of TCAC before and after silver and copper adsorption
- Figure 3.9 The possible binding structure of  $\text{O}=\text{P}-\text{O}^-$  on TCAC with metal ions
- Figure 4.1 Predicted breakthrough curves for adsorption of Ag (I) and Cu (II) in the column under different flow rates
- Figure 4.2 Predicted elution peaks for adsorption of Ag (I) and Cu (II) in the column under different flow rates
- Figure 4.3 Predicted breakthrough curves for adsorption of Ag (I) and Cu (II) in the column under different bed lengths

- Figure 4.4 Predicted elution curves for adsorption of Ag (I) and Cu (II) in the column under different bed lengths
- Figure 4.5 Predicted elution curves for adsorption of Ag (I) and Cu (II) in the column with different initial concentration
- Figure 4.6 Predicted elution curves for adsorption of Ag (I) and Cu (II) in the column with different initial concentration
- Figure 4.7 Predicted elution curves for adsorption of Ag (I) and Cu (II) in the column with different injection time
- Figure 4.8 Predicted elution curves for adsorption of Ag (I) and Cu (II) in the column with the same injection amount of metal ions

## **List of Symbols, Nomenclature or Abbreviations**

AAS	Atomic absorption spectroscopy
B.E.	Binding energy
EDTA	Ethylene diamine tetra acetic acid
EE	Elovich's equation
FTIR	Fourier transform infrared spectroscopy
ICP-OES	Inductively coupled plasma - optical emission spectrometry
ID	Intrapartical diffution
TCAC	TPP-alkalization chitosan bead
TCB	TPP-chitosan bead
TPP	Sodium tripolyphosphate
XPS	X-ray photoelectron Spectra
XRD	Powder X-ray diffraction
$b$	Langmuir constant related to the affinity of binding sites, L/mg
$Bi_m$	Mass transfer Biot number
$c_{i0}$	Concentration of metal ion $i$ in the feed, mg/L

$c_e$	Equilibrium concentration of remaining metal ions in the solution, mg/L
$c_{e,i}$	Measured concentration of copper and silver ions in the liquid after equilibrium, mg/L
$C_p$	Concentration of the solute within the pores inside the particle, mM
$C_p^*$	Concentration of solute in equilibrium with $C_p$ , mM
$C_s$	Concentration of the solute adsorbed in the stationary phase, mM
$C_i$	Concentration of metal ion $i$ in the bulk liquid, mM
$c_t$	Measured concentration of copper and silver ions presented in the liquid phase after equilibration time $t$ , mg/L
$Des\%$	Desorption ratio of copper and silver ions desorbed by agents
$D_{a,i}$	Apparent dispersion coefficient, $\text{cm}^2/\text{s}$
$D_c$	Intraparticle diffusion, $\text{cm}^2/\text{s}$
$D_{L,i}$	Dispersion coefficient of metal ion $i$ , $\text{cm}^2/\text{s}$
$D_m$	Molecular dispersion, $\text{cm}^2/\text{s}$
$D_{\text{mech}}$	Mechanical dispersion, $\text{cm}^2/\text{s}$
$D_p$	Dispersion coefficient in the particle, $\text{cm}^2/\text{s}$
$E_{sw}$	Percent swelling of beads in the equilibrium
$F$	Phase ratio, equal to $V_s/V_m$ or $(1-\varepsilon)/-\varepsilon$
$i$	Metal ion

$K$	Equal to $q_{\max}/c_{i0}$
$K_f$	Lumped mass transfer coefficient, $s^{-1}$
$k_f$	External mass transfer coefficient, $cm/s$
$k_F$	Freundlich constants indicating adsorption capacity, $mg/g$
$k_m$	Diffusion coefficient $mg/(g \cdot h^{1/2})$
$k_{p2}$	Rate constant of second-order kinetic model, $g/(mg \cdot h)$
$k_1$	Rate constant of pseudo-first order kinetic model, $h^{-1}$
$L$	Bed length, $cm$
$m$	Empirical constant related to $Pe_d$
$n$	Freundlich constants indicating intensity
$Pe_d$	Peclet number of molecular diffusion
$Pe$	Peclet number
$Q$	Flow rate, $L/h$
$q$	Amount of metal ions adsorbed per mass unit of adsorbent, $mg/g$
$q_e$	Amount of metal ions adsorbed per mass unit of adsorbent at equilibrium, $mg/g$
$q_i^*$	Amount of metal ion $i$ adsorbed on the stationary phase in equilibrium with the mobile phase concentration $C_i$ , $mg/g$

$q_i$	Amount of metal ions adsorbed per mass unit of adsorbent, mg/g
$q_s/q_{\max}$	Maximum amount of metal ions adsorbed per mass unit of adsorbent, mg/g
$q_t$	Amounts of metal ions adsorbed per mass unit of adsorbent at time $t$ , mg/g
$R^2$	Coefficient of determination of a linear regression
$Re$	Reynolds number
$r_c$	Radius of the pore in the particle, cm
$r_p$	Radius of the chitosan gel beads, cm
$Sh$	Sherwood number
$t$	Time, h
$u$	Interstitial velocity, cm/s
$V$	Volume of the solution, L
$W$	Mass of the biosorbent, g
$W_d$	Weight of the dried test beads, g
$W_s$	Weight of swollen test beads, g
$\alpha$	Initial adsorption rate, mg/(g·h)
$\alpha_d$	Empirical constant related to $Pe_d$
$\beta$	Desorption constant, g/(mg·(lnh))

$\varepsilon$	Porosity of bed
$\varepsilon_p$	Percentage of macro-pore on the beads
$\eta$	Fluid's absolute viscosity, Pa·s
$\rho$	Packed-bed density, g/L
$\rho_f$	Fluid's density, g/L
$\tau$	Porous medium tortuosity

NPLATE Number of the plate assumed in the column

# **Chapter 1 Introduction**

## **1.1 Background**

Due to the rapid industrialization the global metal demand is ever increasing, but the reserves of high-grade ores are diminishing. It is therefore important to explore the alternative sources of industrial metals. Concurrently, the rapid industrialization generates a variety of industrial wastes, which usually contain toxic heavy metals. Metal accumulation in the environment as a result of mining and metallurgical activities is arising as a matter of serious concern. The recovery and/or removal of metal ions from hydrometallurgical waste solutions prior to their release to the environment are essential in preserving the ecosystem as well as from an economical perspective.

Silver is one of the most essential elements in nearly every industry, such as ethylene oxide industry, photo voltaic industry, batteries, water purification, and even in medical. In 2010, it was reported that the industrial demand of silver was 13.8 million kg and forecasted to be 18.8 million kg in 2015 ("The Future of Silver Industrial Demand ", 2011). Silver can be obtained from three sources: (1) silver ores, (2) by-products of other metal ores, (3) wastewater from photographic processing industry. Although there are some silver-bearing ores on the earth, none of them contains silver as its major component. In the province of Newfoundland and Labrador (NL), silver has been found to be distributed with relatively low contents in massive base metal sulfide ores. It has been reported there would be up to 1600 g silver, 50 g gold and a few amount of other precious metals present per 1000 kg of copper ore in NL (Yao, 2014). After floatation of

a typical silver-bearing ore, the concentrate probably contains 1.7% silver, 10-15% lead, and 10-15% copper (Hoffmann, 2015). Green and cost-effective methods are required to recover the relative low content of silver from flotation concentrates.

Currently, three methods are extensively used to extract or recover silver ions from aqueous solution: chemical precipitation, electrolytic refining and biosorption. Chemical precipitation is the oldest technique which consumes many chemicals and produces solid waste with metallic compounds. Electrolytic refining is widely applied for silver extraction or recovery industry. Generally, a direct electrical current flows through silver-bearing solution between two electrodes, and then the silver ions are reduced on the cathode (Hosseini et al., 2005). However, the low concentration of silver in the leaching elution increase the operation cost of conventional methods. Biosorption, especially with the dead biomass, is well-known to have good removal and recovery abilities in the diluted solution with lower operation cost. Recovery of silver through biosorption is beneficial from both environmental and process-economic perspectives.

However, selecting proper biomass from the huge biomass pool is the key when applying biosorption, because various biomass materials have distinct affinities for certain metals. The well-known biomass capable of binding silver is fungi, yeast, chitosan, and some resins (Das, 2010). Chitin and chitosan, extracted from shrimp and crab shells, have emerged as promising biosorbents because of their high affinity to metals and large quantities in the world, especially in NL. Particularly, chitosan is a more flexible and soluble polymer than chitin, which is more popular in different applications as solutions, gels, or film and fibers (Rinaudo, 2006). The presence of amino groups makes chitosan an

efficient metal scavenger, capable of retaining metal ions from wastewater (Kyzas et al., 2009; Machado et al., 2009; Monier, 2012; Ngah & Fatinathan, 2010; Vijayaraghavan et al., 2011; Zhang et al., 2015). Nevertheless, the poor stability of chitosan in aqueous acidic media limits its application as a biosorbent, because many industrial effluents tend to be acidic. Chemical modifications of chitosan are thereby essential to improve its chemical stability, mechanical strength and adsorption capacity in acidic media.

Although numerous researches dedicated to the sorption of metal ions by modified chitosan, most of them focus on the evaluation of sorption performances and only a few of them aim at gaining a better understanding of sorption mechanisms. Moreover, the majority of studies in the biosorption area focused on the sorption of monometallic system; insufficient research has been carried out for the competitive adsorption from bimetallic or multi-metallic environment. It was also noted that comprehensive modeling and simulation of the fixed bed adsorption of metal ions in the biosorption area were seldom reported. Compared with the stirred-tank biosorption process, the dynamic column process is preferred because it is more productive, easily to be recycled and produces less secondary waste. Mathematical modeling of fixed bed biosorption is an efficient alternative to experimental investigation for a good prediction on the selective/competitive uptake of metal ions under different operating conditions.

## **1.2 Objective and scope of study**

Based on the importance of the silver recovery in the future and the lack of related research of eco-friendly biosorption process in the area, the objectives of this study are to

a) synthesize the crosslinked chitosan beads to selectively adsorb silver in ionic form from bimetallic solution; b) identify the competitive biosorption mechanism of silver and copper on biosorbents c) determine the competitive adsorption isotherm and kinetic parameters for the uptake of silver and copper ions on the prepared chitosan beads; d) use a proper mathematical model to simulate the fixed bed adsorption of silver and copper ions under various conditions.

The scope of the study is as follows:

a) Biosorbent preparation

Chitosan was chosen as the raw biomass to prepare biosorbents for silver and copper uptake and TPP was chosen as the crosslinking agent. Design of experiments (DOE) was applied to screen the proper crosslinked chitosan beads with high silver uptake capacity and selectivity in binary solution.

b) Biosorption equilibrium and kinetic studies

Through the isotherm study, the biosorption equilibrium of silver and copper can be quantified. Kinetic studies can give information of the mechanism of biosorption and the rate-controlling steps.

c) Identification of biosorption mechanism

Metal adsorption through biosorption is complex and various with different biosorbents and metals. Thus, potential implementation strategies should be involved to support the results of sorption equilibrium and kinetic studies, such as FTIR, XPS,

and XRD, which are essential to identify the interaction between metals and biosorbents.

d) Simulation of fixed bed adsorption of silver and copper ions

Linear driving force model was selected for the simulation of fixed bed adsorption of silver and copper ions by the newly synthesized chitosan beads. Empirical correlations were used to estimate two important model parameters, axial dispersion coefficient and lumped mass transfer coefficient. The effects of flow rate, bed length, sample concentration and injection time on the breakthrough and elution of silver and copper ions from the column were studies.

### **1.3 Thesis Outline**

This thesis includes five chapters. Chapter 1 is the introduction that consists of the background, scope of research and the objectives of this study. Chapter 2 mainly reviews the most relevant research on the biosorption of silver. Chapter 3 presents the synthesis of the crosslinked chitosan biosorbent, the isotherm, kinetic and desorption studies of silver and copper ions on the newly synthesized sorbent, as well as the potential sorption mechanism. Chapter 4 shows the modeling and simulation of fixed bed adsorption of silver and copper ions on the synthesized various operation conditions based on the isotherm and kinetic parameters obtained through batch experiments. The major conclusions from this study and recommendations for future works are summarized in Chapter 5.

## **Chapter 2 Literature Review**

### **2.1 Importance of metal recovery in industry**

Along with the advancement of industry, more metals, especially precious metals, have been used in different areas, resulting in a noticeable increase in the volume of aqueous wastewater produced with metal ions. The direct disposal of wastewater is not only damaging to the environment, but also a waste of resources. Heavy metals are barely degraded in soil or water by microorganisms and have serious effects on living creatures (Lenart-Boroń & Boroń, 2014); most precious metals are scarce and non-renewable on the earth but irreplaceable in industry. At present, conventional methods, for the removal of metals and industrial cycling techniques have been combined to deal with those types of wastewater, such as chemical precipitation, membrane and ion exchange (Peter, 1995). However, due to the low concentration of metal ions in wastewater, the cost of operation is higher than the profit from the recycled metals and the secondary pollution, e.g. sludge cannot be avoided. Therefore, an alternative method is needed with efficient recovery of metals from wastewater to develop a win-win situation between the environment and industry. Recently, biosorption has been proposed and is regarded as a promising method to remove and recycle metal ions in the wastewater on account of its inexpensive resources and high efficiency in concentrating metals from even very dilute aqueous solutions (Fu & Wang, 2011).

## **2.2 Biosorption and biosorbents**

### **2.2.1 Available raw materials**

Current research in this area focuses on a number of solid materials for biosorption, and microorganisms are one of the most popular materials. Generally, all types of microorganism have good uptakes towards all types of metal ions. For example, the capacity of *Pseudomonas putida* (a type of bacteria) for Cu(II) is 96.9 mg/g (Uslu & Tanyol, 2006); one gram of *Cladosporium cladosporioides* (a type of fungi) can adsorb 81mg Au(III) (Pethkar et al., 2001); and the capacity of *Fucus vesiculosus* (a type of algae) for Au(III) is 69 mg/g (Mata et al., 2009). Although living biomass has high capacities for metal ions, non-living biomass is preferred because of its low cost, simple operating environment, etc.

Besides, other biomass was also reported (Park et al., 2010) to have good performance in biosorption of metals, such as industrial (activated sludge, food/beverage wastes) wastes, agricultural (rice straws, wheat bran) wastes, natural residues (tree barks) and other biomaterials (Chitosan-driven materials, cellulose-driven materials). When referring to the activated sludge, which has two existing forms, the maximum biosorption capacities of aerobic activated sludge for Cu<sup>2+</sup>, Mn<sup>2+</sup>, Zn<sup>2+</sup>, and Fe<sup>3+</sup> are 65.79, 44.84, 64.94, and 75.76 mg/g, respectively, while the capacities of anaerobic activated sludge are 59.88, 49.02, and 62.50, respectively (Wu et al., 2012). Wheat bran has been studied in the biosorption of Cd(II), Pb(II), Cr(III), Cr(VI), Cu(II), etc. and the capacities of wheat bran are different in each case corresponding to the variation in the structures of

wheat bran (Farooq et al., 2010). Marin and Ayele (Marin & Ayele, 2003) found that the preference of spruce sawdust for metal ions are Zn < Ni < Cd < Cu < Pb due to the different cations of the sawdust in the biosorption process. It is reported that chitosan-based materials have outstanding sorption for toxic metals (Hg), precious metals (Pd, Pt) and metal anions (Mo and V) and can be modified to have selectivity for the target metals (Wang & Chen, 2014).

Though research on the biosorption has been done for years and many raw materials were applied, exploring better biosorbents with lower cost and higher efficiency is needed to deal with more complicated situations arising with the development of industry. Chitosan, having around 70-90% deacetylation of chitin, is one of the cheapest and most abundant biopolymers in the world (Wlnterowd, 1995). It is mainly sourced from crab and shrimp shells, and some are extracted from fungal biomass, insect cuticle or squid pen (Eric Guibal, 2004). Although chitin can be used as biosorbent whose cost is lower than chitosan, the capacity of chitosan is five or six times greater than that of chitin due to its free amino and hydroxyl groups (Bailey et al., 1999). Moreover, chitosan is well-known for its unique properties, such as biodegradability, hydrophilicity, non-toxicity, and adsorption capacity (Ngah et al., 2011). Therefore, an increasing number of researchers began to study the application of chitosan in biosorption.

### **2.2.2 Chitosan based biosorbents**

Among a variety of raw materials, chitosan has attracted special attention by researchers because of two major merits: its low cost, which is related to it being the second most

abundant polysaccharide in the world after cellulose (Peter, 1995); and its outstanding adsorption behavior, especially for metal ions.

Chitosan is the N-deacetylated form of chitin, which is normally hydrophobic in aqueous systems at near neutral or higher pH (Kumar, 2000). It has two functional groups in its structure: amine groups and hydroxyl groups, whose components, N and O, are the key atoms for adsorption. It has been proven that the binding capacity of chitosan is more than 1 mmol metal/g, which is larger than that of other materials (Masri et al., 1974). In recent years, chitosan has been investigated mainly on the biosorption of biomacromolecules (e.g., dye, peptide, enzyme, protein), heavy metals, and precious metals (Kumar, 2000). As for biomacromolecules, it is reported that, due to its unique polycationic structure, chitosan has outstanding behaviour for adsorbing many classes of dyes, including disperse, acid, reactive, sulfur and direct dyes (Crini & Badot, 2008). For example, the capacity of chitosan for acid dyes can reach 600-900 mg/g (Wong et al., 2004); the mechanism of this adsorption is mainly the attraction between anionic sulphonate groups of dissolved dye molecules and the protonated amino groups and the alkyl groups. Another major biosorption of biomacromolecules is drug delivery (e.g., insulin, antitumor, ocular) because the chitosan matrix formation can swell gradually in an acid solution and has a mucoadhesive cationic nature (Kumar, 2000). In addition, chitosan nanoparticles are widely applied in gene delivery due to the positively charged amine groups (Duceppe & Tabrizian, 2010). In the adsorption of metal ions, heavy metals have been widely studied: cadmium (Cd), mercury (Hg), copper (Cu), nickel (Ni), zinc (Zn), lead (Pb), manganese (Mn) and iron (Fe). For instance, Cd is extremely toxic to

humans and the ecosystem, even in low concentration; it was found that, with the same amount of activated carbon and chitosan, the adsorption capacities of Cd are almost the same, but activated carbon is much more expensive (Hydari et al., 2012). Besides, Cu(II) is mostly common in wastewater and its removal has been studied for years. Chitosan beads showed excellent adsorption capacity for Cu (80.71 mg/g); this value is slightly lower than that of chitosan flakes, in which the capacity of Cu is 100 mg/g (Ngah et al., 2002). The capacity of Cu is much better than that of algae and bacterium whose capacities are between 30-48 mg/g (Zhou et al., 2009). Because of the promising performance of chitosan in adsorbing heavy metals, some researchers started to study the application of chitosan in recovering precious metal ions in the aqueous system. The known factors affecting adsorption are pH, temperature, some chelating ions, and other metal ions. Based on the research (Laus et al., 2010), Cd(II), Cu(II) and Pb(II) have the optimum pH values for adsorption at 7.0, 6.0, and 5.5, respectively. However, the optimum adsorption condition of different precious metals varies according to valence, atomic radius and ionization energy. For example, with the increase in pH, the adsorption capacity of chitosan gel for Au ions remained constant until pH was greater than six; for Pt, the adsorption decreased when  $pH > 4$  (Fujiwara et al., 2007).

Although chitosan is a promising biosorbent with unique merits, it still has some drawbacks that affect its application in industry. Chitosan is a semi-crystalline polymer because its insolubility will be changed when immersing it into organic or mineral acids, such as acetic acid and hydrochloric acid (Fujiwara et al., 2007). The amino groups on the molecular backbone are one of the most important adsorption sites, but they can also

be protonated under acidic conditions and increase the solubility of chitosan (Li et al., 2008). Generally, most wastewater is slightly acidic so it is important to make chitosan insoluble. Therefore, modifications are made on either primary amino groups or secondary hydroxyl groups of chitosan before utilizing it. Crosslinking has been widely used, which involves introducing new molecules to react with amine groups to reduce potential protonated sites; this reaction also decreases the adsorption capacity of chitosan. For example, the capacity of chitosan for Fe(III) is 47 mg/g, but that of epichlorohydrin-crosslinked chitosan (EPI-chitosan) is only 34 mg/g; moreover, the capacity of glutaraldehyde-crosslinked chitosan (GLA-chitosan) beads for Fe(III) is just 1/3 of that of chitosan beads (Suc & Ly, 2013). Furthermore, it was found that, compared with chitosan found in nature, GLA-chitosan has lower adsorption ability than EPI-chitosan because of the different crosslinking process (Baroni et al., 2008). The adsorption capacity varies when changing the molar ratio of the crosslinking agent and chitosan (Baroni et al., 2008); therefore, though crosslinking would reduce the potential binding sites on the chitosan, optimal modifications can strengthen the mechanism and insolubility as well as to retain excellent adsorption performance.

Grafting new functional groups to form chitosan derivatives or complexes has been studied to improve the capacity of cross-linked chitosan. Three heteroatoms are most commonly introduced: nitrogen from an amino acid or N-carboxymethyl; phosphorus from orthophosphoric acid or methanesulphonic acid; and sulphur from carbon disulphide or thiourea (Varma et al., 2004). More specialized structures, such as crown ethers or EDTA can also be grafted on the chitosan. For instance, chitosan complexes containing

montmorillonite, have been developed to adsorb dye in the wastewater, which has 53 mg/g capacity of Congo red (Wang & Wang, 2007). It was also reported that N-alkylation of chitosan with cellobiose has better adsorption performance of Pb(II) than natural chitosan, because it introduced other binding sites (though the reaction consumed some amine groups on the chitosan) (Pestov et al., 2008). Magnetic composite, a special component like Fe<sub>3</sub>O<sub>4</sub>, could also increase the biosorption capacity of chitosan (Chen et al., 2012; Zhou et al., 2010). Moreover, it was reported that grafting an S atom to chitosan usually increases the sorption capacity and selectivity of “soft” metal ions (such as Ag and Pt) (Wang & Chen, 2014). Arrascue et al. (2003) found that chitosan grafting of sulfur compounds increased the capacity of Au(III), which is larger than 2 mmol/g with GLA crosslinking. Interestingly, different chitosan derivatives or complexes selectively adsorb specific types of organic compounds or metal ions (Wang & Wang, 2007), which benefits the recovery process in industry. For instance, it was found that GLA-chitosan has a higher capacity of Au(III) (565 mg/g) than that of Pd(II) (180 mg/g), indicating that this adsorbent can selectively adsorb Au(III) from at least binary solutions (Mack et al., 2007). Imprinting technology is developed to enhance the selectivity of chitosan and was recently proved to be effective. It was found that the imprinted chitosan beads have much higher adsorption capacity and selectivity for hemoglobin than the non-imprinted ones (Guo et al., 2004). An enhancement by 20% in the removal capacity of Ag(I) was also developed in the Ag-imprinted chitosan membrane when comparing that of the non-imprinted one (Shawky, 2009).

Another problem of chitosan in adsorption is its slow adsorption kinetics, which is mainly caused by the mass transfer of biosorbates from the bulk of the liquid phase to the adsorption sites inside the particles. Porosity measurements have verified the fact that chitosan is formed by a single-phase homogeneous gel matrix rather than a two-phase heterogeneous one (Guibal, 2004). Therefore to improve the diffusion property, physical modifications are applied to form different porous polymers, such as nanoparticles, beads, membranes, sponges, and fibers. Meanwhile, these modifications on chitosan structures can also enhance the permeability, selectivity and durability of biosorbents (Wang & Chen, 2014). Cross-linked chitosan beads are studied to replace chitosan flakes because of its expansion of the polymer network, improved mass transfer properties, and enhanced hydrodynamic properties (Guibal, 2004). Fixed-bed columns are usually filled with chitosan beads due to the easy recycling of the beads after adsorption. Chitosan fibers have been considered for the recovery of dyes and amino acids; hollow fibers are mainly applied for the continuous adsorption of target metals and their desorption (Guibal, 2004).

In general, chemical modifications are the most influential factors for in the adsorption capacity of chitosan; however, most of the chemicals used are more or less toxic, such as glutaraldehyde and thiourea, which weaken the advantage of biosorption. Tripolyphosphate (TPP) is known for its environmental-friendly properties and low cost, leading to the studies and development in wide-spread applications. There are two crosslinking processes between chitosan and TPP: coacervation and ionic-crosslinking. The former is cured in pH values higher than 7 and fewer  $P_3O_{10}^{5-}$  can react with amine

groups, while the latter is cured in pH values lower than 7 and  $\text{P}_3\text{O}_{10}^{5-}$  was attracted with protonated amine groups (Mi et al., 1999). However decreasing the solubility of chitosan, TPP also introduces -OH (one possible binding site) to chitosan biosorbent. In the past few years, TPP has been mainly used in the synthesis of chitosan biosorbent for drug delivery because of its simple preparation, non-toxicity and undesirable effects. In addition, due to the electrostatic interaction between chitosan and TPP, the particle size can be controlled by altering the chitosan: TPP ratio, pH and the molar mass can be changed, making it a promising drug delivery agent (Morris et al., 2011). Shu & Zhu (2002) developed TPP-crosslinked chitosan beads with good mechanical strength which need approximately ten times higher force to break the beads than that of sulfate-crosslinked chitosan or citrate-crosslinked chitosan beads. Recently, the unique merits of TPP-crosslinked chitosan have caught scientists' attention and led to studies on its adsorption of organics (dye and protein) and metals. S. Reyna G. applied TPP-crosslinked chitosan into the adsorption of red dye and the results showed nearly a 98% removal ratio (Sanchez-Duarte et al., 2012). Similarly, Z. Tang found that the TPP-crosslinked chitosan has a fast adsorption rate of neutral lipase and almost 98% removal ratio as well (Tang et al., 2007). In addition, there is some research on the adsorption of metal ions through TPP-crosslinked chitosan, such as the uptake of copper ions by TPP crosslinked magnetic chitosan (Lee et al., 2001), or adsorption of  $\text{Ag}(\text{I})$  and  $\text{Au}(\text{III})$  by TPP crosslinked magnetic chitosan (Donia et al., 2014); but they are not applied into industry.

Though numerous chitosan-based biosorbents are being developed and the number is increasing, the materials to modify the chitosan are limited; thus, the process of synthesis is the key which leads to the various types of biosorbents. To identify the characteristics of different chitosan biosorbents, analytical techniques are needed during the biosorption research. Brunauer–Emmett–Teller (BET) is a method to test the specific surface area of a material, but it does not work effectively when applied to the measurement of chitosan biosorbents. The scanning electron microscope (SEM) is widely used to measure the surface morphology of chitosan biosorbents by scanning analytes with a focused beam of electrons. It shows visible images of surface structures of specimen to supplement its adsorption mechanism through various analytical modes. Whereas the resolution of the SEM is not high enough to show individual atoms, the transmission electron microscope (TEM), measuring the inner morphology, can supplement the limitations of SEM. TEM transmits a beam of electrons through an ultra-thin specimen, which makes them interact with the specimen when it passes through ("Transmission electron microscopy,"). In addition, the determination of active sites on the biosorbents is important to measure the potential capacity and possible binding process; and those functional sites on chitosan are majorly determined by the degree of deacetylation (DD) and the degree of substitution (DS). Potentiometric titration is widely used to estimate DD and DS, which is similar to direct titration of a redox reaction (Kong, 2012). Besides, nuclear magnetic resonance (NMR) is applied to identify the degree of N-acetylation (DA), which reflects chemical structures, properties and structure–properties relationships of biosorbents (Kasaai, 2010). To analyse the specific functional groups, Fourier transform infrared spectroscopy (FTIR)

is the most widely used technique to obtain an infrared spectrum of absorption and it can simultaneously collect spectral data in a wide spectral range ("Fourier transform infrared spectroscopy,"). Based on the peaks of different spectral ranges, functional groups on the sorbents can be characterised. Further, the bonds between biosorbents and sorbates can as well be identified through the shifts of characteristic peaks. In order to study the strength of the bonds and the states of involved atoms, energy dispersive X-ray spectroscopy (EDS), X-ray diffraction (XRD) analysis and X-ray photoelectron spectroscopy (XPS) are applied the biosorption research. EDS is an analytical technique based on the principle that each element has its own atomic structure with a unique set of peaks on the X-ray emission spectrum ("X-ray spectroscopy"). It is usually used to supplement the analysis of SEM for elemental analysis or chemical characterization of specimen. XRD is good at analysing the crystallographic structure and chemical composition of metal bounded on the biosorbent, using X-ray, neutron, or electron diffraction on powder samples ("X-ray diffraction,"); particularly when reduced metals are produced during the biosorption process. XPS is a surface-sensitive quantitative spectroscopic technique that measures oxidation state of metal bounded on the biosorbents and its ligand effects ("X-ray photoelectron spectroscopy"). According to the survey spectra and high resolution spectra, different binding sites can be assigned by the calculated binding energy. With the application of a least-squares peak analysis software, XPSPEAK, the shifts of peaks of binding sites and the element atomic percentages will be integrated and calculated; then the state of metal in the bond can be tracked in the existing database (Amaral et al., 2005). Additionally, because the diffusion is a controlling process in the

uptake by chitosan-based biosorbents, specifically the ionic crosslinked chitosan beads; thus the swelling ratio is introduced to test the swelling characteristics of biosorbents. This test is carried out in dissolution media at different pH values, in which the biosorbents are immersed for a certain time; and then the change in weights of biosorbents is measured.

The performance of biosorbents is directly reflected by its capacity and removal ratio, and supplemented by its equilibrium isotherms and uptake kinetics. There are three commonly used methods to determine the concentrations before and after adsorption: atomic absorption spectroscopy (AAS), inductively coupled plasma (ICP) and UV-Visible spectroscopy. In analytical chemistry, AAS can be used for measuring the concentration of a particular element without the effect from other existing elements in the sample ("Atomic absorption spectroscopy,"). Moreover, the continuous source AAS is widely-spread in the measurement of continuous adsorption, such as the column test. ICP has wide applications where a high-density plasma is needed ("Inductively coupled plasma,"); optical emission spectrometry (OES) is one of its applications which is an atomic emission spectroscopy for the detection of trace metals; mass spectrometry (MS) is a mass spectrometry for detecting metals and several non-metals at low concentrations. UV-Vis spectroscopy is mainly used for the quantitative determination of organic compounds and biological macromolecules, sometimes for the qualitative determination of metal ions; and its continuous spectrum can be used for the continuous adsorption as well. Equilibrium studies, measuring the sorption capacity, are commonly known as adsorption isotherms; these plot the concentrations of the adsobate in the solid phase

versus that in the liquid phase, so that the most fitted appropriate correlation for this equilibrium curve can be established (Wang & Chen, 2014). According to various experimental data in different biosorption systems, increasing equilibrium isotherm equations are created, including Langmuir, Freundlich, BET, Toth, Temkin, Redlich-Peterson, Sips, Frumkin, Harkins-Jura, Halsey, Henderson and Dubinin-Radushkevich isotherms (Wang & Chen, 2014). In fact, those existing isotherms are only empirical equations with thermodynamic assumptions and restrictions, which cannot 100% fit any equilibrium curve; and researchers will find more equilibrium equations based on the new biosorption systems. However, a mathematical equilibrium isotherm is essential for obtaining reliable prediction of adsorption parameters to quantitatively compare the performance of different biosorbents in varied experimental conditions (Crini & Badot, 2008). An ideal biosorbent for recovery should not only have a large capacity but also a fast adsorption rate. Thus, adsorption kinetics are studied to explain the adsorption rate and also to provide information on the affecting factors (Crini & Badot, 2008); it plots the concentrations of the adsobate in the liquid phase versus time or the uptake capacity versus time, so that the most fitted appropriate correlation for this kinetic curve can be established. The pseudo-first-order equation, the pseudo-second-order equation and intraparticle diffusion models are most commonly used in biosorption. Though biosorption kinetics studies are not developed because of the difficult simulation of complex sorption processes, it is indispensable when studying the adsorption mechanism, the surface properties and affinity of the biosorbent as well as the equilibrium isotherm.

### **2.3 Adsorption mechanism**

The interaction between biosorbents and biosorbates depends on the biosorbates, their chemistry, their chemical and physical nature, the pH of the solution, and other components in the system (Wang & Chen, 2014). In general, the affecting factors can be divided into two types: physical and chemical factors. There are four main categories of physical ones: the physical nature of the material, source and synthesis, process conditions, and physical properties of the biosorbents (Gerente et al., 2007). For example, the value of pH will affect the competition on the binding sites between metal ions and protons (Gerente et al., 2007). The parameters that affect chemical adsorption are solution pH, biosorbate selectivity, and biosorbent structure. For instance, the degree of deacetylation of chitosan influences the density of amine groups on the surface of chitosan and therefore the capacity for metal ions (Gerente et al., 2007). Because of those parameters influencing the adsorption performance, the mechanism is composed of three categories: physical adsorption, chemical adsorption and chemical reaction. However, among numerous papers dedicated to the removal of organic components by chitosan, most of them focus on the adsorption performances and its industrial application, but not the understanding of adsorption mechanisms (Crini & Badot, 2008). On the contrary, several hypotheses of the adsorption structure between chitosan and metal ions has been proposed.

### **2.3.1 Physical adsorption**

Physical adsorption is a process in which the electronic structure of the atom is seldom changed ("Physical adsorption,"), including van der Waals forces, hydrophobic and electrostatic interactions, and ion exchange between the sorbate and the sorbent surface (Matsusaki et al., 2008). Van der Waals forces is not electronic attraction, but the repulsive forces between molecules or atoms; hydrophobic interaction is the adsorption between the non-polar sites of the sorbent and hydrophobic molecules in the polar solvent, clustering or forming micelles, such as alkanes and fats in the wastewater; electrostatic interaction is the attraction between electrically charged particles, the major physical adsorption involved in chitosan-based biosorption. In general, its mechanism may be included in the sorption of metal complexes because the interaction occurs between the free metal anions (metal ions with ligands) and protonated amine groups (Guibal, 2004). For instance, it was reported that electronic attraction is the dominant type when the polyaminated chitosan beads adsorbed Cu-EDTA chelate anions (Juang & Ju, 1997).

Ion exchange is the exchange between both positively or negatively charged ion-containing solution and resins (functionalized porous or gel polymer). In acidic media, due to the cationic behavior of chitosan, the protonation of amine groups adsorb metal anions by ion exchange, not chelation. It was found that the ion-exchange is process-controlling in the adsorption only at low Pb(II) ion concentrations (Ngah & Fatinathan, 2010). In general, in most cases, the chelation is the most common mechanism of chitosan adsorption.

In chemistry, complexation is a coordination complex or metal complex containing a central atom or ion, and the binding molecular or ion are regarded as ligands ("Coordination complex,"). Chelation, one type of complexation, which is the interaction between the functional groups on the chitosan and adsorbates; and it always involves more than one coordinating bond between functional sites and one metal ion or organic compound. Pearson's definition of chelation is the theory of the hard and soft acids and bases (HSB) (Pearson, 1963), and the affinity and stability of chelating ligands for adsorbates differs according to the various experimental conditions (pH, adsorbate concentration, adsorbate and ligand ratio), physical state of the chitosan (powder, bead, or membrane), and DA, which confirms that the chelation process was easier when the chitosan has a large DA (Rhazi et al., 2002). The amino group is the key site on the chitosan with free electron pairs which can form coordinating bonds with metal ions. Two adsorption models have been widely accepted (Guibal, 2004): the "bridge model" and the "pendant model". In the "bridge model", the interaction normally occurs between different chains, involving metal ions and several amine groups; but inversely, as to the "pendant model", the metal ion is only bonded with an amine group in a chitosan chain (Guibal, 2004). Nevertheless, the variation of chitosan-based biosorbents and different adsorption systems lead to more complicated mechanisms of chelation. It was reported that two chelation models exist in the same system when changing the pH of adsorption:  $[\text{Cu}(-\text{NH}_2)]^{2+}, 2\text{OH}^-$ ,  $\text{H}_2\text{O}$  is more stable for pH between 5 and 5.8, and  $[\text{Cu}(-\text{NH}_2)^2]^{2+}, 2\text{OH}^-$  is more stable at pH larger than 5.8 (Vold et al., 2003).

### **2.3.2 Chemical reduction**

Because of the amino and hydroxyl groups on the backbone of chitosan, the metal ions can be reduced during the adsorption process in some certain conditions (Dambies et al., 2001). In addition, some crosslinking agents or grafted components can also introduce reducing ends on the chitosan-based biosorbents. It was found that GLA-crosslinked chitosan beads could partly reduce Cr(VI), Mo(V) and Cu(II) to Cr(III), Mo(VI) and Cu(I) (Dambies et al., 2001). The reason may be the residues on glutaraldehyde - aldehyde groups, which do not react with amino groups, reduce the metal ions (E Guibal et al., 1999). However, some research indicates that not chitosan itself, but the products of its hydrolysis are the main reducing agents in H[AuCl<sub>4</sub>]/chitosan solutions causes the fast Au(III) reduction to Au(0) particles (Pestov et al., 2015). Besides, the reducing ability of chitosan is often applied into the formation of metal nanoparticle-chitosan (NPs-chitosan) by exposure of chitosan to a solution containing metal salts under thermal treatment, such as AgNPs, AuNPs (Wei et al., 2010). The metal nanoparticles that are formed strongly bound to chitosan, which encouraged us to investigate their catalytic performance. Currently XPS, XRD, <sup>13</sup>C and <sup>1</sup>H NMR analysis (Dambies et al., 2001; Pestov et al., 2015) are common techniques to detect the reduced metals; whereas the redox is hard to comprehensively be verified because those detecting methods can also cause the chemical reaction to some degree (Warren, 1969; Watts, 1994).

## **2.4 Column test and mathematic modeling**

The batch test is commonly used to obtain isotherm and kinetics parameters of biosorbents, but it is not enough to confirm their application in the industry. The performance in fixed-bed systems has attracted more attention by scientists to test the possibility of industrial application recently. Moreover, the biosorbents in the column can separate different kinds of adsorbates in the aqueous system based on its various affinities and the regeneration by some chemicals. There are two major continuous biosorption reactors: the down-flow bed reactor and the up-flow bed reactor; though the former one is more energy-effective due to its gravitational forces, the latter one is applied more extensively because it is easier to be controlled and has higher operation yield (Park et al., 2010).

### **2.4.1 Breakthrough curve and elution curve**

The breakthrough curve is mostly observed in continuous biosorption because it can not only give column information, such as the number of theoretical plates, the capacity or separation factors (Weber Jr & Liu, 1980); but also represent feasibility and economics of the sorption phenomena. Besides, the breakthrough curve can also reflect the conditions of the column which means that: (a) there are short circuits in the column if the elution has residues once inputting the solution; (b) the mass transfer is too slow if the breakthrough is significantly spread. Generally, for the same column, the shape of the breakthrough curve is determined by the flow rate and solute concentration; with increasing flow rate and solute concentration, the breakpoint and adsorption capacity are

decreased because of the insufficient contact time (Sankararamakrishnan et al., 2008). A breakthrough curve is usually expressed in terms of the initial adsorbate concentration in the elution as a function of flow time ( $t$ ) or volume of effluent for a given bed height (Sankararamakrishnan et al., 2008). In spite of the adsorption capacity, the regeneration of biosorbents is also a significant characteristic; because it is efficient to be applied into columns, thereby reducing the cost of operation. Thus several papers studied the selectivity of elution conditions, such as the type of desorption agents, pH, ion strength, size of chitosan, etc. HCl, HNO<sub>3</sub>, H<sub>2</sub>SO<sub>4</sub>, Thiorea, and EDTA are common desorption agents. For example, EDTA is found effective in desorbing metal ions as it has strong chelating affinity to them (Jeon & Park, 2005); H<sub>2</sub>SO<sub>4</sub> and Thiorea are typically better for the desorption of precious metals because of S atoms (Lin & Lien, 2013); and HNO<sub>3</sub> and HCl are mostly used in the desorption because they are much cheaper and their desorption abilities are not bad in certain conditions (Kang et al., 2004; Kavaklı et al., 2006). An elution curve is usually expressed in terms of the adsorbate concentration in the elution as a function of flow time ( $t$ ) or volume of effluent for a given bed height. Because of the different affinities of desorption agents to the adsorbates, different components in the solution can be separated and recovered through the column. There are also some papers working on the optimization of elution conditions to maximize the efficiency of the adsorbents in the column; such as changing the concentration of desorption agent or the pH of the eluent (Tang et al., 2007). In addition, combining the breakthrough curve and elution curve, the real performance of the column can be explained clearly and provide precise information in the industrial application.

## 2.4.2 Mathematical model

The mathematical model here is a description of the mass transfer in the adsorption-desorption continuous system (fixed-bed or column) using mathematical concepts and language, predicting the breakthrough and elution curves. Compared to the experiment, mathematical modeling needs no experimental equipment and chemicals but gives accurate predictions of breakthrough and elution curves based on the isotherm and kinetics parameters. Currently, many mathematical models, reported for liquid-solid adsorption, have been simplified based on different rate-controlling steps like axial dispersion and sorption equilibrium.

Originally, the fixed-bed or column is assumed to be uni-dimensional and only have two independent variables, the time  $t$  and the column length  $z$ . To study the band profile of the components in the column, the differential mass balance is introduced. Guiochon et al. (2006) provided the general differential mass balance in the bulk mobile phase and deduced the solution of the mass transfer (Equation 2.1) according to several fundamental assumptions: a) the column is radically homogeneous with constant axial dispersion; b) the mobile phase is hardly compressed and the sample components keep stable in both phases; c) the solvent or the weak solvent is not adsorbed in the isotherm; d) the thermal effects and the influence of the heat of adsorption on the band profile are neglected (Guiochon et al., 2006).

$$\text{The derivation: } \frac{\partial C_i}{\partial t} + F \frac{\partial C_{s,i}}{\partial t} + \mu \frac{\partial C_i}{\partial z} = D_{L,i} \frac{\partial^2 C_i}{\partial z^2} \quad (2.1)$$

where  $F$  is the phase ratio,  $V_s/V_m$ , equal to  $(1-\varepsilon)/-\varepsilon$ . The first two terms on the left-hand side represent the accumulation in the mobile and stationary phases, respectively; the third term is the convection; the term on the right-hand side represents diffusion.

Because of the different properties of the chromatography, the mass transfer kinetics is different. When the mass transfer between two phases is fast, the concentration of the component in the stationary phase  $C_{s,i}$  can be represented by  $q_i$ , and the stationary phase concentration in equilibrium with  $C_{s,i}$  is:

$$C_{s,i} = q_i = f_i(C_1, C_2, \dots, C_i, \dots, C_n) \quad (2.2)$$

and when the mass transfer kinetics is slow, such as in the liquid-solid chromatography and ion-exchange chromatography, the  $C_{s,i}$  can be represented as:

$$\frac{\partial C_{s,i}}{\partial t} = g_i(C_1, C_2, \dots, C_i, \dots, C_n, C_{s,i}, \dots, C_{s,n}) \quad (2.3)$$

#### 2.4.2.1 General rate model

Currently, the most precise model to describe the mass conservation and transport in the basic stage of the model is the general rate model, considering all the possible contributions to the mass transfer kinetics, which is widely used when the impact of particle size distribution cannot be neglected. This model includes two parts:

(a) the bulk model can be written as follows:

$$\mu \frac{\partial C}{\partial t} + \frac{\partial C}{\partial t} + F \frac{\partial \bar{q}}{\partial t} = D_L \frac{\partial^2 C}{\partial z^2} \quad (2.4)$$

where  $D_L$  is the axial dispersion coefficient, and the term  $\partial\bar{q}/\partial t$  is the rate of adsorption averaged over the particle. For a spherical particle, the equation is:

$$\partial\bar{q}/\partial t = k_f(C - C_p \Big| r = R_p)/R_p \quad (2.5)$$

where  $k_f$  is the external mass transfer coefficient and  $C_p$  is the concentration of the solute within the pores inside the particle (Guiochon et al., 2006).

(b) The particle model can be divided into micro-pore control ( $r_c \ll 1$  mm) and macro-pore control ( $r_c = 1 - 5$  mm) according to the size of adsorbents. For the micro-pore control model, the equation can be written as follows (Guiochon et al., 2006):

$$\frac{\partial q}{\partial t} = D_c \left( \frac{\partial^2 q}{\partial r^2} + \frac{2}{r} \frac{\partial q}{\partial r} \right) \quad (2.6)$$

where  $D_c$  is the diffusion coefficient of the solute into the particle and  $q$  is the stationary phase concentration. For the macro-pore control model, the equation can be written as follows (Guiochon et al., 2006):

$$\varepsilon_p \frac{\partial C_p}{\partial t} + (1 - \varepsilon_p) \frac{\partial C_s}{\partial t} = D_p \left( \frac{\partial^2 C_p}{\partial r^2} + \frac{2}{r} \frac{\partial C_p}{\partial r} \right) \quad (2.7)$$

where  $\varepsilon_p$  is the internal porosity of the particle,  $D_p$  is the diffusion coefficient of the solute in the particle pores, and  $C_s$  is the concentration of the solute adsorbed by the stationary phase. When assuming the kinetics of adsorption-desorption is infinitely fast,  $C_s$  can be related to the linear adsorption isotherm equation:

$$\frac{\partial C_s}{\partial t} = k_{ads}(C_p - C_p^*) \quad (2.8)$$

where  $C_p^*$  is concentration of solute in equilibrium, which is commonly obtained through the Langmuir isotherm or Freundlich isotherm.

It is proved that the predictions of general rate model were very consistent with the experimental data, such as the analysis of Solanesol adsorption on macro-porous Resins (Du et al., 2008), the adsorption of  $Pb^{2+}$  in a fixed bed of ETS-10 adsorbent (Lv et al., 2008). However, the problem of using this model is to make a detailed analysis of the significance of all the contributions, and then obtaining all the four parameters through experiments, which require numerous experiments and sufficient facilities.

#### 2.4.2.2 Lumped kinetic model

Simpler models, such as the various lumped kinetic models, were developed by generally sacrificing accuracy in describing the suspended-particle batch adsorption process (Rowe et al., 1999). It is formed based on a kinetic equation, lumping all the slow kinetics in a single rate coefficient; so the mass balance equation is then written:

$$\frac{\partial C_i}{\partial t} + F \frac{\partial C_s}{\partial t} + \mu \frac{\partial C_i}{\partial z} = D_L \frac{\partial^2 C_i}{\partial z^2} \quad (2.9)$$

and when the kinetics of adsorption-desorption is slower than the other steps of the column process, the kinetic equation can be presented as:

$$\partial C_s / \partial t = k_a C - k_d C_s \quad (2.10);$$

while if the slowest step is the mass transfer kinetics, the kinetic equation is:

$$\partial C_s / \partial t = K_f (C - C^*) \quad (2.11).$$

Though some steps are simplified in the lumped kinetic models, good agreement was found between the experimental and calculated data in the column with slow kinetics and the diffusion coefficient mostly equaled the axial dispersion (Bak et al., 2007; Pérez-Martínez et al., 2015).

#### 2.4.2.3 Equilibrium-Dispersive model

When the mass transfer kinetics is fast but not infinitely fast, it can be assumed that the mobile and the stationary phases are constantly in equilibrium. Thus, the equilibrium-dispersive model was created; the mass balance equation for component  $i$  is as follows:

$$\frac{\partial C_i}{\partial t} + F \frac{\partial q_s}{\partial t} + \mu \frac{\partial C_i}{\partial z} = D_{a,i} \frac{\partial^2 C_i}{\partial z^2} \quad (2.12)$$

where  $D_{a,i}$  is the apparent dispersion coefficient which lumped the axial dispersion, non-equilibrium effects and finite kinetics of adsorption-desorption.

This model is usually applied into HPLC columns with high efficiency because of the assumptions of simplified process (Quiñones et al., 2000). Therefore in the lab-scale experiments this model is difficult to get good agreement between model and experiment.

#### **2.4.2.4 Ideal model**

When there is no axial dispersion and the two phases are constantly at equilibrium, which means the column efficiency is infinite; then the mass transfer equation can be simplified as the ideal model:

$$\frac{\partial C_i}{\partial t} + F \frac{\partial q_i}{\partial t} + \mu \frac{\partial C_i}{\partial z} = 0 \quad (2.13)$$

This simplest model focuses on the the effects of the nonlinear thermodynamics of phase-solid equilibrium, which are in good agreement with the experiment for large samples, highly efficient columns and small dispersive effects of the column efficiency (Guiochon et al., 2006). The application of this model is scarce in the literature because of its strict assumptions.

#### **2.4.3 Mass transfer effect on column test**

Mass transfer is the movement of mass, like phase, fraction or component, from one point to another. It is extensively applied in many chemical engineering processes, such as absorption, evaporation, adsorption, drying, precipitation, membrane filtration, and distillation ("Mass transfer,"). Specifically, in the column, the mass transfer includes (i) radial diffusion from the center of the flow stream to the surface of biosorbents; (ii) film diffusion from the mobile phase into the stationary phase (inside of biosorbents); (iii) diffusion from the stagnant mobile phase into the biosorbents pores. Moreover, in the general sense, the mass transfer can also contain adsorption-desorption, ion-exchange, and complexation (Guiochon et al., 2006) . The most important coefficients are bulk

diffusion coefficients, axial dispersion coefficients, external film mass transfer resistance, intraparticle pore diffusion coefficients and viscosity of flow stream. The values of those parameters are affected by temperature, pressure, viscosity, concentration, molecular diffusion and the size of biosorbents; and these values result in different column performance. It is reported that with different flow rate, the film diffusion coefficient and axial dispersion coefficient vary, leading to different breakthrough curves for the adsorption of copper ions (Ko et al., 2001).

## **Chapter 3 Competitive Adsorption of Ag(I) and Cu(II) on Chitosan Beads Cross-linked with Sodium Tripolyphosphate**

### **3.1 Introduction**

These years, biosorption has been considered as a promising technology for the removal of heavy metals or the recovery of precious metals because of its low cost and high capacity (Park et al., 2013). Chitosan, produced from chitin, is one of the popular biosorbents that has been widely studied in the removal of different heavy metals from aqueous solution (Guibal, 2004; Li et al., 2008). Amine groups, however, as one of major biosorption sites on chitosan, could lead to its solubility in acid solution (Kumar et al., 1999), limiting the application in real situations. Therefore, chemical modifications have been studied to increase its stability in acid solution and improve its metal sorption performance. Crosslinking is a common modification to strengthen the mechanical structure and decrease the solubility by consuming or grafting the primary amino group and hydroxyl group. Besides, crosslinked beads can be used in the column commercially without causing clogging and high pressure like powder (Miretzky & Cirelli, 2009).

Four common cross-linkers, i.e., glutaraldehyde, ethylene glycol diglycidyl ether (EGDE), tripolyphosphate (TPP) and epichlorohydrin (EPI) have been applied to immobilize chitosan powder. Therefore, because of the non-toxicity and low-cost, TPP is a promising crosslinking agent for the chitosan beads, as well as due its simpler synthesis process (Sureshkumar et al., 2010). It is reported that the ionic reaction of chitosan-TPP is significantly influenced by the pH of the TPP solution and the chitosan solution (Mi et al.,

1999). In the acid aqueous solution, the interaction between TPP and chitosan is controlled by ion-crosslinking; with the increase of pH, more OH<sup>-</sup> will compete with P<sub>3</sub>O<sub>10</sub><sup>5-</sup> and coagulate with chitosan, preserving more free -NH<sub>3</sub><sup>+</sup> (Mi et al., 2003). However, there are few studies about the adsorption of metals with TPP crosslinked chitosan beads, such as the improvement of sorption performance and mechanism.

Except for the enhancement of metal adsorption, the understanding of adsorption mechanism is also important to study because it can help to further improve the property of chitosan beads effectively. Based on the available functional groups on chitosan, four possible adsorption mechanisms can be applied: electrostatic attraction/ion exchange with protonated amino groups, chelation/coordination on amino groups in a pendant fashion or in combination with vicinal hydroxyl groups (Donia et al., 2007; Guzman et al., 2003).

Electrostatic attraction and ion exchange both occur at the low pH of 2-4 and react with protonated amine groups on chitosan (Guibal, 2004). While for the former one, -NH<sub>3</sub><sup>+</sup> usually interact with free metal anions which can be regarded as metal complexes which will be discussed later. For the latter one, the mechanism probably is the exchange of H<sup>+</sup> on the protonated amine groups with metal cations, and is hardly dependent on the pH.

Chelation and coordination both form a complex with ions in the solution and functional groups on chitosan; the difference is that the chelation focuses on metal ion complexes and the coordination explains the metallic atoms. Thus in the adsorption of chitosan, the mechanism of coordination is seldom mentioned; and it is proved that chelation plays an important role (Guibal et al., 2006). These years, many studies have been done about the

adsorption mechanism of copper ions and two models are accepted by the majority: (i) the pendant model, which is the coordination of Cu<sup>2+</sup> with one amine group or C<sub>3</sub>-hydroxyl group and certain amount of water molecule or -OH<sup>-</sup>. (ii) the bridge model, which is the coordination of Cu<sup>2+</sup> with one amine group and C<sub>3</sub>-hydroxyl group, and then bonded with certain amount of water molecule or -OH<sup>-</sup> (Lü et al., 2008). Besides, fewer studies about the adsorption of silver were reported, especially the adsorption mechanism. But -NH<sub>2</sub> on the chitosan is reported to be involved in the Ag<sup>+</sup> adsorption via ion exchange (acidic solution) or chelation (neutral or basic solution) (Donia et al., 2007). Some research mentioned about the reduction of silver ions during the adsorption process, but the detailed mechanism was not confirmed (Kumar et al., 2013).

Although adsorption of cross-linked chitosan on metal ions has been widely studied, rarely has research studied the separation of metal ions in binary solution; especially when the two metal ions were in the same group in the periodic table due to their similar properties. Thus it is meaningful to study the competitive adsorption of copper and silver ions because silver ions exist in the wastewater of copper mining and the amount is valuable if it is recovered. Besides, TPP-crosslinked beads are environment-friendly and cost-effective with simple synthesis steps.

## **3.2 Materials and Methods**

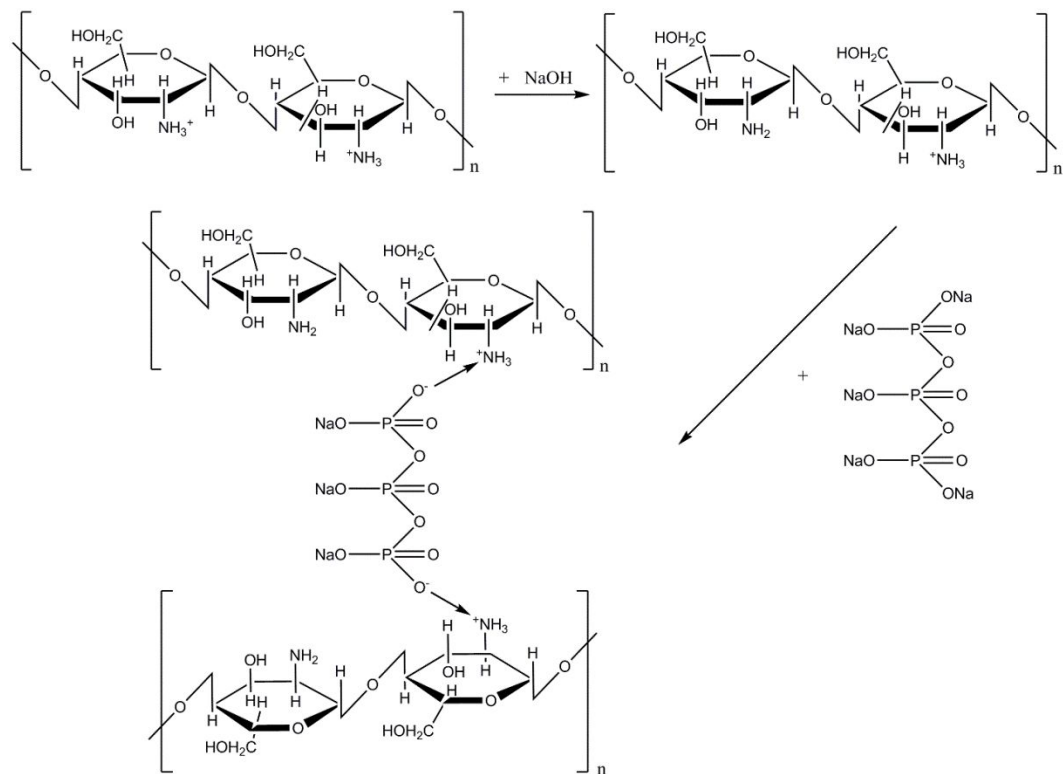
### **3.2.1 Materials and chemicals**

Chitosan and sodium tripolyphosphate (TPP) were purchased from Fisher (Canada). Weight-average molecular weight (Mw) and deacetylation degree are 100,000 – 300,000 g/mol and 90%, respectively. Copper nitrate, silver nitrate standard solution (100 mM) and acetic acid was provided by Fisher Scientific. All other materials were of reagent grade purity. Deionized (DI) water was used throughout the study.

### **3.2.2 Preparation of cross-linked chitosan beads**

Chitosan solution was prepared by dissolving 4.00 g chitosan powder into 100 ml of 4% (v/v) acetic acid. The TPP solution was prepared by dissolving 5.00 g TPP powder in 100 mL of water. To synthesis TPP-chitosan bead (TCB) with the conventional method, the chitosan solution was dropped into TPP solution (pH = 8.6) directly using a syringe, with a needle of 1.5 mm; which coagulated the chitosan gel to spherical uniform chitosan gel beads and thereby cross-linked for certain time. To synthesis TPP-alkalization chitosan bead (TCAC) with the novel method, the chitosan solution was dropped into 250 ml of 0.50 M NaOH to get wet chitosan beads firstly and the beads were alkalized for 24h; after that the alkalized chitosan beads were immersed in TPP solution (pH = 8.6) for cross-linking for 1 h. The formation of cross-linked TPP-beads by the interaction between phosphate groups of tripolyphosphate and amino group of chitosan is schematically represented in Scheme 1. The beads were separated by filtration, washed four times with

deionised water and air dried before use in adsorption experiments. Dried beads were spherical and slightly yellowish in color (Figure 3.1).



Scheme 1. Alkalization and cross-linking of chitosan with sodium tripolyphosphate



Figure 3.1 Dried TCAC

### 3.2.3 Swelling rate test

The swelling characteristics of TPP beads were determined by immersing dried test beads to swell at 25°C in HNO<sub>3</sub> (pH = 2), H<sub>2</sub>O (pH = 6) and NaOH (pH = 10) for 24 h; thereby beads were removed from the swelling medium and were blotted with a piece of paper towel to absorb excess water on surface. The swelling ratio of test beads was calculated from the following expression:

$$E_{sw} = (W_s - W_d) / W_d \quad (3.1)$$

where  $E_{sw}$  is the percent swelling of beads in the equilibrium,  $W_s$  is the weight of swollen test beads and  $W_d$  is the weight of the dried test beads.

### 3.2.4 Batch sorption tests

Stock solutions of certain concentration of Ag(I) and Cu (II) ions were prepared using analytical-reagent grade silver(I) nitrate solutions and copper(II) nitrate solutions, respectively. The initial pH of the adsorption of Ag(I) and Cu(II) ions onto TPP beads was kept original (pH = 5.0).

Adsorption equilibrium study was conducted using 0.10 g of TPP beads at room temperature. The experimental solutions contain a measured concentration (0.2 mM – 2.0 mM) of copper and silver ions and the adsorbent, which was equilibrated in a 500 mL Erlenmeyer flask at 150 rpm using an Innova® 43 console incubator shaker. After 48 h of equilibration, 20–100 µL of the solution was withdrawn from the experimental mixture, and copper and silver concentrations were estimated using ICP-OES. The amount of copper and silver ions adsorbed onto the TPP bead at time  $t$ , was calculated by:

$$q_i = \frac{(c_{0,i} - c_t)V}{W} \quad (3.2)$$

where  $q_i$  (mg/g) is the quantity of copper and silver ions adsorbed on TPP bead,  $c_{0,i}$  is the initial concentration (mg/L) of copper and silver ions used in the experiment,  $c_t$  is the measured concentration (mg/L) of copper and silver ions presented in the liquid phase after equilibration time  $t$ ;  $V$  is the volume of the solution (L);  $W$  is the mass of the TPP beads (g).

The batch kinetic studies were carried out using 0.3 g adsorbent in 300 mL solution of 1.0 mM of Ag(I) and Cu(II) ions. The adsorption time was varied from 0 to 1600 min.

Adsorption kinetics experiments were performed by the batch method, where approximately 0.3 g of beads were suspended in a 300 mL of Ag(I) and Cu(II) solution of 1 mM at 150 rpm using an Innova® 43 console incubator shaker; The temperature was 300 K for times varying from 0 to 48 h. The concentrations of the residual cation (mg/L) in collected samples was tested by ICP-OES.

Desorption studies were conducted using 0.10 g TCAC loaded with 100 ml of 1mM Ag(I) and Cu(II) ions solution under the optimum conditions. The TCAC were agitated with 50 mL EDTA, Na<sub>2</sub>S<sub>2</sub>O<sub>3</sub> or H<sub>2</sub>SO<sub>4</sub> solution of various concentrations for certain time; the pH was adjusted by an accumet™ AB15 Basic and BioBasic™ pH/mV/°C Meter using 1M NaOH and 1M H<sub>2</sub>SO<sub>4</sub>. The final concentration of metal ions in the aqueous phase was determined by Atomic absorption spectrometer, and the initial and final pH was tested by an accumet™ AB15 Basic and BioBasic™ pH/mV/°C Meter. The ratio of copper and silver ions desorbed onto the TPP bead at time *t*, was calculated by:

$$Des\% = \frac{c_{e,i}V}{q_iW} \times 100\% \quad (3.3)$$

where *Des%* is the desorption ratio of copper and silver ions desorbed by agents, *q<sub>i</sub>* (mg/g) is the quantity of copper and silver ions adsorbed on TPP bead, *c<sub>e,i</sub>* is the measured concentration (mg/L) of copper and silver ions in the liquid after equilibrium, *V* (L) is the volume of the solution and *W* is the mass of the TPP beads (g).

### **3.2.5 ICP-OES**

The concentrations of Ag (I) and Cu (II) ions in the solutions were measured by PerkinElmer® Optima™ 5300DV Inductively Coupled Plasma Optical Emission Spectrometer (ICP-OES) equipped with WinLab 32 for ICP v.4.0.0.0305 software. Sample solutions were diluted 20 times with 2% HNO<sub>3</sub> solution for the simultaneous measurement of all analytes. Standard solutions containing 0.0, 0.01, 0.1, 1.0, and 10.0 mg/L Ag (I) and Cu (II) in 2% HNO<sub>3</sub> were used to get the calibration curves. Yttrium (10 mg/L) was used as an internal standard to account for any difference between the sample matrix and calibration standards. Check standard solutions were prepared from PlasmaCal standards. Analysis on Ag was conducted at wavelengths of 338.290 nm, 328.068 nm and 243.774 nm, analysis on Cu was performed at wavelengths of 327.393 nm, 324.755 nm and 224.698 nm. Reported values were the mean of three consecutive replicate measurements and were corrected for dilution.

### **3.2.6 ATR-FTIR**

The infrared spectra were recorded with a Bruker Alpha FTIR Spectrometer, using the Single Bounce Diamond ATR accessory. The beads were dried at room temperature in a fuming hood for 24 h. The spectra were obtained with the average of 24 scans, at a 4 cm<sup>-1</sup> spectral resolution. Peak identification was obtained from the correspondent second-derivative spectra in the range between 4000 and 400 cm<sup>-1</sup>.

### **3.2.7 XPS**

X-ray photoelectron Spectra were performed on a ULTRA spectrometer (Kratos Analytical) at the Alberta Centre for Surface Engineering and Science (ACSES), University of Alberta. The base pressure in the analytical chamber was lower than  $5 \times 10^{-8}$  Pa. Monochromatic Al K $\alpha$  X-ray radiation was used as the excitation source (1486.6 eV), and operated at 144 W. Survey spectra were collected for binding energy spanning from 0 to 1100 eV with a pass energy of 80 eV with a step of 0.4 eV. High resolution spectra for the C 1s, O 1s, N 1s, Ag 3d and Cu 2p regions were obtained, using a pass energy of 40 eV with a step of 0.1 eV. The resolution for the instrument is 0.55 eV for Ag 3d. Due to their insulating nature, chitosan beads surfaces were charged, resulting in a shift toward higher binding energy. Thus, the binding energies of the photoelectron peaks were calibrated, assigning a binding energy of 284.8 eV to the C-C of C 1s peak, present as a carbon surface contaminant. The deconvolution of the high resolution spectra was made using XPSPEAK version 4.1, utilizing the Gaussian/Lorenzian sum function.

### **3.2.8 XRD**

Powder X-ray diffraction studies were carried out using a Rigaku Ultima-IV XRD with Cu source, set up via Bragg-brentano configuration and a graphite monochromator. The scan range was 5.0000 – 100.0000 deg., the scan speed was 1.000 deg./min, and the scan axis was 2 theta//theta.

### **3.3 Results and Discussion**

#### **3.3.1 Sorbent screening and characterization**

According to the research study of Mi and co-workers (Mi et al., 1999), protonated amino group on chitosan reacted more easily with  $P_3O_{10}^{5-}$  at low pH of TPP solution. In another word, gel beads prepared in acidic TPP solution have a higher degree of ionic crosslinking. Therefore, in this study, pH 8.6 of TPP solution was selected to control the degree of crosslinking of chitosan. Table 3.1 summarizes the performances of TCAC and TCC beads prepared under different conditions for the adsorption of Ag (I) and Cu (II) from monometallic and bimetallic solutions. Results indicate that alkalization before crosslinking helps to obtain chitosan gel beads with higher total uptake capacity, and TCAC beads provided much more binding sites for Ag (I) than TCC beads. It is clearly that beads with lower degree of crosslinking (TCAC) are favorable to Ag (I) binding, whereas beads with higher degree of crosslinking (TCC) tend to bind more Cu (II). This reveals the adsorption of Ag (I) and Cu (II) take place at different sorption sites and amine group on chitosan is more selective to Ag (I).

As illustrated in Table 3.1, concentration of STPP solution does not have significant influence on the sorbent performance. Therefore, TCAC beads prepared by crosslinking with 5.0% (w/v) STPP solution were selected for the remaining isotherm and kinetic studies.

Through the FTIR spectra of chitosan powder, TPP-crosslinked chitosan beads with or without alkalization, shown in Fig. 3.2, several peaks, characteristic for chitosan and

sodium tripolyphosphate are observed in the spectrum to explain the reason of the difference. The intense band around  $3628\text{ cm}^{-1}$  should be assigned to free –OH, indicating that the hydroxyl group (from sodium tripolyphosphate solution) was introduced in the synthesis process. Amine functional groups show characteristic peaks  $1650\text{ cm}^{-1}$  and  $1576\text{ cm}^{-1}$ , and are assigned to –NH deformation vibration. The shift of amine groups on chitosan beads indicate the reaction between tripolyphosphate and amine groups. The intense band around  $3273\text{ cm}^{-1}$  should be assigned to the stretching vibration of  $\text{NH}_3^+$ ; and due to the alkalization, the intermolecular hydrogen-bonded O-H gives a broad peak at  $3550$ - $3230\text{ cm}^{-1}$ , which overlaps peak of  $-\text{NH}_3^+$ . Sharp peaks at  $1212\text{ cm}^{-1}$  and  $1127\text{ cm}^{-1}$  are caused by P-O-H vibration of HO-P=O groups; similarly, the peak at  $1150\text{ cm}^{-1}$  should be assigned to associated C-N stretching, respectively. Further, the strong intense band around  $1068\text{ cm}^{-1}$  should be assigned to the alcohol C-O stretching vibration of –CH<sub>2</sub>-OH groups.

Therefore, similar with other's results (Mi et al., 1999), the crosslinking mechanism with alkalization could be coacervation (Figure 3.3a) and that without alkalization could be a combination of coacervation and ionic-crosslinking (Figure 3.3a & 3.3b). When chitosan beads were dropped into sodium hydroxide for alkalization, the OH<sup>-</sup> ions reacted with protonated amino group of chitosan on the surface of the beads. After the formation of a gelled outer layer with OH<sup>-</sup> ions, P<sub>3</sub>O<sub>10</sub><sup>5-</sup> was more difficult to diffuse into the beads, preserving more free –NH<sub>3</sub><sup>+</sup>. However, when the chitosan beads were dropped in TPP solution directly, the P<sub>3</sub>O<sub>10</sub><sup>5-</sup> and OH<sup>-</sup> ions in the solution would compete to react with the amino groups, leading to less free amino groups inside the beads and higher density of

TPP-crosslinking. Thus, although the TPP can provide available functional groups for adsorption, it consumes the existing ones as well. In total, there is an optimal density of TPP-crosslinking to maximize the adsorption ability of beads. In this study, the optimal synthesis condition should include alkalization.

Table 3.1 Adsorption studies\* of two types of TPP-crosslinked chitosan beads from monometallic and bimetallic solutions

No.	Alkalization	Crosslinking time (h)	Conc. of TPP (%)	Conc. of chitosan (%)	Capacity (mg/g)	
					Ag (I)	Cu (II)
1	NO	1	5	4	8.25	-
2	NO	1	5	4	-	16.50
3	YES	1	5	4	28.30	-
4	YES	1	5	4	-	8.90
5	NO	1	5	4	5.80	7.15
6	NO	1	10	4	6.65	7.94
7	Yes	1	5	4	31.54	3.89
8	Yes	1	10	4	32.28	4.84

\* Batch sorption tests were carried out at  $T=25^{\circ}\text{C}$  for 24.0 h.

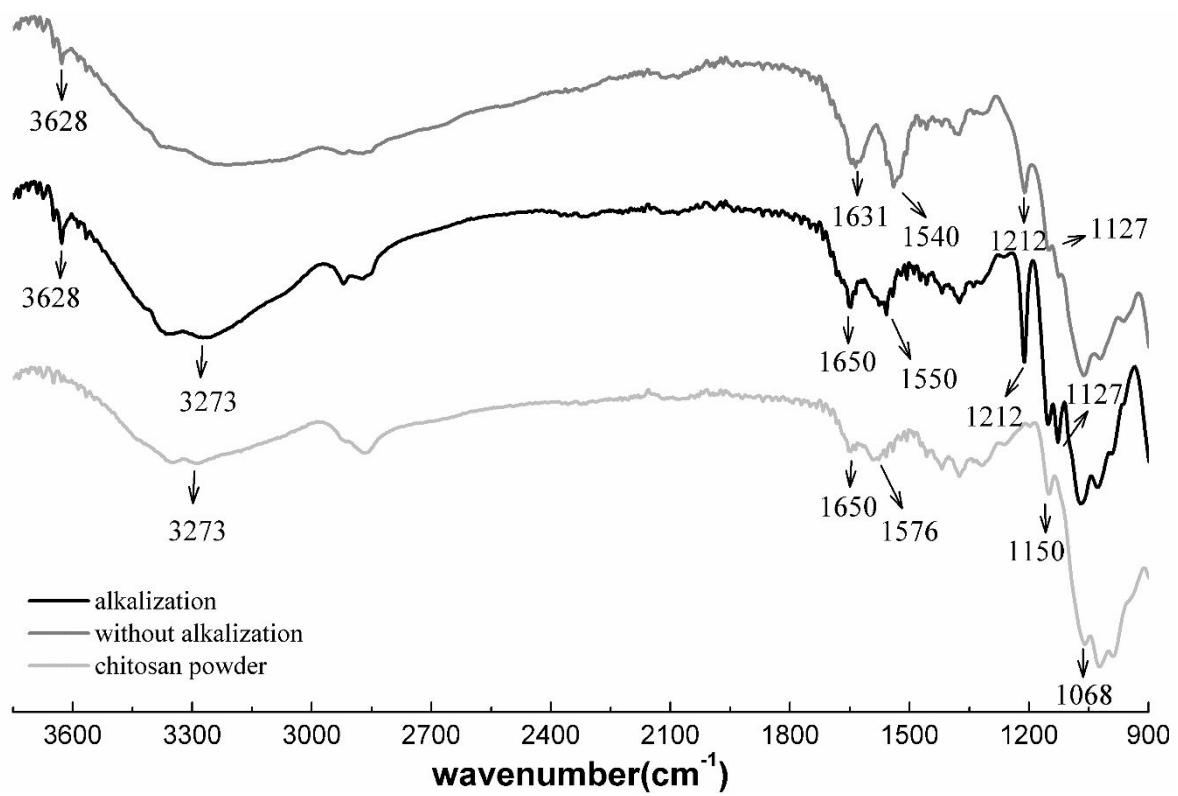


Figure 3.2 ATR-IR of chitosan powder, TPP-crosslinked chitosan beads with and without alkalization before crosslinking

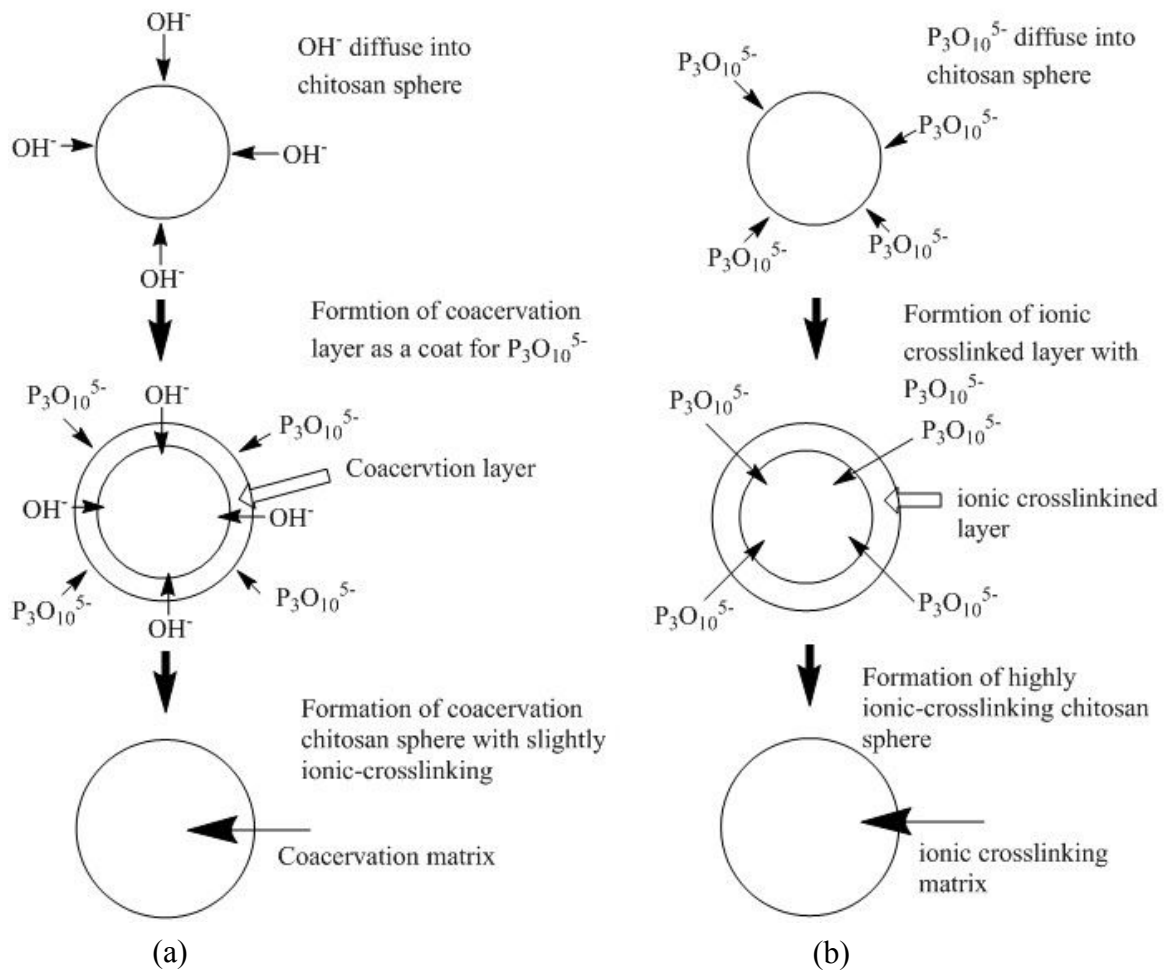


Figure 3.3 crosslinking mechanism of TPP chitosan beads: coacervation (a); ionic-crosslinking (b)

### 3.3.2 Swelling properties

A convenient proof of crosslinking is the swelling behavior of the TPP beads in various pH values of aqueous media. The swelling ability of two types of chitosan beads was evaluated in dissolution media of pH 2, 6, 10. Table 3.2 shows the equilibrium swelling behavior of two kinds of TPP beads synthesized from different crosslinking densities of TPP to chitosan (cured with or without alkalization). It was indicated that swelling ability

of the TPP beads was quite different according to different pH values of the dissolution medium. In pH 2 media, the chitosan beads prepared by curing with or without alkalization displayed different swelling characteristics due to the variation of ionic-crosslinking density of the beads. In pH 2 of dissolution media, the chitosan gel beads prepared by curing with alkalization (TCAC) swelled quickly and gradually dissolved within 12 h, whereas chitosan gel beads prepared by curing without alkalization (TCB) did swell largely but were not dissolved in this media (Table 3.2). In this pH, the swelling of chitosan-TPP beads was mainly attributed to the scission of ionic-crosslinked chain. With the increase of pH of dissolution medium, the ionic-crosslinked chain of TPP beads didn't dissociate and the swelling percentages were getting smaller, so the swelling of chitosan-TPP beads in this medium would be mainly attributed to the hydration or ionization of unbound -NH<sub>2</sub> sites in chitosan. However, the swelling percentages of TCAC were still higher than 100% which means alkalization before crosslinking preserves free amine groups from being bonded.

Table 3.2 Swelling percentage of two types of TPP beads in different pH

Bead Type	E <sub>sw</sub>		
	pH = 2	pH = 6	pH = 10
TCB	0.65	0.27	0.24
TCAC	/	1.35	1.26

' / ': beads were dissolved after swelling.

### 3.3.3 Adsorption isotherm

The relation between the adsorbed amount and the equilibrium concentration in the aqueous phase is very important in optimizing the sorption process and understanding the

sorption behavior. For investigating the effect of Ag(I) and Cu(II) concentrations on the adsorption of TCAC, experiments were conducted with certain volume of solutions having initial concentrations varying from 0.2 mM to 2.0 mM and a fixed mass of 0.1 g of adsorbent. The Langmuir and Freundlich equations (LeVan & Vermeulen, 1981) were used in this study to describe the equilibrium of Ag(I) and Cu(II) ions adsorption onto TCAC.

The non-linear form of Langmuir isotherm is expressed as:

$$q_e = \frac{bq_s c_e}{1 + bc_e} \quad (3.4)$$

where  $c_e$  is the equilibrium concentration of remaining metal ions in the solution (mg/L);  $q_e$  is the amount of metal ions adsorbed per mass unit of adsorbent at equilibrium (mg/g);  $q_s$  is the maximum amount of metal ions adsorbed per mass unit of adsorbent (mg/g) and  $b$ , the Langmuir constant related to the affinity of binding sites (L/mg), is a measure of the energy of adsorption.

The Freundlich isotherm expresses adsorption on multilayer and energetically heterogeneous surfaces. It is an empirical equation suitable for high and middle-concentration range. The non-linear Freundlich isotherm is given as:

$$q_e = k_F c_e^{1/n} \quad (3.5)$$

where  $k_F$  and  $n$  are Freundlich constants indicating adsorption capacity (mg/g) and intensity, respectively.

Fig. 3.4 shows the plot based on Langmuir and Freundlich isotherm models; the calculated values of Langmuir and Freundlich parameters are given in Table 3.3.

Based on the correlation coefficients, TCAC has a good fit to Langmuir model both for the adsorption of both Ag(I) and Cu(II). From Fig. 3.4, it is clear that the saturation of Ag(I) on the TCAC can be increased with the increase of the concentration; and in Table 3.3, it can be observed that the maximum capacity of TCAC for Ag(I) is promising, more than 1 mmol/g; but regarding to the equilibrium time, the adsorption rate is the major barrier because of the slow mass transfer rate. Freundlich parameter,  $n$  indicates the favourability of the adsorption. It is shown that  $n$  values more than 1, suggesting that the adsorption intensity is favorable at high concentration. For the adsorption of Cu(II), the maximum capacity of TCAC for Cu(II) is 13.9 mg/g, which is much lower than that for Ag(I). Because of the low capacity, the experiment data observed for the isotherm has higher errors, leading to lower  $R^2$ . While compared with the Freundlich isotherm, the Langmuir isotherm fits better and describes the real situation well.

Table 3.3 Isotherm parameters of the adsorption of Ag(I) and Cu(II) on TCAC at T=25°C

Metal	Langmuir			Freundlich		
	$b$ L mg <sup>-1</sup>	$q_s$ mg g <sup>-1</sup>	$R^2$	$K_F$	$n$	$R^2$
Ag(I)	0.008	167.98	0.98	3.57	1.51	0.96
Cu(II)	0.41	14.37	0.90	5.56	4.57	0.85

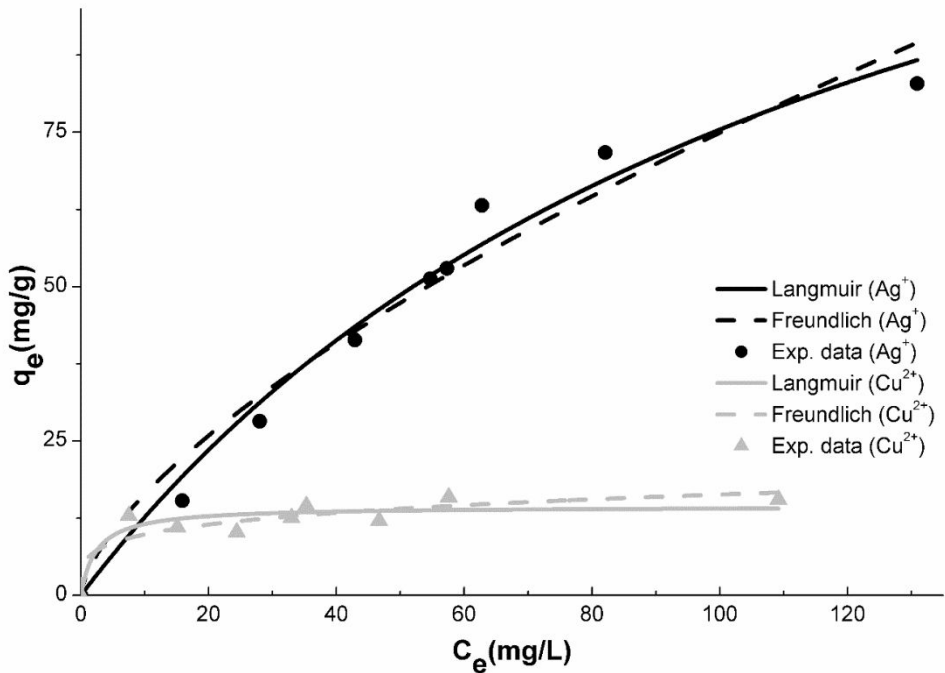


Figure 3.4 Non-linear Langmuir and Freundlich isotherm for the adsorption of Ag(I) and Cu(II) ions onto TCAC in a binary metal solution

### 3.3.4 Adsorption kinetics

To understand the effect of contacting time on Ag(I) and Cu(II) adsorption onto TCAC, experiments were conducted with 300 mL of solution having 1 mM Ag(I) and Cu(II) ions and 100 mg of adsorbent. 3 mL of the sample was analyzed at various intervals to estimate the concentration of dissolved Ag(I) and Cu(II) as a function of equilibration time.

Several adsorption kinetic models have been applied to understand the adsorption kinetics and the rate limiting step during adsorption process. Some of the rate determining steps includes diffusion control, chemical reactions and particle diffusion (Ngah et al., 2002).

The first-order rate equation (Yuh-Shan, 2004), widely used to describe the adsorption of pollutants from wastewater, can be presented as follows:

$$\frac{d_{q_t}}{d_t} = k_1(q_e - q_t)$$

(3.6)

where  $q_e$  and  $q_t$  (mg/g) are the amounts of Ag(I) or Cu(II) ions adsorbed onto TCAC at equilibrium and at time  $t$ , respectively, and  $k_1$  ( $\text{h}^{-1}$ ) is the rate constant of pseudo-first order kinetic model. Integrating Eq. (3.6) with boundary conditions of  $q_t = 0$  at  $t=0$  and  $q_t = q_e$  at  $t=t$  gives

$$q_t = q_e(1 - \exp(-k_1 t)) \quad (3.7)$$

The non-linear relationship of  $q$  against  $t$  was used to determine the  $k_1$  and correlation coefficient,  $R$ . The non-linear form of the first-order model for the sorption of Ag(I) and Cu(II) onto chitosan are given in Fig. 3.5a. The first-order model did not adequately describe the sorption result of Ag(I) ion onto TCAC; the correlation coefficients ( $R^2$ ) between the predicted and the experimental values for the entire data set of Ag(I) and Cu(II) are 0.96 and 0.98, respectively (Table 3.4). First of all, a disadvantage of this model for Ag adsorption is that it does not fit well the experimental data for the whole range of contact time and the plots are only linear over the first 30 min, approximately. Moreover, according to the situation in this experiment, there are two possible explanations: since after 48 h, the adsorption of both metal ions still did not reach equilibrium, leading to the lack of data to fit an accurate kinetic model; it may be caused

by complicated combinations, which tends to become immeasurably slow. For copper, however, the first-order model fits not bad, indicating that the adsorption of Cu(II) is fast and simple.

The second-order rate equation (Ho, 2006), mainly applied in the chemical adsorption with sharing or exchange of electrons between functional groups and metal ions, can be presented as follows:

$$\frac{d_{q_t}}{d_t} = k_{p2}(q_e - q_t)^2 \quad (3.8)$$

where  $q_e$  and  $q_t$  (mg/g) are the amounts of Ag(I) or Cu(II) ions adsorbed onto TCAC at equilibrium and at time  $t$ , respectively, and  $k_{p2}$  (g mg<sup>-1</sup> h<sup>-1</sup>) is the rate constant of second-order kinetic model. Integrating Eq. (3.8) with boundary conditions of  $q_t=0$  at  $t=0$  and  $q_t=q_e$  at  $t=t$ , yields,

$$\frac{1}{q_t} = \frac{1}{q_e} + \frac{1}{k_{p2}q_e^2 t} \quad (3.9)$$

The straight-line plots of  $\log 1/ q_t$  against  $1/t$  were used to determine the  $k_{p2}$  and correlation coefficient,  $R$ . The linearized form of the second-order model for the sorption of Ag(I) and Cu(II) onto chitosan are given in Fig. 3.5b. The second-order model did well describe the sorption results of Ag(I) ions as well as Cu(II) ions onto TCAC; the correlation coefficients ( $R^2$ ) between the predicted and the experimental values for the entire data set are both 0.98 (Table 3.4). For adsorption of Ag(I), the second-order model fits better than the first-order model which indicates more than one adsorption

mechanism involve in the adsorption of Ag(I); for adsorption of Cu(II), second-order model fits as well as the first-order model, indicating that the biosorption of TCAC for Cu(II) as solid surfaces are homogeneous.

Because the previous adsorption rate models cannot describe the definite mechanism, and mass transfer in sphere would be a crucial factor in adsorption process in such size ( $d_p = 1$  mm after swelling) of TCAC. The simplified intraparticle diffusion equation (Ngah & Fatinathan, 2010), proposed by Weber-Morris Model, can be presented as follows:

$$q_t = k_m t^{1/2} \quad (3.10)$$

The straight-line plots of  $\log q_t$  against  $t^{1/2}$  were used to determine the  $k_m$  and correlation coefficient,  $R^2$ . The linearized form of the intraparticle diffusion model for the sorption of Ag(I) and Cu(II) onto chitosan are given in Fig. 3.5c. The intraparticle diffusion model did well to describe the sorption results of Ag(I) ions, but not Cu(II) ions onto TCAC; the correlation coefficients ( $R^2$ ) between the predicted and the experimental values for the entire data set are 0.97 and 0.88, respectively (Table 3.4). For adsorption of Ag(I), the intraparticle diffusion model fits not bad which indicates mass transfer cannot be ignored in the adsorption of Ag(I) and it is probably the reason why the equilibrium time is longer than usual; moreover, the slope is not equal to zero, indicating that the intraparticle diffusion is not the sole rate-limiting step. For adsorption of Cu(II), intraparticle diffusion model fits well after certain time of adsorption, suggesting adsorption of copper ions was controlled by other factors in the initial time.

These years, some research started to apply gas adsorption model into aqueous-solid situation to explain the adsorption on the surface, which is affected by the concentration. Elovich's equation (Chien & Clayton, 1980), which can describe the adsorption occurred on the heterogeneous surface is presented as follows:

$$\frac{d_{q_t}}{d_t} = \alpha e^{-\beta q} \quad (3.11)$$

where  $q_t$  (mg/g) are the amounts of Ag(I) or Cu(II) ions adsorbed onto TCAC at equilibrium and at time  $t$ , respectively, and  $\alpha$  and  $\beta$  is the initial adsorption rate and the desorption constant, respectively. Integrating Eq. (3.11) with boundary conditions yields,

$$q_t = (1/\beta) \ln(\alpha\beta) + (1/\beta) \ln t \quad (3.12)$$

The straight-line plots of  $\log q_t$  against  $\ln t$  were used to determine  $\alpha$ ,  $\beta$  and correlation coefficient,  $r$ . The linearized form of the Elovich's equation for the sorption of Ag(I) and Cu(II) onto chitosan are given in Fig. 3.5d. The Elovich's equation did both well describe the sorption results of Ag(I) and Cu(II) ions onto TCAC; the correlation coefficients ( $R^2$ ) between the predicted and the experimental values for the entire data set are 0.97 and 0.98 (Table 3.4), respectively. For adsorption of Ag(I), the Elovich's equation fits the experimental data as well as the intraparticle equation, suggesting that there might be two different adsorption mechanisms in the adsorption of silver. For adsorption of Cu(II), the theoretical curve of Elovich's equation model pass through nearly all the experimental data points, indicating the sorption of Cu(II) ions onto TCAC occurs on the surface of TCAC predominantly.

Table 3.4 Kinetic parameters for Ag(I) and Cu(II) adsorption on TCAC

Kinetic Equation	Rate Parameters		
	Ag(I)	Cu(II)	
Pseudo-first order			
$k_1$	$\text{h}^{-1}$	0.1535	0.319
$q_e$	$\text{mg g}^{-1}$	42.77	7.35
$R^2$		0.96	0.98
Pseudo-second order			
$k_2$	$\text{g mg}^{-1} \text{ h}^{-1}$	0.0038	0.0458
$q_e$	$\text{mg g}^{-1}$	49.57	8.22
$R^2$		0.98	0.98
Intraparticle diffusion			
$k_m$	$\text{g mg}^{-1} \text{ h}^{-0.5}$	7.07	1.24
$R^2$		0.97	0.88
Elovich			
$\alpha$	$\text{mg g}^{-1} \text{ h}^{-1}$	34.98	6.66
$\beta$	$\text{g mg}^{-1} (\ln h)^{-1}$	0.12	0.63
$R^2$		0.97	0.98

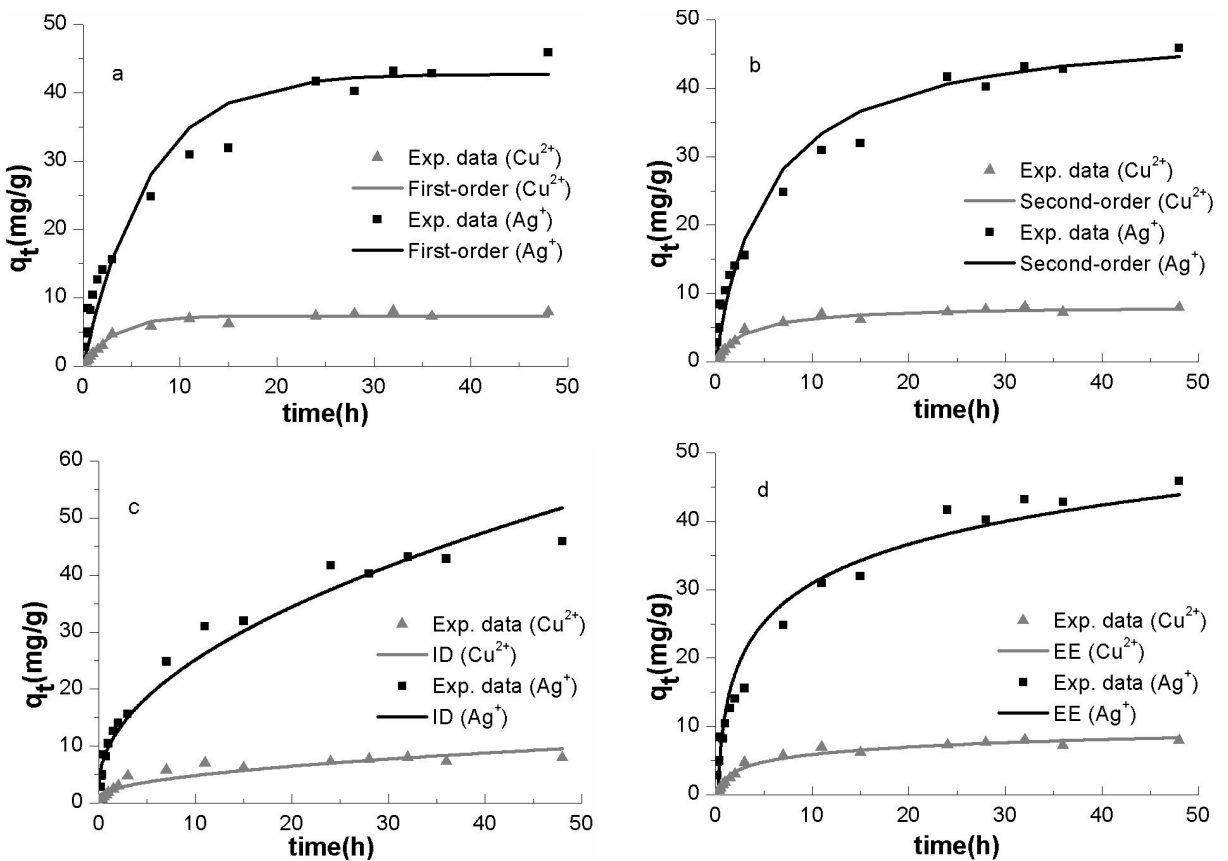


Figure 3.5 Comparison of different kinetic models (a. First-order, b. Second-order, c. Intrapartical diffution (ID), d. Elovich's equation(EE)) for the sorption of Ag(I) and Cu(II) ions onto TCAC

### 3.3.5 Sorption Mechanism

#### 3.3.5.1 FTIR

To further study the mechanism of the adsorption on TCAC, Fourier transform infrared spectroscopy (FTIR) of the TPP-crosslinked chitosan beads, before and after adsorption, are shown in Fig. 3.6; several peaks, characteristic for chitosan and sodium tripolyphospahte are observed in the spectrum.

After adsorption, the intensity of the adsorption bands was changed and shifted to lower or higher wavenumbers. The big shift of peak at  $3628\text{ cm}^{-1}$  in Fig. 3.6 indicates that the hydroxyl and amine groups are involved in the adsorption of both copper and silver ions. The large shift of the peak at  $1068\text{ cm}^{-1}$ , to  $1058\text{ cm}^{-1}$  in  $\text{Cu}^{2+}$  adsorption and  $1056\text{ cm}^{-1}$  in  $\text{Ag}^+$  adsorption respectively, is probably caused by the coordination between C-O with metal ions. The shift of spectrum at peak  $3273\text{ cm}^{-1}$  indicate that at least either of these two functional groups of  $\text{N-H}^+$  and  $\text{O-H}$  is involved in the adsorption of copper ions and silver ions. Moreover, the  $-\text{NH}_2$  groups ( $1650\text{ cm}^{-1}$ ) become available for absorbing cooper ions and silver ions which leads to the shift to higher wavenumber ( $1652\text{ cm}^{-1}$ ) and lower wavenumber ( $1647\text{ cm}^{-1}$ ), respectively. Furthermore, the adsorption of binary metal ions has the similar change of this peak as that of single silver ions, which indicates that the adsorption of silver ions is dominant. The sharp peaks( $1127\text{ cm}^{-1}$  and  $1212\text{ cm}^{-1}$ ), assigned to P-O-H vibration, are disappeared after adsorption, which reflects the interaction between  $\text{Cu}^{2+}$  ( $\text{Ag}^+$ ) and  $\text{O-P=O}$ . Therefore, the P-O stretching vibration has the similar affinity of  $\text{Ag}^+$  and  $\text{Cu}^{2+}$ .

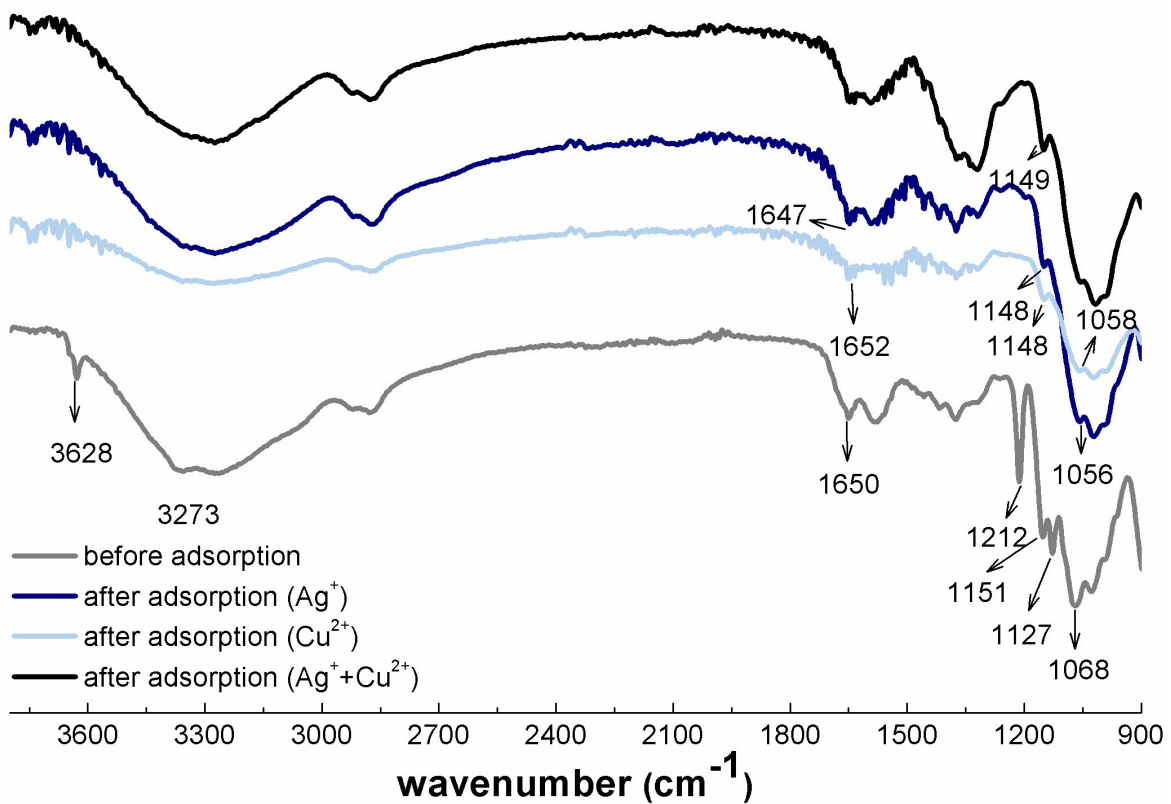


Figure 3.6 ATR-IR of TCAC before and after adsorption in  $\text{AgNO}_3$  and  $\text{Cu}(\text{NO}_3)_2$  Solution

### 3.3.5.2 XPS

XPS spectra have widely been used to identify the existence of a particular element and to distinguish the different forms of the same element in a material. The studied material could be characterized by recording the photoemission bands C 1s, N 1s, O 1s and P 2s, 2p.

Fig. 3.7 shows the total spectrum for TCAC and its appropriate curve-fit before and after adsorption. It can be found that silver and copper ions were adsorbed on the beads. Two

observed peaks of Cu 2p<sub>3/2</sub> and Cu 2p<sub>1/2</sub>, at 933.3 eV and 953.3 eV were assigned to Cu(II), probably coordinating with –OH or forming complexes with –O<sup>–</sup> and H<sub>2</sub>O (Huang et al., 2012), which is in agreement with the results of FTIR. Two observed peaks of Ag 3d<sub>3/2</sub> and Ag 3d<sub>5/2</sub>, at 374.6 eV and 368.6 eV can be assigned to the combination of Ag(I) and Ag(0) according to the database (Moulder et al., 1992). For Ag(I), it may be ion-exchanged with the functional groups on TCAC or form a complex. For the presence of the reduced silver, it could either be attributed to the interaction with chitosan, like –NH<sub>2</sub>, or could also be a result from the specific experimental conditions that have to be applied in XPS analysis, of high and endured vacuum (Vieira et al., 2011). Another obvious change is the disappearance of P after adsorption, indicating P was involved in the adsorption. Besides, the observed peaks, at 190.5 eV and 133.3 eV, can be assigned to Na<sub>5</sub>P<sub>3</sub>O<sub>10</sub>. Thus, there are two possible reasons to explain the disappearance of P around that range of binding energy: (i) most of P<sub>3</sub>O<sub>10</sub><sup>5–</sup> was involved in the adsorption and it's a chemical process; (ii) due to adsorption of silver and copper on the beads, the proportion of P became smaller and it was hard to detect them.

Fig. 3.8a shows the N 1s spectrum for TCAC and its appropriate curve-fit before and after adsorption. The slightly shift (+ 2eV) was observed and referenced to the N 1s peak at 399.3 eV which was assigned to –NH<sub>2</sub> (amine) as the basic structural unit of chitosan (Boufi et al., 2013). This higher B.E. peak observed indicates that some N atoms existed in a more oxidized state on the beads' surfaces due to metal ion adsorption. This phenomenon can be attributed to two possible adsorptions: (i) the formation of -NH<sub>2</sub>R<sup>n+</sup> complexes, in which a lone pair of electrons in the nitrogen atom was donated to the

shared bond between the N and R<sup>n+</sup>, reducing the electron cloud density of the nitrogen atom; (ii) the reduction of metal ion occurred when the nitrogen atom donated the electrons. Due to the alkalization, the amount of protonated amine ( $-\text{NH}_3^+$ ) was extremely small. Besides, the peak (401.4 eV) corresponding to protonated amine was shifted to lower binding energy after adsorption, suggesting there may be a chemical adsorption process on protonated amine.

Fig. 3.8b shows the O 1s spectrum for TCAC and its appropriate curve-fit before and after adsorption. Two peaks were found to fit the spectrum. The peaks at 530.8 eV and 532.7 eV are assigned to oxygen in the oxygen in P<sub>3</sub>O<sub>10</sub><sup>5-</sup> and C-OH in chitosan chain (Huang et al., 2012). The decrease in the intensity of O 1s (532.7 eV) after adsorption indicates that the copper or silver physical adsorption can take place on C-OH; besides, the peak at 530.8 eV shifted to higher B.E. on the O 1s spectrum after adsorption, suggesting the decrease of electron density of oxygen. In this case, oxygen acts as the electron donor when binding with metal ions.

Fig. 3.8c shows the P 2p spectra of TCAC and the fitted curves. P 2p peak at 133.1 eV which is assigned to P<sub>3</sub>O<sub>10</sub><sup>5-</sup> group (Moulder et al., 1992), shifted to 133.5 eV after adsorption. Peak shift at 133.1 eV to higher BE proves the involvement of P<sub>3</sub>O<sub>10</sub><sup>5-</sup> group in metal binding. In addition, the low signals of the intensity, especially after adsorption, indicated that the crosslinking density of TCAC beads is low. The reason for the dramatic decrease of the intensity of P 2p peak after adsorption could be the increase of Ag (I) and Cu (II) on sorbent surfaces, reducing the proportion of P on the bead surfaces.

Fig. 3.8d presents the TCAC's XP spectrum of Ag 3d core regions and its corresponding curve-fit. Two peaks of Ag 3d<sub>3/2</sub> and Ag 3d<sub>5/2</sub>, at 374.6 eV and 368.6 eV were observed. Based on the database (Moulder et al., 1992), these two peaks can be assigned to the combination of Ag(I) and Ag(0). For Ag(I), it may be ion-exchanged with the functional groups on TCAC or form a complex. For the presence of the reduced silver, it could either be attributed to the interaction with chitosan, like –NH<sub>2</sub>, or could also be a result from the specific experimental conditions that have to be applied in XPS analysis of high and endured vacuum (Vieira et al., 2011).

Cu 2p<sub>1/2</sub> and Cu 2p<sub>3/2</sub> can also be observed from the XPS spectrum of TCAC after sorption shown in Fig. 3.8e. Cu 2p<sub>1/2</sub> peak at 953.3 eV and Cu 2p<sub>3/2</sub> peak at 933.3 eV are corresponding to an oxidation state (Cu<sup>2+</sup>) of copper (Vieira et al., 2011), suggesting the binding of Cu (II) with oxygen in the 'O-P=O group.

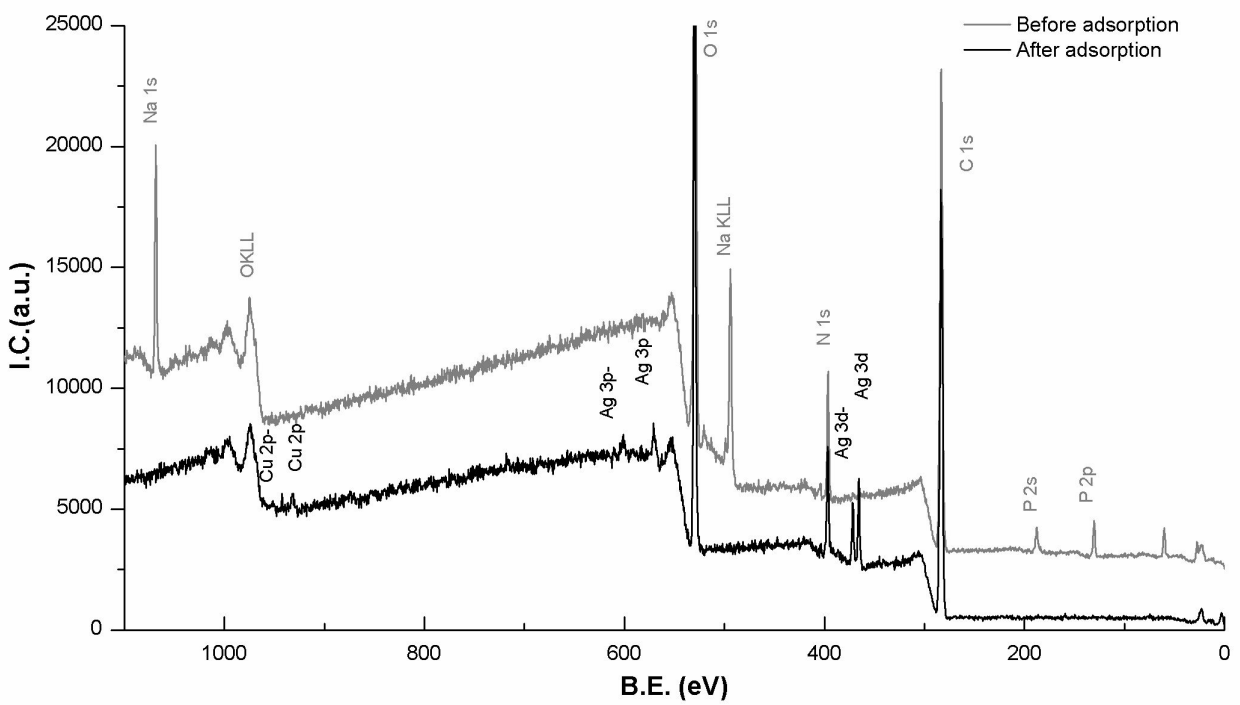
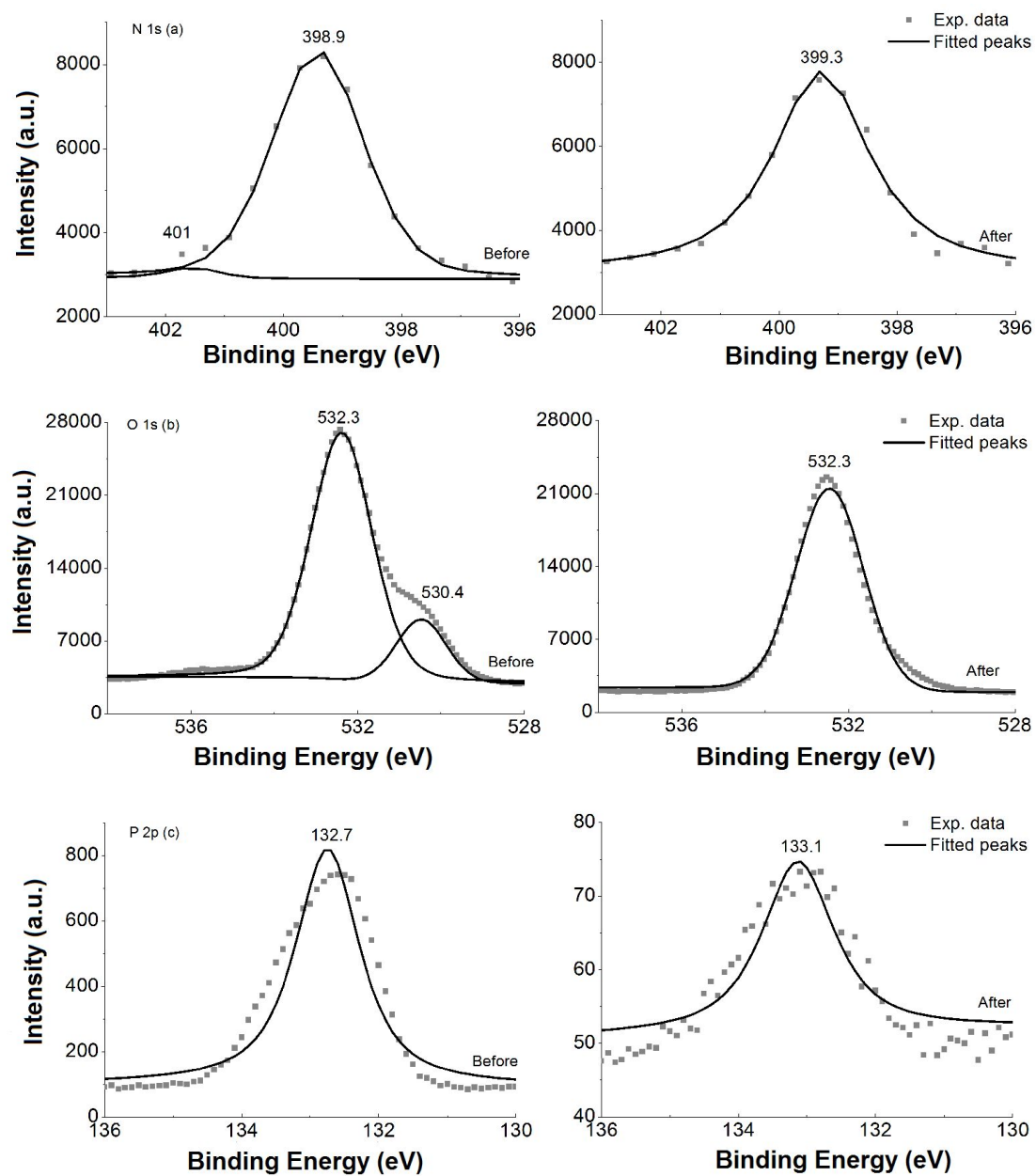


Figure 3.7 XPS spectra of TCAC before and after silver and copper sorption



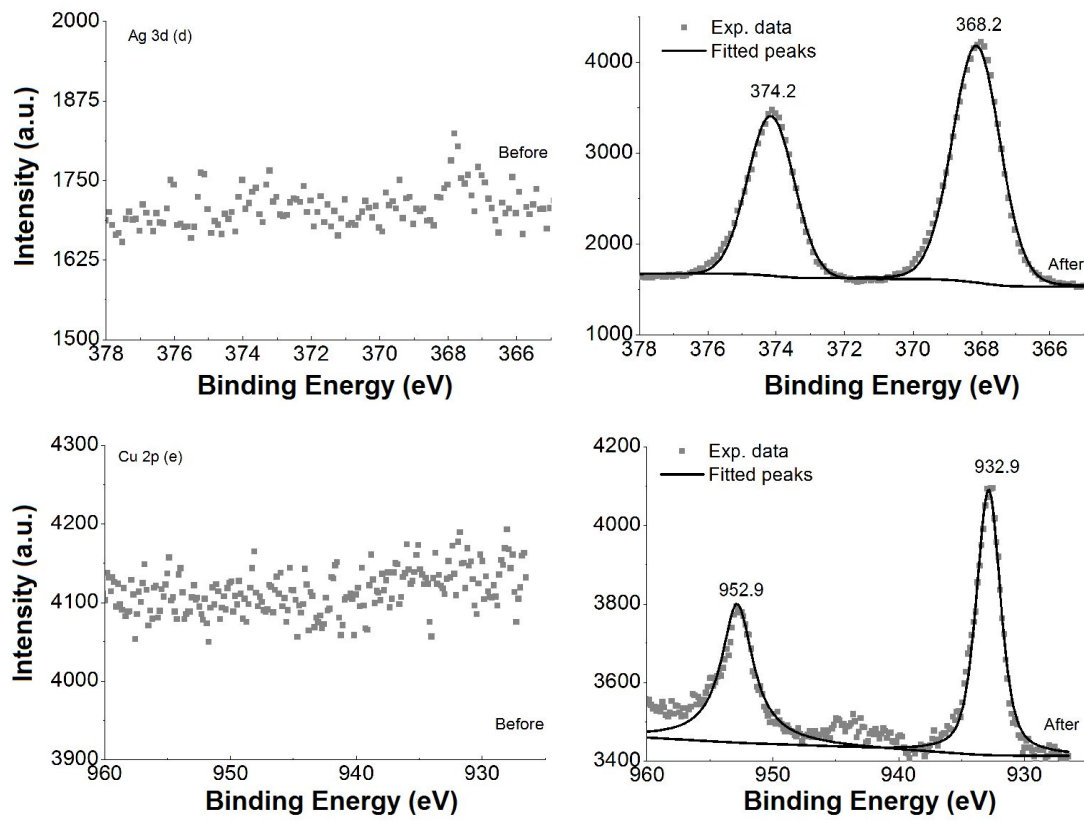


Figure 3.8 Fitted high-resolution photoemission spectra of N 1s (a), O 1s (b), P 2p (c), Ag 3d (d), and Cu 2p (e) before and after metal uptake for TCAC beads

### 3.3.5.3 XRD

Fig. 3.9 shows the XRD patterns of TCAC before and after Ag(I) and Cu(II) adsorption. In both situations, TCAC exhibited a broad peak at  $2\theta = 20.3^\circ$  due to the amorphous state of the chitosan. In the pattern of TCAC after adsorption, a spread diffraction peak was appeared between a  $2\theta$  angle of  $38^\circ$  and  $40^\circ$ , corresponding to metallic silver, which was agreement with the results of XPS that the existence of Ag(0). Moreover, the insignificant peak of Ag(0) is probably caused by the small amount of reduced Ag(I). Besides, no Cu(0) was detected, with the assumption that the noisy background did not hide the peak of

metallic copper, two possible results could be concluded; (i) there was no reduction occurred on Cu(II), the adsorption of copper was completion or ion exchange; (ii) Cu(II) was reduced to Cu(I). According to the results of XPS, it is probably that only silver ion had the reduction during the adsorption.

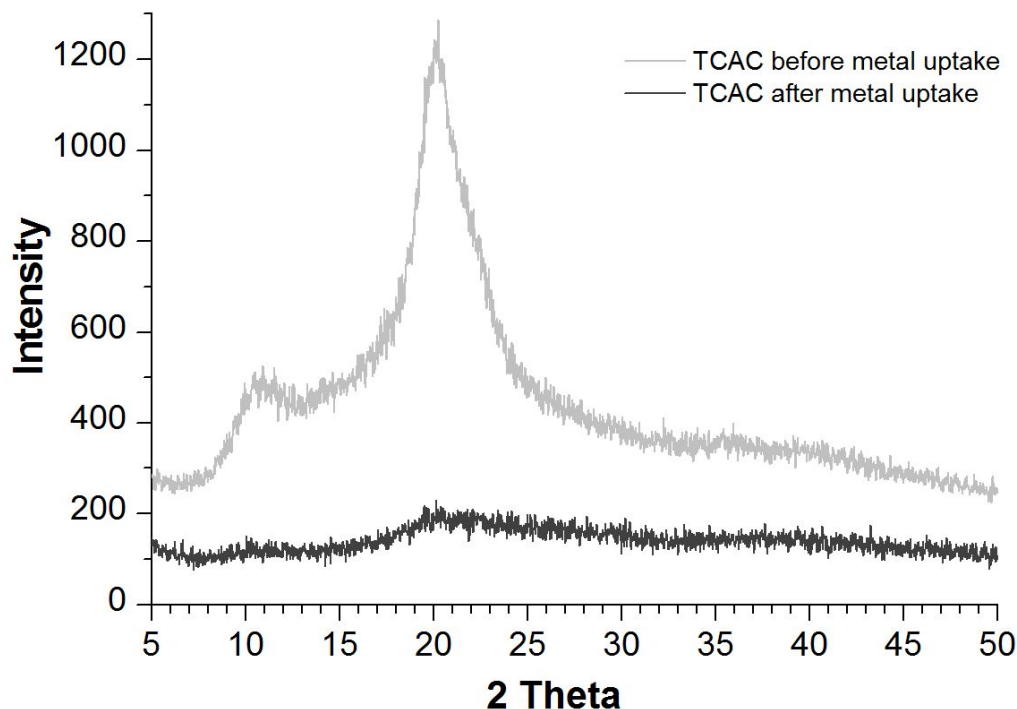


Figure 3.9. XRD patterns of TCAC beads before and after metal uptake

According to the results of desorption, the adsorption of silver ion is sensitive with pH which indicates that ion exchange or electrostatic attraction is involved in the adsorption process. Due to slightly acidic environment of binary solution, some free  $-NH_2$  are protonated again and selectively adsorb precious metal ions from transition metals, which is in agreement with the results of FTIR; because precious metal ions usually exist as

metal anions in acidic solution (Mack et al., 2007). From the results of XPS and ATR-FTIR, it was found that the phosphorus of  $\text{P}_3\text{O}_{10}^{5-}$  was not directly involved into adsorption, but the binding site of  $\text{P}_3\text{O}_{10}^{5-}$  did change after adsorbing Cu(II) or Ag(I). One possible binding site could be introduced by TPP:  $\text{O}=\text{P}-\text{O}^-$ , like its congeners, as it can form molecular geometry of complexes with metal ions and functional groups on TCAC (Shinde et al., 2013). The possible binding process is shown in Fig. 3.9. It is similar with “pendant or bridge model” which is generally accepted as the adsorption of copper ions bonded to one or more nitrogen and oxygen atoms (Skorik et al., 2005). The physical adsorption of silver and copper ions on the beads may be considered to consist of two processes: (i) the binding of metal ions to the active adsorption sites on the surfaces of the beads (boundary diffusion), and (ii) the transport of metal ions from the surfaces of the beads to the inside of beads (intraparticle diffusion). In the initial stage, the surfaces of the beads were relatively free and the silver and copper ions competitively attached to the available sites on the beads’ surfaces. Hence, the adsorption rate may be dominated by the concentration of metal ions. In the later stage of adsorption, as most of the adsorption sites on the beads’ surfaces were occupied, the metal ions had to find available adsorption sites inside the beads; from then on, intraparticle diffusion started to control the adsorption and slowed down the adsorption rate. Based on the results of kinetics, the Elovich’s equation could fit adsorption isotherm of both silver and copper ions, indicating that initially, the competitive abilities of those two metal ions are similar; while the intraparticle diffusion equation fitted the adsorption of silver ion better, suggesting the silver ion has better competitiveness inside the beads. It could as well be proved through

the results of isotherm. In the lower concentration, the maximum adsorption capacities of these two ions were similar; but with the increase of concentration, the capacity of silver ion grew faster and the difference became larger. XPS and FTIR analyses clearly revealed that the oxygen (hydroxyl groups) and phosphate (phosphorous groups) atoms were the main binding site for copper ions to form surface complexes as well as silver ion; because the TPP crosslinking here was like a coating process and most phosphate atoms were on the surface of beads. However, pronated amine groups in chitosan were the main binding sites for Ag(I) which was inside the beads and had the affinity to silver anions. Moreover, from the comparison of adsorption capacities of TCB and TCAC, it was found that freer –NH<sub>2</sub> had larger effect on the adsorption of silver ions.

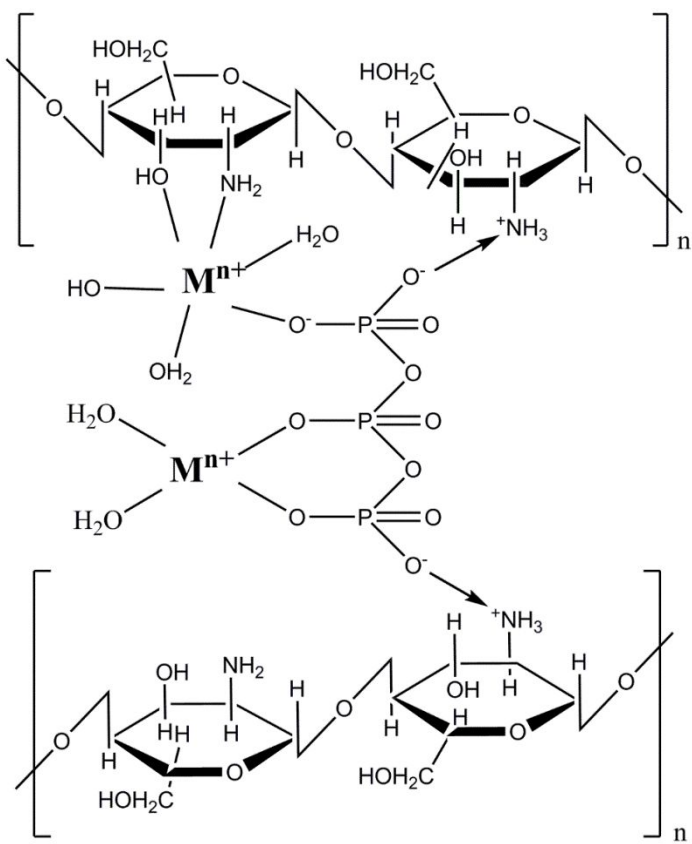


Figure 3.9 The possible binding structure of  $\text{O}=\text{P}-\text{O}^-$  on TCAC with metal ions

### 3.3.6 Desorption of metal ions

To apply TCAC into column and real industrial plants, the desorption process is important. Various factors are involved in the efficiency of desorption agents and desorption rate, which are heavily depend on the adsorption mechanism. In general, adsorbed metal ions can be desorbed by proper acid and some chelating agent. Chitosan was reported to have good solubility in most acid, except sulfuric acid (Eric Guibal, 2004), thus  $\text{H}_2\text{SO}_4$  was chosen in this study; but after several pre-experiments, it was found that  $\text{pH}=3$  is the lowest condition that TCAC can tolerate. Besides, EDTA is

known as a very strong chelating agent for many metals (widely used in the adsorption of copper), which was thought to replace the amine group or the hydroxyl group to coordinate with metal ions (Dawson, 1969). As shown in Table 3.5, pH after desorption was increased but not significant with the increase of desorption ratio, indicating that ion exchange was involved in the adsorption while not dominant. With the same concentration of  $\text{Na}_2\text{S}_2\text{O}_3$ , the introduction of EDTA increased the desorption rate of copper largely and the desorption efficiency of silver slightly; which the influence on silver probably due to the lower initial pH because the single EDTA can hardly desorb silver from biosorbents.  $\text{Na}_2\text{S}_2\text{O}_3$  can desorb both silver and copper but with different desorption rate, which EDTA can only desorb copper and the desorption rate is fast. That is in agreement with different adsorption mechanisms for these two metals proposed before. Interestingly, both  $\text{Na}_2\text{S}_2\text{O}_3$  and  $\text{H}_2\text{SO}_4$  are efficient for desorbing silver, which is probably caused by the complex adsorption mechanism for silver ions and needs to be studied further.

Table 3.5 Desorption study of Ag(I) and Cu(II) on TCAC

Desorption agent	Desorption time	Final pH			Ag(I) desorption ratio			Cu(II) desorption ratio		
		2.5 h	8 h	24 h	2.5 h	8 h	24 h	2.5 h	8 h	24 h
0.1 M Na <sub>2</sub> S <sub>2</sub> O <sub>3</sub> pH = 6.1		7.8	7.8	7.8	96%	96%	96%	58%	77%	95%
0.1 M Na <sub>2</sub> S <sub>2</sub> O <sub>3</sub> & 75 ppm EDTA pH = 5.3		7.8	7.8	7.8	100%	100%	100%	80%	88%	98%
0.01 M EDTA & 0.1 M H <sub>2</sub> SO <sub>4</sub> pH = 3		3.4	3.5	3.76	53%	72%	96%	97%	97%	97%
0.01 M EDTA pH = 4.7		5.6	5.8	6.1	8%	8%	8%	99%	99%	99%

### 3.4 Conclusion

TPP-crosslinked beads can be used as an effective adsorbent for silver ion recovery from binary solutions with copper ions. The crosslinking agent (TPP) can not only improve the chemical stability of the chitosan beads in slightly acid solutions, but also provide effective functional groups for adsorption. Besides, alkalization (-NH<sub>3</sub><sup>+</sup>) was neutralized to prevent from reacting with crosslinker TPP) before crosslinking lowered the crosslinking density as well as the reaction time, leading to higher adsorption capacity, especially for silver ions. The Langmuir isotherm model can describe the adsorption isotherm of silver ions in TCAC very well, but due to the low capacity, the isotherm data of Cu(II) adsorption cannot be fitted well with either Langmuir or Freundlich isotherm. Initially, on

the surface of beads, the adsorption rate may be dominated by the concentration of metal ions. After that, the metal ions competitively diffuse into the beads for further adsorption which is much slower than the surface adsorption. Most of the cooper ions were adsorbed on the surface of beads with oxygen (hydroxyl groups) and phosphate (phosphorous groups) atoms; while silver ions were absorbed not only on the surface, but also inside the beads with nitrogen atoms. Moreover, a reduction of silver ions probably occurred because of some reducing ends of monomers and polysaccharides on chitosan, such as  $\text{--NH}_2$ .

## **Chapter 4 Simulation of the Fixed Bed Adsorption of Ag (I) and Cu (II) onto TCAC sorbents**

### **4.1 Introduction**

The majority of biosorption studies in heavy metal removal or precious metal recovery were investigated in the stirred-tank batch mode (Goel et al., 2005), for the measurement of sorbent capacity, adsorption isotherm and kinetic parameters. For industrial application of biosorption as a low-cost metal removal alternative to conventional processes such as ion exchange, precipitation etc., fixed-bed adsorption is preferable because of its ability to process large quantities of feed under cyclic-batch operating mode (Aksu & Gönen, 2004; Naja & Volesky, 2006). In addition, the fixed-bed adsorption column can effectively separate different components from fluid and easily be regenerated, which meets the need of industrial utilization (Izatt et al., 2010; Naja & Volesky, 2006).

Based on the two different ways sample solutions fed to the column, the performance of a fixed-bed column is usually evaluated through the concept of the breakthrough curve and elution peaks (Han et al., 2009; Lee & Chen, 2001). In fixed-bed adsorption, if the feed concentration is a step function, breakthrough curves of the sample solutes are obtained. However, a pulse of feed solution leads to the attainment of elution profiles of solutes. Usually, breakthrough curves are dependent on many factors, such as the flow rate, sample concentration and pH of effluent, particle size of biosorbents, etc. The time of the breakthrough point and the shape of the breakthrough have been found to highly related to the sample concentration and the flow rate (Aksu & Gönen, 2004). Elution, in a

biosorption experiment, is the process of extracting the adsorbate from the biosorbent by washing with a solvent (also called eluent) ("Elution,"). Because the loading samples are in a small volume, the elution profiles are more complex and sensitive to the affecting factors, such as flow rate, sample concentration, injection time than the breakthrough curves (Lee & Chen, 2001).

Mathematical modeling is a very efficient approach to predict the dynamic performance of fixed-bed adsorption processes. Since no equipment and chemicals are involved, numerical simulation is becoming increasingly important for good prediction of column adsorption and for more detailed information of process scale-up.

In the fixed bed biosorption process, the fluid-solid interaction is quite complex. Four basic mass transfer steps are widely accepted to describe the behavior of biosorption process (Nakhli et al., 2014): (a) liquid phase mass transfer; (b) film diffusion; (c) intraparticle diffusion; (d) the adsorption-desorption reaction. In mass transfer modeling, the intrinsic sorption reaction is assumed to be fast and single-resistance models or dual-resistance model of the diffusion processes (steps 2 and 3) are considered as rate limiting. In surface reaction modeling (SRM), mass transfer is assumed to be fast, and the sorption reaction (step 4) becomes the rate-limiting step (Chatterjee & Schiewer, 2014). For passive biosorption process, chemical reactions usually do not take place; hence the mass transfer model is more accurate. So far, several mass transfer mathematical models have been developed for the fixed bed adsorption of gas (Mulgundmath et al., 2012), proteins (Yun et al., 2009), organic chemicals (Sansalone & Ma, 2010), and metal ions (Escudero et al., 2013; Lim & Aris, 2014) by various types of the adsorbents, such as

organic wastes, active carbon, inorganic compound, etc. However, research on the fixed bed adsorption of metal ions by chitosan gel beads is scarce (Guibal et al., 1999; Osifo et al., 2009; Sankararamakrishnan et al., 2008). Chitosan and chitosan derivatives are very promising biosorbents, demonstrating high capacity and good selectivity towards transition metals; it is therefore important and valuable to study the on-column separation of metal ions by chitosan based sorbents and the mass transfer characteristics of metal ions in the fixed bed column.

Following the batch mode sorption of Ag (I) and Cu (II) on TCAC beads presented in Chapter 3, this chapter mainly aims to examine the performance of the TCAC beads for the separation of Ag (I) and Cu (II) ions from aqueous solutions in a fixed-bed column. Linear driving force model was applied to simulate the breakthrough curves and elution profiles of Ag (I) and Cu (II) from the fixed-bed column. The effects of flow rate, bed length, sample concentration and injection time on column performance and the separation of the two metal ions were evaluated.

## 4.2 Mathematical Model

In physical biosorption processes, the transfer of metal ions from the liquid phase to the solid phase includes four steps (Heeter & Liapis, 1998): (1) convective mass transfer along with the flow, (2) film diffusion (transfer from the bulk of the liquid phase to the external surface of the sorbent), (3) intraparticle diffusion (intraparticle mass transfer for

pore diffusion and intraparticle convection), and (4) interaction between the adsorbates and active sites on the sorbent.

The general mass balance of each adsorbate (metal ion in biosorption) can be described by: Input + Generation = Output + Accumulation + Consumption. Since no chemical reactions are involved, the mass balance equation is simplified into: Input = Output + Accumulation.

To derive a proper mass balance of the column biosorption process, some assumptions are made below (Guiochon et al., 2006):

- 1.The input flow is radially homogeneous and the column is isothermal;
- 2.The phase velocity is constant along the column and independent of the pressure;
- 3.The axial dispersion coefficient is a lumped parameter resulting from all the mechanisms;
- 4.The convention exists when the weak solvent (deionized water) is not adsorbed;
- 5.The thermal effects and influence of the heat of adsorption can be neglected.

In this study, the lumped kinetic model was chosen to analyze the performance of the continuous biosorption of Ag(I) and Cu (II) by TCAC beads . Although the general rate model is the most accurate one, the complex parameters are not easy to obtain correctly, which weaken its advantages; the ideal model is not suitable on account of its strict assumptions. Lumped kinetic model is a simplified equation but it also considers the adsorption on the film and solid; besides, it is frequently used in others' research (Bak et al., 2007; Kaczmarski et al., 2001; Pérez-Martínez et al., 2015).

Then the differential mass balance equation for metal ion  $i$  is presented as follows when assuming  $u$  and  $D_{L,i}$  are constant:

$$\frac{\partial C_i}{\partial t} + \frac{1-\varepsilon}{\varepsilon} \frac{\partial q_i}{\partial t} + u \frac{\partial C_i}{\partial z} = D_{L,i} \frac{\partial^2 C_i}{\partial z^2} \quad (4.1)$$

The following initial and boundary conditions are considered:

$$\text{I.C.: } t < 0, 0 \leq z \leq L, C_i = 0, q_i = 0 \quad (4.2a)$$

$$\text{B.C.: } t \geq 0, z = 0, D_{L,i} \frac{\partial^2 C_i}{\partial z^2} \Big|_{z=0} = u(C_i - C_{i0}); \quad (4.2b)$$

$$z = L, \frac{\partial C_i}{\partial z} \Big|_{z=L} = 0 \quad (4.2c)$$

where  $C_i$  (mM) is the concentration of metal ion  $i$  in the bulk liquid,  $C_{i0}$  (mM) is the concentration of metal ion  $i$  in the feed,  $q_i$  (mM) is amount of metal ions adsorbed by TCAC beads;  $u$  (m/s) is the interstitial velocity,  $z$  is the coordinate along the length of the column,  $t$  (h) is the time,  $\varepsilon$  is the porosity of bed,  $D_{L,i}$  (cm<sup>2</sup>/s) is the axial dispersion coefficient, and  $L$  (cm) is the length of the fixed bed.

Using the linear driving force model, the mass balance of metal ion  $i$  on solid phase can be described as (Guiochon et al., 2006):

$$\frac{\partial q_i}{\partial t} = K_f (q_i^* - q_i) \quad (4.3),$$

where  $q_i^*$  (mg/g) is the amount of metal ion  $i$  adsorbed on the stationary phase in equilibrium with the mobile phase concentration  $C_i$ , and  $K_f$  ( $s^{-1}$ ) is the lumped mass transfer coefficient.

For the Langmuir isotherm, we have:

$$q_i^* = \frac{q_{\max} C_i}{1 + b C_i} \quad (4.4)$$

Finally the partial differential equation (Eq. (4.1)) is solved numerically by conversion to the ordinary differential equations (ODEs) using the second order finite difference scheme (Table 4.1). The resulting initial value problems of ODEs were solved using the stiff solver ode15s in MATLAB R2012a.

Table 4.1 Transformation from PDE to ODE

---

PDE	ODE
$D_{L,i} \frac{\partial^2 C_i}{\partial z^2}$	$D_{L,i} \frac{C_{i+1} - 2 \times C_i + C_{i-1}}{h^2}$
$u \frac{\partial C_i}{\partial z}$	$u \frac{C_{i+1} - C_{i-1}}{h}$

---

\*  $h = L/(NPLATE - 1)$

### 4.3 Methodology to determine model parameters

#### 4.3.1 Column parameters

Based on the results of swelling rate test presented in Chapter 3, the parameters of TCAC beads and the column parameters are summarized in Table 4.2.

Table 4.2 Physical parameters of TCAB beads and fixed-bed columns

Average beads diameter, $d_p$ (cm)	0.10
Packed-bed density, $\rho$ (g/cm <sup>3</sup> )	0.55
Porosity of bed, $\varepsilon$	0.57
Cross-sectional area of column (cm <sup>2</sup> )	0.785

#### 4.3.2 Empirical correlations of axial dispersion coefficient ( $D_L$ )

In the past few decades, axial dispersion in packed bed reactors has been measured and discussed in both gas-liquid and liquid-solid systems (Yu et al., 1999). In the chemical engineering area, when considering if the radial contribution is important to the adsorption process, axial dispersion is usually measured as one-dimensional (Yu et al., 1999). In general, the axial dispersion includes two components: mechanical dispersion and molecular dispersion; the correlation equation is:

$$D_L = D_{\text{mech}} + \tau D_m \quad (4.5),$$

where  $D_{\text{mech}}$  (cm<sup>2</sup>/s) is the mechanical dispersion,  $D_m$  (cm<sup>2</sup>/s) is the molecular diffusion, and  $\tau$  is the porous medium tortuosity. Because the value of  $D_{\text{mech}}$  is directly related to the interstitial velocity, scientists proposed an empirical correlation with Peclet number of molecular diffusion ( $Pe_d$ ) to evaluate the dominance part in  $D_L$ .

$$Pe_d = \frac{ud_p}{D_m} = \left( \frac{ud_p \rho_f}{\eta} \right) \left( \frac{\eta}{\rho_f D_m} \right) = Re Sc \quad (4.6),$$

where  $u$  (cm/s) is the interstitial velocity,  $\eta$  is the fluid's absolute viscosity,  $\rho_f$  is the fluid's density g/L.

It is found that when  $Pe_d$  is lower than 0.4, the molecular dispersion is dominant; for a fixed-bed column, it typically varies from 0.1 to 0.5. When  $Pe_d$  is between 0.4 and 5, both of the mechanical and molecular dispersion affect  $D_L$ ; when  $Pe_d$  is larger than 5, the value of  $D_L$  is mostly dependent on the interstitial velocity. Bear provided an empirical equation for axial dispersion when  $Pe_d > 5$  (Yu et al., 1999):

$$D_L = D_m \alpha_d (Pe_d)^m \quad (4.7),$$

where  $\alpha_d$  and  $m$  are empirical constants related to  $Pe_d$ . For the value of  $Pe_d$  greater than 5 but smaller than 10, the value of  $\alpha_d$  is suggested to be 0.5 and  $m$  values between 1 and 1.2; for the value of  $Pe_d$  is greater than 10, the proper values of  $\alpha_d$  and  $m$  are about 1.8 and 1.0, respectively, which means  $D_L$  is totally independent on molecular diffusion.

Other empirical equations reported from open literature, summarized in Table 4.3 were also used to estimate the  $D_L$  values. .

Table 4.3 Empirical axial dispersion correlations

<b>Adsorbent</b>	<b>Adsorbate</b>	<b>Correlation</b>	<b>Source</b>
ETS-10	Pb <sup>2+</sup>	$D_L = 0.44D_m + 0.83ud_p$ (4.8)	Suzuki and Smith (Lv et al., 2008)
Activated carbon	Pb <sup>2+</sup> , Cu <sup>2+</sup> , Cr <sup>3+</sup> , Co <sup>2+</sup>	$\frac{uL}{D_L} = \frac{L}{2r_p \epsilon_b} (0.2 + 0.011 Re^{0.48})$ (4.9)	Chung and Wen equation (Sulaymon et al., 2009)
Mineralized peat	Cu <sup>2+</sup>	$D_L = 3.3110 u^{1.8269}$ (4.10)	Marta, etc. (Izquierdo et al., 2010)

#### 4.3.3 Determination of the overall mass transfer coefficient ( $K_f$ )

To simplify the calculation, all the mass transfer coefficients in the column are usually lumped into an overall coefficient in the linear driving force model, which is easy to estimate through experiments. Normally, this overall mass transfer coefficient can be estimated based on the three mass transfer steps taking place in the column, i.e., mass transfer in bulk fluid, in macro-pores or in micro-pores of porous solids. Therefore, the entire mass transfer resistance in the fixed bed adsorption column consists of the resistances arising from the thin fluid film on the fluid-solid interface, resistances in macro-pores and micro-pores. Thus the relationship between  $K_f$  and its three main components is as follows:

$$\frac{1}{K_f} = \frac{r_p K}{3k_f} + \frac{r_p^2 K}{15\varepsilon_p D_p} + \frac{r_c^2}{15D_c} \quad (4.11)$$

where  $K$  is equal to  $q_{\max}/c_{i0}$ ,  $k_f$  (cm/s) is the external mass transfer coefficient,  $\varepsilon_p$  is the percentage of macro-pore on the beads,  $r_p$  (cm) is the radius of the chitosan gel beads,  $D_p$  (cm<sup>2</sup>/s) is the molecular diffusion coefficient of metal ions in macro-pores,  $r_c$  (cm) is the radius of the pore in the particle,  $D_c$  (cm<sup>2</sup>/s) is the diffusion coefficient in micro-pores, which can be estimated through kinetic studies in Chapter 3 by the following equation (Qiu et al., 2009):

$$q_t = k_m t^{1/2} = 6q_{\max} \left( \frac{D_c}{r_p^2 \pi} \right)^{1/2} t^{1/2} \quad (4.12)$$

Based on the preparation condition, either macro-pore ( $> 50$  nm) or micro-pores ( $< 2$  nm) can be obtained for the chitosan gel beads. Due to the limitation of experimental facility, the real pore size and distribution of the prepared chitosan gel beads cannot be measured in this study. However, the preparation method of the chitosan beads in this study is very similar to the one reported by Mi and co-workers (2002) (Mi et al., 2002). The pore size of chitosan beads in their study is  $1.37 \mu\text{m}$ . Therefore, we assume that the TPP crosslinked chitosan beads prepared in this study also have the uniform macro-pore structure, and the overall mass transfer coefficient  $K_f$  can be calculated by:

$$\frac{1}{K_f} = \frac{r_p K}{3k_f} + \frac{r_p^2 K}{15\varepsilon_p D_p} \quad (4.13)$$

where  $\varepsilon_p$  of the TPP crosslinked gel beads is estimated to be 80.75% based on the same research work by Mi and co-workers (Mi et al., 2002).

To determine the overall mass transfer coefficient  $K_f$ , the film transfer coefficient  $k_f$  is prerequisite. The film transfer coefficient is dependent on the liquid properties, flow rate and the physical properties of biosorbents, the relationship between  $k_f$  and Sherwood number ( $Sh$ ) was proposed by Seader & Henley (2006) as:

$$Sh = \frac{2k_f r_p}{D_m} \quad (4.14)$$

Several empirical correlations (Lv et al., 2008) was summarized in Table 4.4 to estimate  $Sh$  and subsequently the film transfer coefficient,  $k_f$ .

Table 4.4 Empirical correlations for Sherwood number ( $Sh$ ) and its applied ranges

Correlation		Validity
$Sh = 5.4 Re^{1/3} Sc^{1/4}$	(4.15)	$0.04 < Re < 30$
$Sh = \frac{1.09}{\varepsilon_b} Re^{1/3} Sc^{1/4}$	(4.16)	$0.0016 < Re < 55$
$Sh = 2.4 \varepsilon^{0.66} Re^{0.34} Sc^{1/4}$	(4.17)	$0.04 < Re < 52$

## 4.4 Results and Discussion

### 4.4.1 Model parameters

In this study, the two model parameters,  $D_L$  and  $K_f$  were determined using empirical correlations and additive mass transfer resistance in a fixed-bed column, respectively. The flow rate ( $Q$ ) for both elution and breakthrough of the metal ions is in the range of 0.006 L/h to 0.06 L/h.

#### 4.4.1.1 Axial dispersion coefficient ( $D_L$ )

Results of  $D_L$  calculated from different correlations are listed in Table 4.5.  $D_L$  values calculated from Eq. (4.8) for Ag (I) and Cu (II) are quite different from those obtained by the other three correlation equations.  $D_L$  values calculated from Eqs. (4.7), (4.9) & (4.10)) are much lower than those from Eq. (4.8), particularly at lower flow rate. Therefore, in-depth analysis of these four correlation equations is essential to determine the proper  $D_L$  values for Ag (I) and Cu (II). Correlation Eq. (4.7) was originally used in the gas adsorption, the results of  $D_L$  of metal ions in aqueous liquid calculated by this correlation may deviate from the real values (Yu et al., 1999). Eq. (4.9) is applicable for fluids with

flow rate larger than 1 L/h and  $10^{-3} < \text{Re} < 10^3$ , which might not be suitable (Sulaymon et al., 2009). Eq. (4.10) was derived from the experimental measurements in a narrow range of flow rate (around 0.6 ml/min), which may cause large errors when applied in a system with fluid flow rate different from the reported value (Izquierdo et al., 2010). Eq. (4.8) incorporates the contributions of both molecular diffusion and fluid convection to axial dispersion and hence is widely used to estimate  $D_L$  in various systems (Lv et al., 2008). As a result,  $D_L$  calculated from Eq. (4.8) was more appropriate to the dynamic adsorption of Ag (I) and Cu (II) on TCAC beads with the selected flow rate range.

Table 4.5  $D_L$  ( $\text{cm}^2/\text{s}$ ) values for  $\text{Ag}^+$  and  $\text{Cu}^{2+}$  calculated from various correlations

		$\text{Ag}^+$	$\text{Cu}^{2+}$
$Q = 0.006 \text{ L/h}$	Eq. 4.7	$3.890 \times 10^{-6}$	$3.890 \times 10^{-6}$
	Eq. 4.8	$1.833 \times 10^{-4}$	$1.806 \times 10^{-4}$
	Eq. 4.9	$6.110 \times 10^{-6}$	$6.110 \times 10^{-6}$
	Eq. 4.10	$1.250 \times 10^{-5}$	$1.250 \times 10^{-5}$
$Q = 0.06 \text{ L/h}$	Eq. 4.7	$3.889 \times 10^{-5}$	$3.889 \times 10^{-5}$
	Eq. 4.8	$1.778 \times 10^{-3}$	$1.778 \times 10^{-3}$
	Eq. 4.9	$5.833 \times 10^{-5}$	$5.833 \times 10^{-5}$
	Eq. 4.10	$8.333 \times 10^{-4}$	$8.333 \times 10^{-4}$

#### 4.4.1.2 The overall mass transfer coefficient ( $K_f$ )

The flow rate of elution and breakthrough varying from 0.006 L/h to 0.06 L/h, leads to the Re between 0.024 and 0.238. Therefore, in this study, the correlations of Eqs. (4.15) & (4.17) can be applied to determine the value of  $k_f$  if  $Q > 0.012 \text{ L/h}$ , and correlation (4.15)

can be applied to estimate  $k_f$  over the entire range of flow rate. When using the Eq. (4.14-4.17), the approximate ranges of  $k_f$  are shown in Table 4.6. Considering the Re values under the selected flow rate range in this study, Eq. (4.16) provides the most applicable film coefficients of Ag (I) and Cu (II) in the bulk liquid. The external mass transfer coefficient for  $\text{Ag}^+$  is in the range of  $4.428 \times 10^{-4}$  cm/s to  $9.464 \times 10^{-4}$  cm/s; the external mass transfer coefficient for  $\text{Cu}^{2+}$  varies from  $2.364 \times 10^{-4}$  cm/s to  $5.053 \times 10^{-4}$  cm/s.

Table 4.6 The values of  $k_f$  (cm/s) for  $\text{Ag}^+$  and  $\text{Cu}^{2+}$  calculated from various correlations

		$\text{Ag}^+$	$\text{Cu}^{2+}$
$Q = 0.006 \text{ L/h}$	Eq. 4.15	/	$6.593 \times 10^{-4}$
	Eq. 4.16	$4.428 \times 10^{-4}$	$2.364 \times 10^{-4}$
	Eq. 4.17	/	$3.372 \times 10^{-4}$
$Q = 0.06 \text{ L/h}$	Eq. 4.15	/	$1.420 \times 10^{-3}$
	Eq. 4.16	$9.464 \times 10^{-4}$	$5.053 \times 10^{-4}$
	Eq. 4.17	/	$4.356 \times 10^{-4}$

Based on the preparation method of the TCAC beads in this study, the  $K_f$  was determined through macro-pore mass transfer model. Therefore, the macro-pore mass transfer coefficient for  $\text{Ag}^+$  is in the range of  $5.028 \times 10^{-5} \text{ s}^{-1}$  to  $8.389 \times 10^{-5} \text{ s}^{-1}$ , the macro-pore mass transfer coefficient for  $\text{Cu}^{2+}$  is in the range of  $8.000 \times 10^{-5} \text{ s}^{-1}$  to  $1.283 \times 10^{-4} \text{ s}^{-1}$ .

#### **4.4.2 Elution and breakthrough of Ag(I) and Cu (II) from the fixed-bed column**

##### **4.4.2.1 Effect of flow rate**

In this study, four levels of elution flow rate - 0.006 L/h, 0.018 L/h, 0.03 L/h, 0.06 L/h were used to study the effect of flow rate on elution and breakthrough of Ag (I) and Cu (II) ions from the 4.5 cm long column packed and chitosan beads of 1.0 mm in diameter.

Fig. 4.1 shows the predicted breakthrough curves for  $\text{Ag}^+$  and  $\text{Cu}^{2+}$  obtained under different flow rates in terms of  $C_e$  (outlet concentration) versus time. It is obvious that the breakthrough of  $\text{Cu}^{2+}$  is earlier than that of Ag (I) because the maximum biosorption capacity of beads for copper ions is much lower than that for silver ions, leading to the shorter time of saturation. In addition, the fast mass transfer rate of Cu (II) indicated by its higher  $K_f$  value, particularly at higher flow rate, makes the breakthrough curve of Cu (II) steeper than that of Ag (I). Clearly the breakthrough point appeared earlier under the higher flow rate. At higher flow rate, the mass transfer of metal ions in the column tends to increase as illustrated in Table 4.5, therefore, the amount of adsorbed metal ions on the TCAC beads per unit bed height increases with an increase in flow rate, leading to faster column saturation. From the mass transfer correlations, it is observed that the influence of flow rate on the film diffusion is much greater than that on the intraparticle diffusion (Sulaymon et al., 2009), and might change the controlling step in the biosorption process of the column. The mass transfer Biot number ( $Bi_m$ ) is a common method to measure the relationship between the flow rate and the sensitivities of external and internal mass transfer, which is defined as:

$$Bi_m = \frac{k_f r_p}{D_c} \quad (4.18)$$

where  $D_c$  is the diffusion coefficient in the pore model.

Table 4.7 shows that the Biot number decreased with the increase of the flow rate at  $L = 4.5$  cm, indicating that the film diffusion resistance is more sensitive to the biosorption process of the column under the higher velocity. Moreover, the breakthrough points of  $\text{Ag}^+$  and  $\text{Cu}^{2+}$  under the same flow rate are closer with the increase of the flow rate, indicating that the film diffusion resistance is the dominating factor when the flow rate is high. Furthermore, the  $Bi_m$  of  $\text{Cu}^{2+}$  is always smaller than the  $Bi_m$  of  $\text{Ag}^+$ , suggesting that copper ions are more difficult to transfer in the solid particles compared with silver ions, and the adsorption of  $\text{Cu}^{2+}$  is almost on the surface of the beads. These results are consistent with the discussions in Chapter 3.

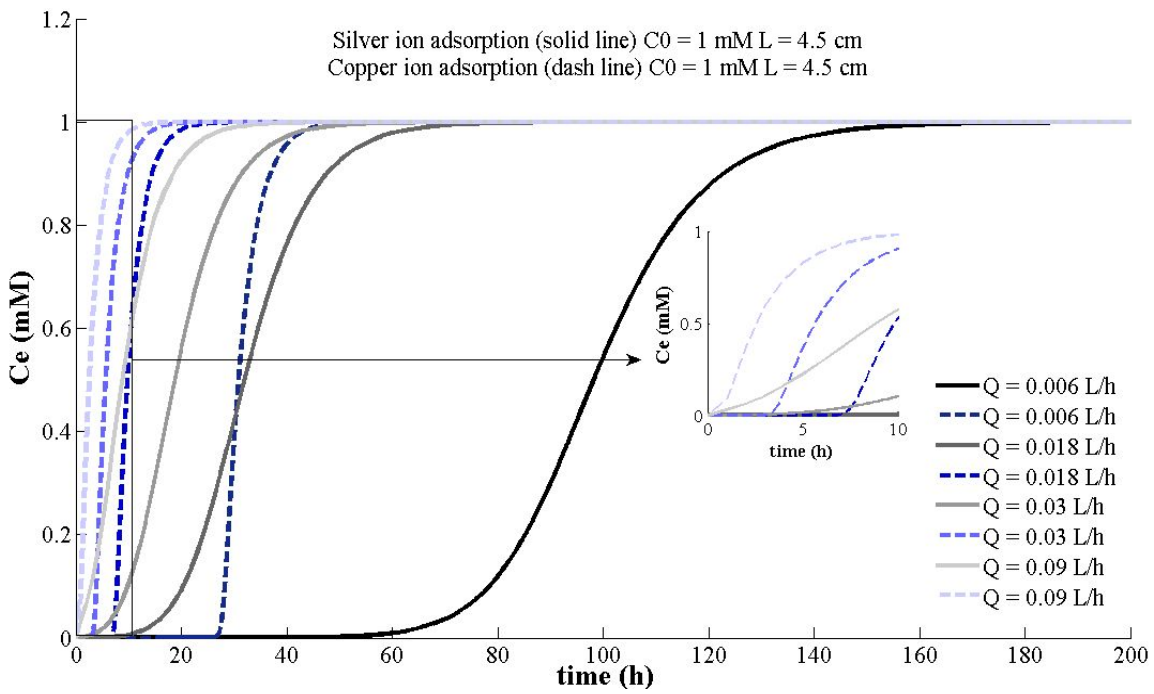


Figure 4.1 Predicted breakthrough curves for adsorption of Ag (I) and Cu (II) in the column under different flow rates

Table 4.7 The values of mass transfer Biot number ( $Bi_m$ ) at different flow rates

Flow rate (L/h)	Metal ions	$Bi_m$
0.006	$\text{Ag}^+$	0.240
	$\text{Cu}^{2+}$	0.130
0.018	$\text{Ag}^+$	0.120
	$\text{Cu}^{2+}$	0.064
0.03	$\text{Ag}^+$	0.085
	$\text{Cu}^{2+}$	0.046
0.06	$\text{Ag}^+$	0.053
	$\text{Cu}^{2+}$	0.029

The influence of flow rate on simulated elution profiles of Ag(I) and Cu (II) from the fixed-bed column is illustrated in Fig. 4.2. The sample concentration is 10 mM for each metal ion and injection time is 0.05 h. It is clear that with the increase of flow rate, the elution time is shorter and the peak is higher and sharper. However, the separation of these two metal ions becomes difficult at higher elution flow rate due to the shorter residence time of metal ions in the column, which makes the metal ions incapable of reaching all the available sorption sites due to the slow mass transfer in the porous solids. Hence, both metal ions elute quickly from the column and separation of the metal ions cannot be attained. Whereas, at lower elution flow rate ( $Q=0.006$  L/h), complete separation of Ag (I) from Cu (II) can be obtained. And the elution order of the two metals is different with the breakthrough order due to the smaller amount of metals ions injected into the column. At lower column loading of metal ions, most of the sorption sites on outer-surface of the beads were occupied by Cu (II), and very less amount of Ag (I) ions can reach the sorption sites in the inner layer of the beads due to the slow mass transfer in the solid particles. Therefore, unlike breakthrough curves, this time Ag (I) eluted earlier than Cu (II) at lower column loading.

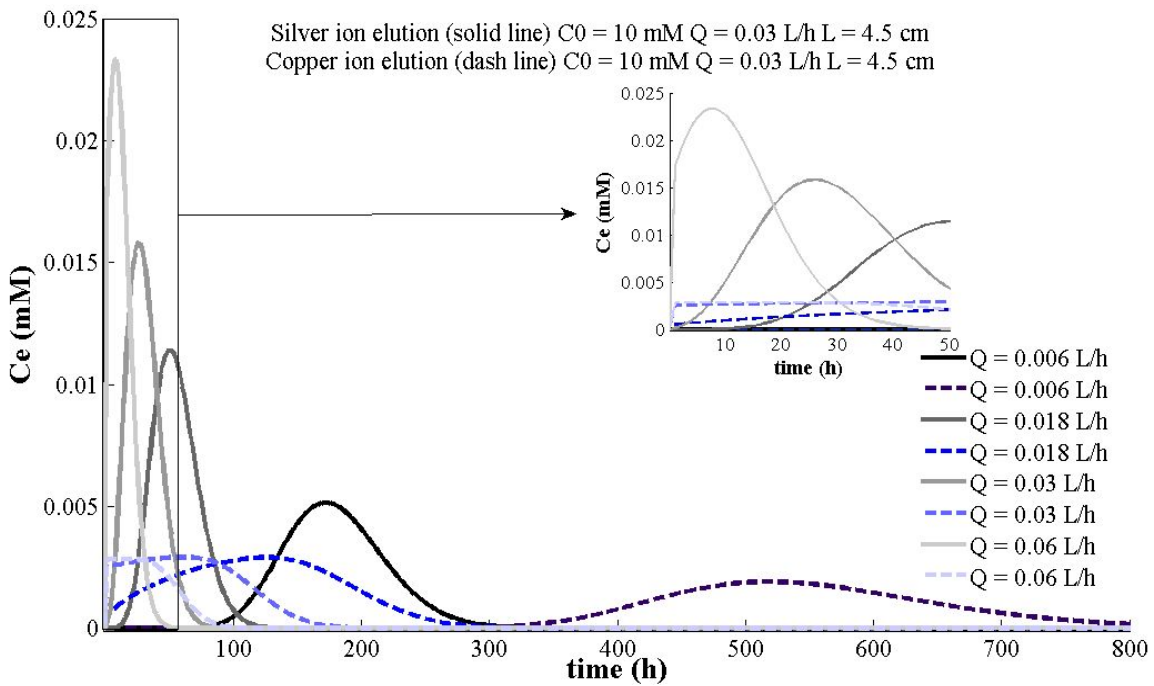


Figure 4.2 Predicted elution peaks for adsorption of Ag (I) and Cu (II) in the column under different flow rates

#### 4.4.2.2 Effect of bed length

The effect of the bed length on the breakthrough and elution of Ag (I) and Cu (II) was determined by four levels – 4.5, 6.5, 8.5, and 10.5 cm of bed length. Fig. 4.3 shows the predicted breakthrough curves for  $\text{Ag}^+$  and  $\text{Cu}^{2+}$  obtained for different bed lengths at  $Q = 0.018 \text{ L/h}$  and sample concentration of 1.0 mM. It is obvious that metal ions take the shortest time to break through the column when bed length is 4.5 cm. With the increase of bed length, longer time is needed for the metal ions to exit from the column. It is also noted that the shapes and slopes breakthrough curves of Ag (I) and Cu (II) with different

bed lengths are almost the same, which stems from the same axial dispersion and mass transfer coefficient.

Peclet number ( $Pe$ ), a dimensionless group number defined as the ratio of the axial convection rate to the axial dispersion rate (Sulaymon et al., 2009), is usually used to demonstrate the different magnitudes of mass transfer by convection and diffusion as:

$$Pe = \frac{uL}{D_L} \quad (4.19)$$

Table 4.8 illustrates  $Pe$  at constant flow rate with different bed lengths. It is found that  $Pe$  increased with the increase of the bed length, indicating that the effect of the axial dispersion in the biosorption process is smaller with the increase of the bed length. This observation is in agreement with the results obtained by Sulaymon and co-workers (Sulaymon et al., 2009). However, the  $Pe$  values for  $\text{Ag}^+$  and  $\text{Cu}^{2+}$  are very close, suggesting that the properties of metal ions have little influence on convection and axial dispersion.

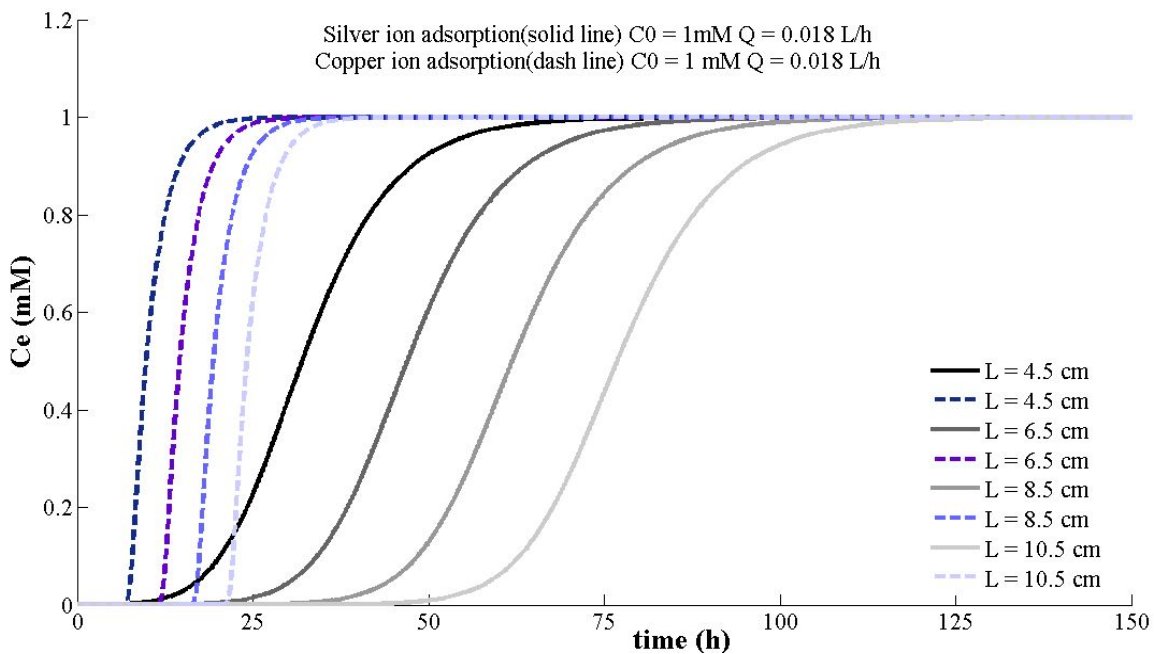


Figure 4.3 Predicted breakthrough curves for adsorption of Ag (I) and Cu (II) in the column under different bed lengths

Table 4.8  $Pe$  values at different bed lengths

<b>Bed length (cm)</b>	<b>Metal ions</b>	<b><math>Pe</math></b>
4.5 cm	$\text{Ag}^+$	0.53
	$\text{Cu}^{2+}$	0.54
6.5 cm	$\text{Ag}^+$	0.77
	$\text{Cu}^{2+}$	0.78
8.5 cm	$\text{Ag}^+$	1.00
	$\text{Cu}^{2+}$	1.02
10.5 cm	$\text{Ag}^+$	1.24
	$\text{Cu}^{2+}$	1.26

The effect of column length (with constant sample concentration and injection time) on the elution profiles of Ag (I) and Cu (II) is presented in Fig. 4.4. By increasing the column length from 4.5 to 8.5 cm, the time which is required for Ag (I) and Cu (II) to elute from the column increases, and the elution profiles of Ag (I) and Cu (II) became more spread and shorter. This is due to the increase in number of binding sites owing to the increase in surface area of the TCAC sorbent. The metal ions had sufficient time to diffuse through the solid particles, leading to the lower concentration in the eluent, but better separation of the two metal ions.

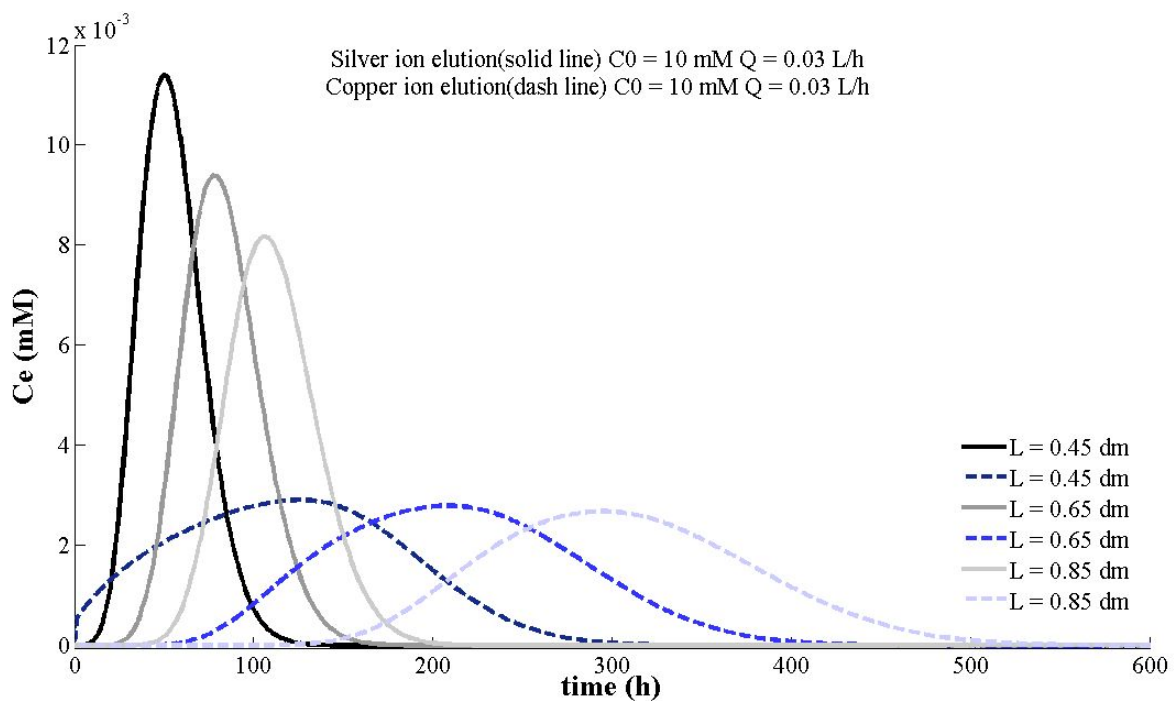


Figure 4.4 Predicted elution curves for adsorption of Ag (I) and Cu (II) in the column under different bed lengths

#### **4.4.2.3 Effect of sample concentration and injection time (*t*)**

For preparative chromatographic separation, column overload through either volume overload or concentration overload is widely applied to separate, with an acceptable resolution, the amount of adsorbates (metal ions in this case) as much as possible. In this study, the effects of concentration overload and volume overload on the elution separation of Ag (I) and Cu (II) from TCAC packed column was investigated. The effect of concentration overloading was studied by keeping the injection time (0.05 h), flow rate (0.006 L/h and 0.06 L/h) and the bed height (4.5 cm) constant and varying the sample concentrations of the feed fluids. The influence of volume overload was performed by making the sample concentration of metal ions (1.0 mM), flow rate (0.006 L/h) and the bed height (4.5 cm) constant and varying the injection time.

Figs. 4.5 and 4.6 demonstrate the effect of sample concentrations on the elution profiles of Ag (I) and Cu (II). It is observed that at lower flow rate (0.006 L/h) increasing the inlet metal ion concentration from 1.0 mM to 10.0 mM has very minor effect on the elution time of the two metal ions, and thus the separation of the metal ions was not significantly affected. The attainment of the complete separation indicate that inlet concentration of metal ions can be further increased because the column was not overloaded due to the relative smaller sample loading in the column (sample loading = flow rate  $\times$  injection time  $\times$  sample concentration). However, at higher flow rate (0.06 L/h), the separation of Ag (I) and Cu (II) can't be obtained for two reasons. First, the slow mass transfer and the short residence time of metals ions make both metal ions elute quickly from the column. Second, the column was heavily overloaded due to the higher injection amount of metal

ions which lead to longer tails for both Ag (I) and Cu (II), therefore complete separation of the metal ions was difficult to achieve.

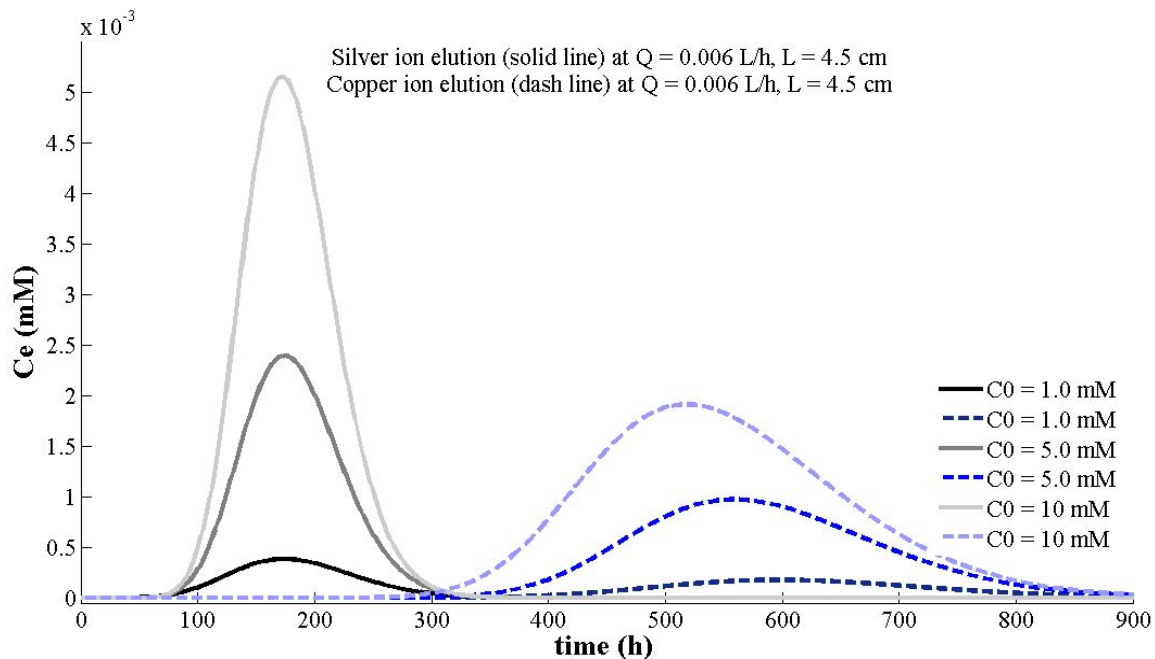


Figure 4.5 Predicted elution curves for adsorption of Ag (I) and Cu (II) in the column with different initial concentration

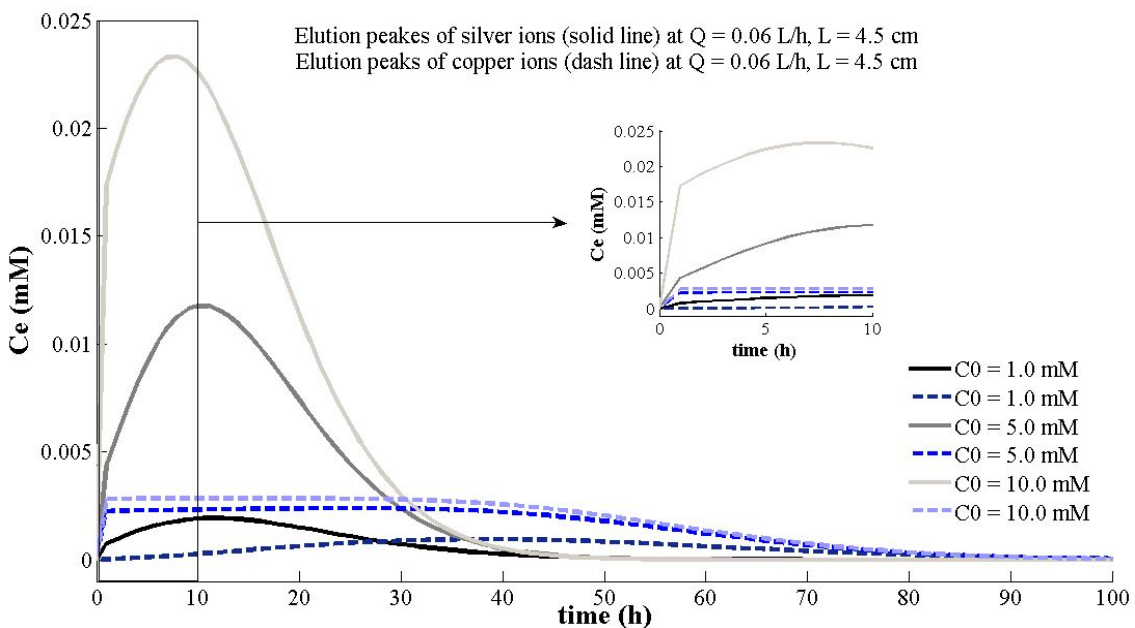


Figure 4.6 Predicted elution curves for adsorption of Ag (I) and Cu (II) in the column with different initial concentration

The effect of injection time on the elution profiles of Ag (I) and Cu (II) is illustrated in Fig. 4.7. As more metal ions were injected in the column when longer injection time was used, relatively longer tails were obtained for Ag (I) and Cu (II), which decreased the separation of metal ions slightly.

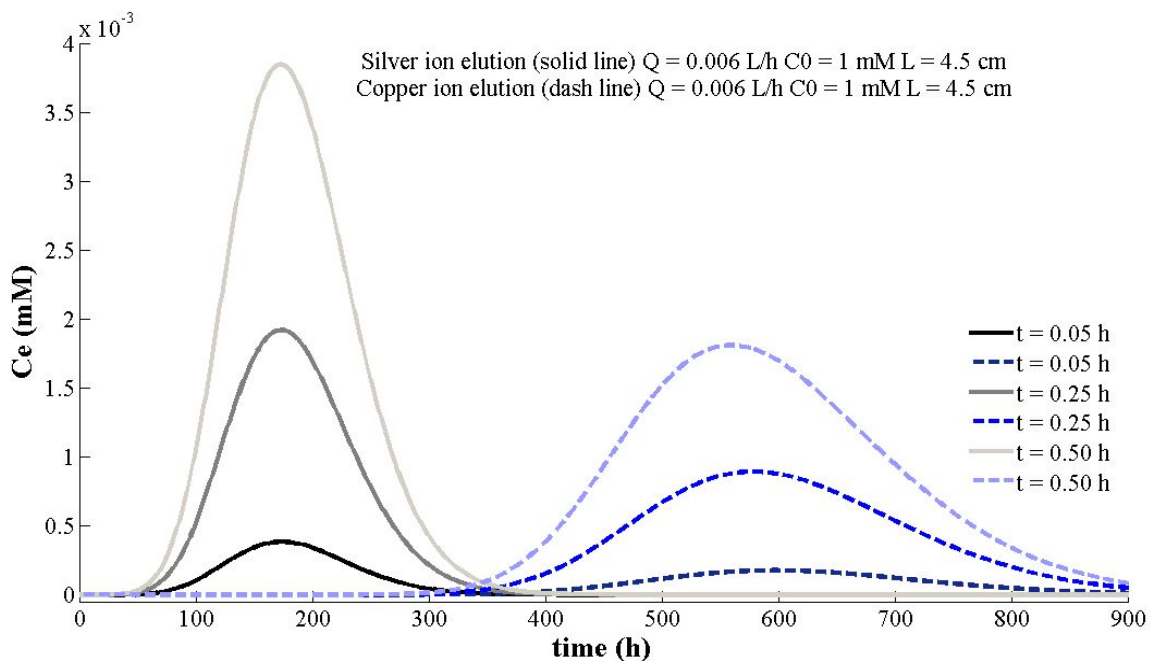


Figure 4.7 Predicted elution curves for adsorption of Ag (I) and Cu (II) in the column with different injection time

A more useful and valuable study is to compare the effects of sample concentration and injection time on the separation of metal ions at fixed sample loading, which is the product of injection concentration and injection volume. Fig. 4.8 showed the calculated elution peaks for Ag (I) and Cu (II) obtained at the same sample loading but with different combinations of sample concentration and injection time at the same flow rate ( $Q = 0.006 \text{ L/h}$ ). It is found that the elution peaks of metal ions are sharper at higher sample concentration and the short injection time, while the elution peaks are more spread when lower sample concentration and longer injection time are used. Moreover, compared with the results of Fig.4.5 and Fig. 4.7, the sample concentration plays a more important role in the separation of the two metal ions. Based on the above analyses, we

conclude high injection concentration and low injection volume is recommended for chromatographic separation.

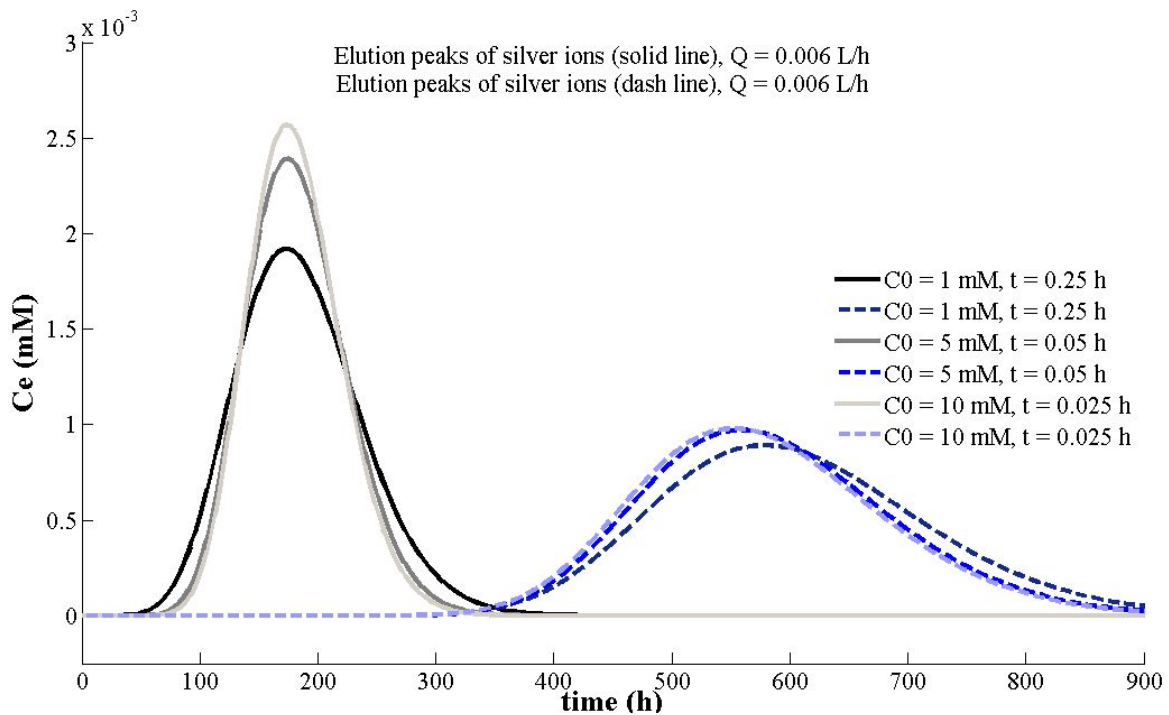


Figure 4.8 Predicted elution curves for adsorption of Ag (I) and Cu (II) in the column with the same injection amount of metal ions

#### 4.5 Conclusion

The lumped kinetic model has been used to describe and predict breakthrough and elution curves for the continuous adsorption of silver and copper ions on TCAC beads. Two important model parameters, namely the overall mass-transfer coefficient ( $K_f$ ), and the axial dispersion coefficient ( $D_L$ ) have been determined using the empirical correlations. Both macro-pore and micro-pore models were used to calculate the overall mass transfer

coefficient ( $K_f$ ) in the fixed bed column and the former one was found to be more suitable. The range of macro-pore mass transfer coefficient for  $\text{Ag}^+$  is in the range of  $5.028 \times 10^{-5}$   $\text{s}^{-1}$  to  $8.389 \times 10^{-5}$   $\text{s}^{-1}$ , and the macro-pore mass transfer coefficient for  $\text{Cu}^{2+}$  is in the range of  $8.000 \times 10^{-5}$   $\text{s}^{-1}$  to  $1.283 \times 10^{-4}$   $\text{s}^{-1}$ ; The range of axial dispersion coefficient for  $\text{Ag}^+$  and  $\text{Cu}^{2+}$  are very close, varying from  $1.806 \times 10^{-4}$   $\text{cm}^2/\text{s}$  to  $1.778 \times 10^{-4}$   $\text{cm}^2/\text{s}$ .

The effects of flow rate, bed length, sample concentration and injection time on the breakthrough and elution of Ag (I) and Cu (II) from the column were investigated. Simulation results indicated that at lower flow rate, longer bed length, lower sample concentration and shorter injection time, the separation of the two metal ions is better. Particularly, when the total loading amount of metal ions are the same, the combination of higher sample concentration and shorter injection time helps to get sharper elution curves and better separation of silver and copper ions. This suggests that concentration overload by increasing the sample concentration is more effective to improve the separation of the two metal ions in fixed-bed columns than volume overload by increasing the injection time.

## **Chapter 5 Conclusions and Recommendations**

### **5.1 Conclusions**

A low-cost and environment-friendly biosorbent, i.e., sodium tripolyphosphate crosslinked alkalized chitosan (TCAC) beads was prepared in this study and used to selectively adsorb Ag (I) ions from the bimetallic solution (containing equal molar concentration of Ag(I) and Cu (II)) through either batch mode and dynamic fixed-bed column separation. A mathematical model was applied to simulate the breakthrough and elution of metal ions from the fixed-bed adsorption column in order to provide practical information for industrial utilization of TCAC beads in wastewater treatment.

Different preparation conditions were used to synthesize TCAC beads and results indicate that alkalization of chitosan before crosslinking is an efficient approach to control the degree of crosslinking of chitosan, and low degree of crosslinking is beneficial to the selective uptake of Ag (I) from aqueous solution containing the same mole concentration of Ag (I) and Cu (II). According to the results of ATR-FTIR and XPS analysis for sorbents before and after metal uptake, silver ions were found to be primarily adsorbed by the amine group in the inner layer of the TCAC beads; whereas copper ions were mainly adsorbed on the outer layer of the beads through phosphorous groups.. The results of desorption process are also in agreement with the mechanism of adsorbing copper and silver ions.

Considering the accuracy and the operability, the lumped kinetic model has been selected to describe and predict breakthrough and elution curves for the continuous biosorption of silver and copper ions on TCAC; the macro-pore model was chosen to simulate the mass transfer in the stationary phase. The external mass-transfer coefficient ( $K_f$ ) and axial dispersion coefficient ( $D_L$ ) are two important parameters affecting the performance of the column under different conditions which have been optimally calculated by proper empirical correlations. The range of macro-pore mass transfer coefficient for  $\text{Ag}^+$  is  $5.028 \times 10^{-5} \text{ s}^{-1}$  to  $8.389 \times 10^{-5} \text{ s}^{-1}$ , and the macro-pore mass transfer coefficient for  $\text{Cu}^{2+}$  is in the range of  $8.000 \times 10^{-5} \text{ s}^{-1}$  to  $1.283 \times 10^{-5} \text{ s}^{-1}$ ; The ranges of axial dispersion coefficient for  $\text{Ag}^+$  and  $\text{Cu}^{2+}$  are almost the same, which is in the range of  $1.806 \times 10^{-4} \text{ cm}^2/\text{s}$  to  $1.778 \times 10^{-4} \text{ cm}^2/\text{s}$ . Four factors are considered when studying the performance of the column under different conditions: flow rate, bed length, initial loading concentration and loading time. The results of breakthrough and elution curves demonstrated that smaller flow rate and longer bed length could extend the appearance time of the breakthrough points and enhance the separation of silver and copper ions in the column. Moreover, smaller initial loading concentrations or shorter loading times can also improve the separation effect. Furthermore, with the same total loading amount of metal ions, decreasing the loading concentration is more effective to improve the separation of two metal ions than shortening the loading time.

## **5.2 Recommendation**

This research work is a meaningful attempt to syntheses chitosan-based biosorbents with enhanced adsorption capacity and good selectivity of silver ions, and to study the separation effects in the continuous system. The alkalization process is applied to reduce the consumption of amine groups (the disadvantage of utilization of TPP in the adsorption area) in crosslinking processes, providing another environmental and effective crosslinker in treating metal ions in the aqueous system.

In addition, with the analysis of ATP-FTIR, XPS, XRD, the selective adsorption mechanism of copper and silver ions is explained clearly which is beneficial for further improvement. There is an interest to examine to competitive adsorption performance in a ternary or multi components system and for other metal ions. For example, the selectivity separation of gold ions from copper, zinc, or lead ions could be investigated in the future.

However, according to the results of isotherm and kinetics in the Chapter 3, the mass transfer of metal ions in the newly synthesized TCAC beads was slow which is also widely reported in others' research. Therefore, further modification is needed to enhance the mass transfer in the chitosan beads, such as increasing the porosity using templates. Considering the promising capacity and low cost of chitosan, it is valuable to do more research to overcome the barrier of chitosan for the practical usage in the future.

## References

- Aksu, Z., & Gönen, F. (2004). Biosorption of phenol by immobilized activated sludge in a continuous packed bed: prediction of breakthrough curves. *Process Biochemistry*, 39(5), 599-613.
- Amaral, I., Granja, P., & Barbosa, M. (2005). Chemical modification of chitosan by phosphorylation: an XPS, FT-IR and SEM study. *Journal of Biomaterials Science, Polymer Edition*, 16(12), 1575-1593.
- Arrascue, M. L., Garcia, H. M., Horna, O., & Guibal, E. (2003). Gold sorption on chitosan derivatives. *Hydrometallurgy*, 71(1), 191-200.
- Atomic absorption spectroscopy. Retrieved March 22, 2015, from [http://en.wikipedia.org/wiki/Atomic\\_absorption\\_spectroscopy](http://en.wikipedia.org/wiki/Atomic_absorption_spectroscopy)
- Bailey, S. E., Olin, T. J., Bricka, R. M., & Adrian, D. D. (1999). A review of potentially low-cost sorbents for heavy metals. *Water research*, 33(11), 2469-2479.
- Bak, H., Thomas, O. R., & Abildskov, J. (2007). Lumped parameter model for prediction of initial breakthrough profiles for the chromatographic capture of antibodies from a complex feedstock. *Journal of chromatography B*, 848(1), 131-141.
- Baroni, P., Vieira, R., Meneghetti, E., Da Silva, M., & Beppu, M. (2008). Evaluation of batch adsorption of chromium ions on natural and crosslinked chitosan membranes. *Journal of hazardous materials*, 152(3), 1155-1163.
- Boufi, S., Vilar, M. R., Ferraria, A. M., & do Rego, A. M. B. (2013). In situ photochemical generation of silver and gold nanoparticles on chitosan. *Colloids and Surfaces A: Physicochemical and Engineering Aspects*, 439, 151-158.
- Chatterjee, A., & Schiewer, S. (2014). Multi-resistance kinetic models for biosorption of Cd by raw and immobilized citrus peels in batch and packed-bed columns. *Chemical Engineering Journal*, 244, 105-116.
- Chen, Y., Hu, J., & Wang, J. (2012). Kinetics and thermodynamics of Cu (II) biosorption on to a novel magnetic chitosan composite bead. *Environmental technology*, 33(20), 2345-2351.
- Chien, S., & Clayton, W. (1980). Application of Elovich equation to the kinetics of phosphate release and sorption in soils. *Soil Science Society of America Journal*, 44(2), 265-268.
- Coordination complex. Retrieved March 22, 2015, from [http://en.wikipedia.org/wiki/Coordination\\_complex](http://en.wikipedia.org/wiki/Coordination_complex)
- Crini, G., & Badot, P.-M. (2008). Application of chitosan, a natural aminopolysaccharide, for dye removal from aqueous solutions by adsorption processes using batch

- studies: A review of recent literature. *Progress in polymer science*, 33(4), 399-447.
- Dambies, L., Guimon, C., Yiacoumi, S., & Guibal, E. (2001). Characterization of metal ion interactions with chitosan by X-ray photoelectron spectroscopy. *Colloids and Surfaces A: Physicochemical and Engineering Aspects*, 177(2), 203-214.
- Das, N. (2010). Recovery of precious metals through biosorption—a review. *Hydrometallurgy*, 103(1), 180-189.
- Dawson, R. M. C. (1969). Data for biochemical research.
- Donia, A. M., Yousif, A. M., Atia, A. A., & Elsamalehy, M. F. (2014). Efficient adsorption of Ag (I) and Au (III) on modified magnetic chitosan with amine functionalities. *Desalination and Water Treatment*, 52(13-15), 2537-2547.
- Donia, A. M., Atia, A. A., & Elwakeel, K. Z. (2007). Recovery of gold (III) and silver (I) on a chemically modified chitosan with magnetic properties. *Hydrometallurgy*, 87(3), 197-206.
- Du, X., Yuan, Q., & Li, Y. (2008). Mathematical analysis of solanesol adsorption on macroporous resins using the general rate model. *Chemical engineering & technology*, 31(9), 1310-1318.
- Duceppe, N., & Tabrizian, M. (2010). Advances in using chitosan-based nanoparticles for in vitro and in vivo drug and gene delivery. *Expert opinion on drug delivery*, 7(10), 1191-1207.
- Elution. Retrieved April 1, 2015, from <http://en.wikipedia.org/wiki/Elution>
- Escudero, C., Poch, J., & Villaescusa, I. (2013). Modelling of breakthrough curves of single and binary mixtures of Cu (II), Cd (II), Ni (II) and Pb (II) sorption onto grape stalks waste. *Chemical Engineering Journal*, 217, 129-138.
- Farooq, U., Kozinski, J. A., Khan, M. A., & Athar, M. (2010). Biosorption of heavy metal ions using wheat based biosorbents—A review of the recent literature. *Bioresource technology*, 101(14), 5043-5053.
- Fourier transform infrared spectroscopy. Retrieved March 22, 2015, from [http://en.wikipedia.org/wiki/Fourier\\_transform\\_infrared\\_spectroscopy](http://en.wikipedia.org/wiki/Fourier_transform_infrared_spectroscopy)
- Fu, F., & Wang, Q. (2011). Removal of heavy metal ions from wastewaters: a review. *Journal of environmental management*, 92(3), 407-418.
- Fujiwara, K., Ramesh, A., Maki, T., Hasegawa, H., & Ueda, K. (2007). Adsorption of platinum (IV), palladium (II) and gold (III) from aqueous solutions onto l-lysine modified crosslinked chitosan resin. *Journal of hazardous materials*, 146(1), 39-50.
- Gerente, C., Lee, V., Cloirec, P. L., & McKay, G. (2007). Application of chitosan for the removal of metals from wastewaters by adsorption—mechanisms and models

- review. *Critical Reviews in Environmental Science and Technology*, 37(1), 41-127.
- Goel, J., Kadirvelu, K., Rajagopal, C., & Garg, V. K. (2005). Removal of lead (II) by adsorption using treated granular activated carbon: batch and column studies. *Journal of hazardous materials*, 125(1), 211-220.
- Guibal, E. (2004). Interactions of metal ions with chitosan-based sorbents: a review. *Separation and Purification Technology*, 38(1), 43-74.
- Guibal, E., Milot, C., Eterradoissi, O., Gauffier, C., & Domard, A. (1999). Study of molybdate ion sorption on chitosan gel beads by different spectrometric analyses. *International journal of biological macromolecules*, 24(1), 49-59.
- Guibal, E., Van Vooren, M., Dempsey, B. A., & Roussy, J. (2006). A review of the use of chitosan for the removal of particulate and dissolved contaminants. *Separation science and technology*, 41(11), 2487-2514.
- Guiochon, G., Felinger, A., & Shirazi, D. G. (2006). *Fundamentals of preparative and nonlinear chromatography*: Academic Press.
- Guo, T., Xia, Y., Hao, G., Song, M., & Zhang, B. (2004). Adsorptive separation of hemoglobin by molecularly imprinted chitosan beads. *Biomaterials*, 25(27), 5905-5912.
- Guzman, J., Saucedo, I., Revilla, J., Navarro, R., & Guibal, E. (2003). Copper sorption by chitosan in the presence of citrate ions: influence of metal speciation on sorption mechanism and uptake capacities. *International journal of biological macromolecules*, 33(1), 57-65.
- Han, R., Wang, Y., Zhao, X., Wang, Y., Xie, F., Cheng, J., & Tang, M. (2009). Adsorption of methylene blue by phoenix tree leaf powder in a fixed-bed column: experiments and prediction of breakthrough curves. *Desalination*, 245(1), 284-297.
- Heeter, G., & Liapis, A. (1998). Frontal chromatography of proteins: Effect of axial dispersion on column performance. *Journal of Chromatography A*, 796(1), 157-164.
- Ho, Y.-S. (2006). Review of second-order models for adsorption systems. *Journal of hazardous materials*, 136(3), 681-689.
- Hoffmann, J. E. (2015). Silver processing. from <http://www.britannica.com/EBchecked/topic/544891/silver-processing>.
- Hosseini, S., Pourmortazavi, S., & Fathollahi, M. (2005). Orthogonal array design for the optimization of silver recovery from waste photographic paper. *Separation science and technology*, 39(8), 1953-1966.

- Huang, P., Cao, M., & Liu, Q. (2012). Adsorption of chitosan on chalcopyrite and galena from aqueous suspensions. *Colloids and Surfaces A: Physicochemical and Engineering Aspects*, 409, 167-175.
- Hydari, S., Sharififard, H., Nabavinia, M., & reza Parvizi, M. (2012). A comparative investigation on removal performances of commercial activated carbon, chitosan biosorbent and chitosan/activated carbon composite for cadmium. *Chemical Engineering Journal*, 193, 276-282.
- Inductively coupled plasma. Retrieved March 22, 2015, from [http://en.wikipedia.org/wiki/Inductively\\_coupled\\_plasma](http://en.wikipedia.org/wiki/Inductively_coupled_plasma)
- Izatt, S., Izatt, N., & Bruening, R. (2010). Metal separations of interest to the Chinese metallurgical industry. *Journal of Rare Earths*, 28, 22-29.
- Izquierdo, M., Gabaldón, C., Marzal, P., & Sempere, F. (2010). Sorption of copper by a highly mineralized peat in batch and packed-bed systems. *Journal of Chemical Technology and Biotechnology*, 85(2), 165-172.
- Jeon, C., & Park, K. H. (2005). Adsorption and desorption characteristics of mercury (II) ions using aminated chitosan bead. *Water research*, 39(16), 3938-3944.
- Juang, R.-S., & Ju, C.-Y. (1997). Equilibrium sorption of Copper (II)-ethylenediaminetetraacetic acid chelates onto cross-linked, polyaminated chitosan beads. *Industrial & engineering chemistry research*, 36(12), 5403-5409.
- Kaczmarski, K., Antos, D., Sajonz, H., Sajonz, P., & Guiochon, G. (2001). Comparative modeling of breakthrough curves of bovine serum albumin in anion-exchange chromatography. *Journal of Chromatography A*, 925(1), 1-17.
- Kang, T., Park, Y., Choi, K., Lee, J. S., & Yi, J. (2004). Ordered mesoporous silica (SBA-15) derivatized with imidazole-containing functionalities as a selective adsorbent of precious metal ions. *Journal of Materials Chemistry*, 14(6), 1043-1049.
- Kasaai, M. R. (2010). Determination of the degree of N-acetylation for chitin and chitosan by various NMR spectroscopy techniques: A review. *Carbohydrate Polymers*, 79(4), 801-810.
- Kavaklı, C., Malci, S., Tunçel, S. A., & Salih, B. (2006). Selective adsorption and recovery of precious metal ions from geological samples by 1, 5, 9, 13-tetrathiacyclohexadecane-3, 11-diol anchored poly (p-CMS-DVB) microbeads. *Reactive and functional polymers*, 66(2), 275-285.
- Ko, D. C., Porter, J. F., & McKay, G. (2001). Film-pore diffusion model for the fixed-bed sorption of copper and cadmium ions onto bone char. *Water research*, 35(16), 3876-3886.

- Kong, X. (2012). Simultaneous determination of degree of deacetylation, degree of substitution and distribution fraction of-COONa in carboxymethyl chitosan by potentiometric titration. *Carbohydrate Polymers*, 88(1), 336-341.
- Kumar, G., Smith, P. J., & Payne, G. F. (1999). Enzymatic grafting of a natural product onto chitosan to confer water solubility under basic conditions. *Biotechnology and bioengineering*, 63(2), 154-165.
- Kumar, M. N. R. (2000). A review of chitin and chitosan applications. *Reactive and functional polymers*, 46(1), 1-27.
- Kumar, P., Ansari, K. B., Koli, A. C., & Gaikar, V. G. (2013). Sorption behavior of thiourea-grafted polymeric resin toward silver ion, reduction to silver nanoparticles, and their antibacterial properties. *Industrial & engineering chemistry research*, 52(19), 6438-6445.
- Kyzas, G. Z., Kostoglou, M., & Lazaridis, N. K. (2009). Copper and chromium (VI) removal by chitosan derivatives—Equilibrium and kinetic studies. *Chemical Engineering Journal*, 152(2), 440-448.
- Laus, R., Costa, T. G., Szpoganicz, B., & Fávere, V. T. (2010). Adsorption and desorption of Cu (II), Cd (II) and Pb (II) ions using chitosan crosslinked with epichlorohydrin-triphosphate as the adsorbent. *Journal of hazardous materials*, 183(1), 233-241.
- Lee, S.-T., Mi, F.-L., Shen, Y.-J., & Shyu, S.-S. (2001). Equilibrium and kinetic studies of copper (II) ion uptake by chitosan-tripolyphosphate chelating resin. *Polymer*, 42(5), 1879-1892.
- Lee, W.-C., & Chen, C.-H. (2001). Predicting the elution behavior of proteins in affinity chromatography on non-porous particles. *Journal of biochemical and biophysical methods*, 49(1), 63-82.
- Lenart-Boroń, A., & Boroń, P. (2014). The Effect of Industrial Heavy Metal Pollution on Microbial Abundance and Diversity in Soils—A Review. *Actinomycetes*, 1012(1013), 107-108.
- LeVan, M. D., & Vermeulen, T. (1981). Binary Langmuir and Freundlich isotherms for ideal adsorbed solutions. *The Journal of Physical Chemistry*, 85(22), 3247-3250.
- Li, C., Hein, S., & Wang, K. (2008). Biosorption of chitin and chitosan. *Materials Science and Technology*, 24(9), 1088-1099.
- Lim, A. P., & Aris, A. Z. (2014). Continuous fixed-bed column study and adsorption modeling: Removal of cadmium (II) and lead (II) ions in aqueous solution by dead calcareous skeletons. *Biochemical Engineering Journal*, 87, 50-61.
- Lin, T.-L., & Lien, H.-L. (2013). Effective and selective recovery of precious metals by thiourea modified magnetic nanoparticles. *International journal of molecular sciences*, 14(5), 9834-9847.

- Lü, R., Cao, Z., & Shen, G. (2008). Comparative study on interaction between copper (II) and chitin/chitosan by density functional calculation. *Journal of Molecular Structure: THEOCHEM*, 860(1), 80-85.
- Lv, L., Zhang, Y., Wang, K., Ray, A. K., & Zhao, X. (2008). Modeling of the adsorption breakthrough behaviors of Pb 2+ in a fixed bed of ETS-10 adsorbent. *Journal of colloid and interface science*, 325(1), 57-63.
- Mack, C., Wilhelmi, B., Duncan, J., & Burgess, J. (2007). Biosorption of precious metals. *Biotechnology Advances*, 25(3), 264-271.
- Machado, M. O., Lopes, E. C., Sousa, K. S., & Airoldi, C. (2009). The effectiveness of the protected amino group on crosslinked chitosans for copper removal and the thermodynamics of interaction at the solid/liquid interface. *Carbohydrate Polymers*, 77(4), 760-766.
- Marin, J., & Ayele, J. (2003). Removal of some heavy metal cations from aqueous solutions by spruce sawdust. II. Adsorption-desorption through column experiments. *Environmental technology*, 24(4), 491-502.
- Masri, M., Reuter, F. W., & Friedman, M. (1974). Binding of metal cations by natural substances. *Journal of Applied Polymer Science*, 18(3), 675-681.
- Mass transfer. Retrieved March 22, 2015, from [http://en.wikipedia.org/wiki/Mass\\_transfer](http://en.wikipedia.org/wiki/Mass_transfer)
- Mata, Y., Torres, E., Blázquez, M., Ballester, A., González, F., & Muñoz, J. (2009). Gold (III) biosorption and bioreduction with the brown alga *Fucus vesiculosus*. *Journal of hazardous materials*, 166(2), 612-618.
- Matsusaki, M., Omichi, M., Maruyama, I., & Akashi, M. (2008). Physical adsorption of human thrombomodulin (ART-123) onto polymeric biomaterials for developing an antithrombogenic blood-contacting material. *Journal of Biomedical Materials Research Part A*, 84(1), 1-9.
- Mi, F.-L., Shyu, S.-S., Chen, C.-T., & Lai, J.-Y. (2002). Adsorption of indomethacin onto chemically modified chitosan beads. *Polymer*, 43(3), 757-765.
- Mi, F.-L., Shyu, S. S., Lee, S. T., & Wong, T. B. (1999). Kinetic study of chitosan-tripolyphosphate complex reaction and acid-resistive properties of the chitosan-tripolyphosphate gel beads prepared by in-liquid curing method. *Journal of Polymer Science Part B: Polymer Physics*, 37(14), 1551-1564.
- Mi, F.-L., Sung, H.-W., Shyu, S.-S., Su, C.-C., & Peng, C.-K. (2003). Synthesis and characterization of biodegradable TPP/genipin co-crosslinked chitosan gel beads. *Polymer*, 44(21), 6521-6530.
- Miretzky, P., & Cirelli, A. F. (2009). Hg (II) removal from water by chitosan and chitosan derivatives: a review. *Journal of hazardous materials*, 167(1), 10-23.

- Monier, M. (2012). Adsorption of  $Hg^{2+}$ ,  $Cu^{2+}$  and  $Zn^{2+}$  ions from aqueous solution using formaldehyde cross-linked modified chitosan–thioglyceraldehyde Schiff's base. *International journal of biological macromolecules*, 50(3), 773-781.
- Morris, G. A., Castile, J., Smith, A., Adams, G. G., & Harding, S. E. (2011). The effect of prolonged storage at different temperatures on the particle size distribution of tripolyphosphate (TPP)–chitosan nanoparticles. *Carbohydrate Polymers*, 84(4), 1430-1434.
- Moulder, J., Stickle, W., Sobol, P., & Bomben, K. (1992). Handbook of X-ray Photoelectron Spectroscopy; Perkin-Elmer Corporation: Eden Prairie, MN, 1992. *There is no corresponding record for this reference*, 52-53.
- Mulgundmath, V., Jones, R., Tezel, F., & Thibault, J. (2012). Fixed bed adsorption for the removal of carbon dioxide from nitrogen: breakthrough behaviour and modelling for heat and mass transfer. *Separation and Purification Technology*, 85, 17-27.
- Naja, G., & Volesky, B. (2006). Behavior of the mass transfer zone in a biosorption column. *Environmental science & technology*, 40(12), 3996-4003.
- Nakhli, A., Bergaoui, M., Khalfaoui, M., Möllmer, J., Möller, A., & Lamine, A. B. (2014). Modeling of high pressure adsorption isotherm using statistical physics approach: lateral interaction of gases adsorption onto metal–organic framework HKUST-1. *Adsorption*, 20(8), 987-997.
- Ngah, W. W., Endud, C., & Mayanar, R. (2002). Removal of copper (II) ions from aqueous solution onto chitosan and cross-linked chitosan beads. *Reactive and functional polymers*, 50(2), 181-190.
- Ngah, W. W., & Fatinathan, S. (2010). Adsorption characterization of Pb (II) and Cu (II) ions onto chitosan-tripolyphosphate beads: kinetic, equilibrium and thermodynamic studies. *Journal of environmental management*, 91(4), 958-969.
- Ngah, W. W., Teong, L., & Hanafiah, M. (2011). Adsorption of dyes and heavy metal ions by chitosan composites: A review. *Carbohydrate Polymers*, 83(4), 1446-1456.
- Osifo, P. O., Neomagus, H. W., Everson, R. C., Webster, A., & vd Gun, M. A. (2009). The adsorption of copper in a packed-bed of chitosan beads: Modeling, multiple adsorption and regeneration. *Journal of hazardous materials*, 167(1), 1242-1245.
- Park, D., Yun, Y.-S., & Park, J. M. (2010). The past, present, and future trends of biosorption. *Biotechnology and Bioprocess Engineering*, 15(1), 86-102.
- Park, S.-I., Kwak, I. S., Won, S. W., & Yun, Y.-S. (2013). Glutaraldehyde-crosslinked chitosan beads for sorptive separation of Au (III) and Pd (II): Opening a way to design reduction-coupled selectivity-tunable sorbents for separation of precious metals. *Journal of hazardous materials*, 248, 211-218.

- Pearson, R. G. (1963). Hard and soft acids and bases. *Journal of the American Chemical Society*, 85(22), 3533-3539.
- Pérez-Martínez, Y., Montesinos-Cisneros, R., Guerrero-Germán, P., Guzman-Zamudio, R., & Tejeda-Mansir, A. (2015). Batch Equilibrium and Kinetic Studies of Plasmid pCI Adsorption onto Perfusion Particles. *Journal of Liquid Chromatography & Related Technologies*, 38(2), 196-200.
- Pestov, A., Nazirov, A., Modin, E., Mironenko, A., & Bratskaya, S. (2015). Mechanism of Au (III) reduction by chitosan: Comprehensive study with <sup>13</sup>C and <sup>1</sup>H NMR analysis of chitosan degradation products. *Carbohydrate Polymers*, 117, 70-77.
- Pestov, A. V., Skorik, Y. A., Kogan, G., & Yatluk, Y. G. (2008). N-alkylation of chitosan by β-halopropionic acids in the presence of various acceptors. *Journal of Applied Polymer Science*, 108(1), 119-127.
- Peter, M. G. (1995). Applications and environmental aspects of chitin and chitosan. *Journal of Macromolecular Science, Part A: Pure and Applied Chemistry*, 32(4), 629-640.
- Pethkar, A., Kulkarni, S., & Paknikar, K. (2001). Comparative studies on metal biosorption by two strains of Cladosporium cladosporioides. *Bioresource technology*, 80(3), 211-215.
- Physical adsorption. Retrieved March 22, 2015, from [http://en.wikipedia.org/wiki/Physical\\_sorption](http://en.wikipedia.org/wiki/Physical_sorption)
- Qiu, H., Lv, L., Pan, B.-c., Zhang, Q.-j., Zhang, W.-m., & Zhang, Q.-x. (2009). Critical review in adsorption kinetic models. *Journal of Zhejiang University Science A*, 10(5), 716-724.
- Quiñones, I., Cavazzini, A., & Guiochon, G. (2000). Adsorption equilibria and overloaded band profiles of basic drugs in a reversed-phase system. *Journal of Chromatography A*, 877(1), 1-11.
- Rhazi, M., Desbrieres, J., Tolaimate, A., Rinaudo, M., Vottero, P., Alagui, A., & El Meray, M. (2002). Influence of the nature of the metal ions on the complexation with chitosan.: Application to the treatment of liquid waste. *European Polymer Journal*, 38(8), 1523-1530.
- Rinaudo, M. (2006). Chitin and chitosan: properties and applications. *Progress in polymer science*, 31(7), 603-632.
- Rowe, G., Margaritis, A., Lan, Q., Bassi, A., & Zhu, J. X. (1999). A new kinetic model of protein adsorption on suspended anion-exchange resin particles. *Biotechnology and bioengineering*, 65(6), 613-621.
- Sanchez-Duarte, R. G., Sanchez-Machado, D. I., Lopez-Cervantes, J., & Correa-Murrieta, M. A. (2012). Adsorption of allura red dye by cross-linked chitosan from shrimp waste. *Water Science & Technology*, 65(4), 618-623.

- Sansalone, J., & Ma, J. (2010). Parametric analysis and breakthrough modeling of phosphorus from Al-oxide filter media. *Journal of Environmental Engineering*, 137(2), 108-118.
- Sankararamakrishnan, N., Kumar, P., & Chauhan, V. S. (2008). Modeling fixed bed column for cadmium removal from electroplating wastewater. *Separation and Purification Technology*, 63(1), 213-219.
- Seader, J., & Henley, E. (2006). Separation Process Principles Powerpoint slides.
- Shawky, H. A. (2009). Synthesis of ion-imprinting chitosan/PVA crosslinked membrane for selective removal of Ag (I). *Journal of Applied Polymer Science*, 114(5), 2608-2615.
- Shinde, R. N., Pandey, A., Acharya, R., Guin, R., Das, S., Rajurkar, N., & Pujari, P. (2013). Chitosan-transition metal ions complexes for selective arsenic (V) preconcentration. *Water research*, 47(10), 3497-3506.
- Shu, X., & Zhu, K. (2002). Controlled drug release properties of ionically cross-linked chitosan beads: the influence of anion structure. *International Journal of pharmaceutics*, 233(1), 217-225.
- Skorik, Y. A., Gomes, C. A., Podberezskaya, N. V., Romanenko, G. V., Pinto, L. F., & Yatluk, Y. G. (2005). Complexation models of N-(2-carboxyethyl) chitosans with copper (II) ions. *Biomacromolecules*, 6(1), 189-195.
- Suc, N. V., & Ly, H. T. Y. (2013). Lead (II) removal from aqueous solution by chitosan flake modified with citric acid via crosslinking with glutaraldehyde. *Journal of Chemical Technology and Biotechnology*, 88(9), 1641-1649.
- Sulaymon, A. H., Abid, B. A., & Al-Najar, J. A. (2009). Removal of lead copper chromium and cobalt ions onto granular activated carbon in batch and fixed-bed adsorbers. *Chemical Engineering Journal*, 155(3), 647-653.
- Sureshkumar, M., Das, D., Mallia, M., & Gupta, P. (2010). Adsorption of uranium from aqueous solution using chitosan-tripolyphosphate (CTPP) beads. *Journal of hazardous materials*, 184(1), 65-72.
- Tang, Z.-X., Shi, L.-E., & Qian, J.-Q. (2007). Neutral lipase from aqueous solutions on chitosan nano-particles. *Biochemical Engineering Journal*, 34(3), 217-223.
- Tang, Z. X., Qian, J. Q., & Shi, L. E. (2007). Optimization of elution conditions of chitosan gel and the study of its adsorbent mechanism. *Journal of Applied Polymer Science*, 103(3), 1495-1506.
- The Future of Silver Industrial Demand (2011): The Silver Institute.
- Transmission electron microscopy. Retrieved March 22, 2015, from [http://en.wikipedia.org/wiki/Transmission\\_electron\\_microscopy](http://en.wikipedia.org/wiki/Transmission_electron_microscopy)

- Uslu, G., & Tanyol, M. (2006). Equilibrium and thermodynamic parameters of single and binary mixture biosorption of lead (II) and copper (II) ions onto *Pseudomonas putida*: effect of temperature. *Journal of hazardous materials*, 135(1), 87-93.
- Varma, A., Deshpande, S., & Kennedy, J. (2004). Metal complexation by chitosan and its derivatives: a review. *Carbohydrate Polymers*, 55(1), 77-93.
- Vieira, R. S., Oliveira, M. L. M., Guibal, E., Rodríguez-Castellón, E., & Beppu, M. M. (2011). Copper, mercury and chromium adsorption on natural and crosslinked chitosan films: an XPS investigation of mechanism. *Colloids and Surfaces A: Physicochemical and Engineering Aspects*, 374(1), 108-114.
- Vijayaraghavan, K., Winnie, H. Y. N., & Balasubramanian, R. (2011). Biosorption characteristics of crab shell particles for the removal of manganese (II) and zinc (II) from aqueous solutions. *Desalination*, 266(1), 195-200.
- Vold, I. M., Vårum, K. M., Guibal, E., & Smidsrød, O. (2003). Binding of ions to chitosan—selectivity studies. *Carbohydrate Polymers*, 54(4), 471-477.
- Wang, J., & Chen, C. (2014). Chitosan-based biosorbents: modification and application for biosorption of heavy metals and radionuclides. *Bioresource technology*, 160, 129-141.
- Wang, L., & Wang, A. (2007). Adsorption characteristics of Congo Red onto the chitosan/montmorillonite nanocomposite. *Journal of hazardous materials*, 147(3), 979-985.
- Warren, B. E. (1969). *X-ray Diffraction*: Courier Corporation.
- Watts, J. F. (1994). X-ray photoelectron spectroscopy. *Vacuum*, 45(6), 653-671.
- Weber Jr, W., & Liu, K. (1980). Determination of mass transport parameters for fixed-bed adsorbers. *Chemical Engineering Communications*, 6(1-3), 49-60.
- Wei, D., Ye, Y., Jia, X., Yuan, C., & Qian, W. (2010). Chitosan as an active support for assembly of metal nanoparticles and application of the resultant bioconjugates in catalysis. *Carbohydrate research*, 345(1), 74-81.
- Wlnterowd, J. G. (1995). Chitin and chitosan. *Food polysaccharides and their applications*, 67, 441.
- Wong, Y., Szeto, Y., Cheung, W., & McKay, G. (2004). Adsorption of acid dyes on chitosan—equilibrium isotherm analyses. *Process Biochemistry*, 39(6), 695-704.
- Wu, Y., Zhou, J., Wen, Y., Jiang, L., & Wu, Y. (2012). Biosorption of heavy metal ions ( $Cu^{2+}$ ,  $Mn^{2+}$ ,  $Zn^{2+}$ , and  $Fe^{3+}$ ) from aqueous solutions using activated sludge: Comparison of aerobic activated sludge with anaerobic activated sludge. *Applied biochemistry and biotechnology*, 168(8), 2079-2093.
- X-ray diffraction. Retrieved March 22, 2015, from [http://en.wikipedia.org/wiki/X-ray\\_crystallography#Overview\\_of\\_single-crystal\\_X-ray\\_diffraction](http://en.wikipedia.org/wiki/X-ray_crystallography#Overview_of_single-crystal_X-ray_diffraction)

- X-ray photoelectron spectroscopy. Retrieved March 22, 2015, from [http://en.wikipedia.org/wiki/X-ray\\_photoelectron\\_spectroscopy](http://en.wikipedia.org/wiki/X-ray_photoelectron_spectroscopy)
- X-ray spectroscopy Retrieved March 22, 2015, from [http://en.wikipedia.org/wiki/X-ray\\_spectroscopy](http://en.wikipedia.org/wiki/X-ray_spectroscopy)
- Yao, S. (2014). *Silver Biosorption Study by Using Seaweed-based Sorbents*. Memorial University of Newfoundland.
- Yu, D., Jackson, K., & Harmon, T. (1999). Dispersion and diffusion in porous media under supercritical conditions. *Chemical engineering science*, 54(3), 357-367.
- Yuh-Shan, H. (2004). Citation review of Lagergren kinetic rate equation on adsorption reactions. *Scientometrics*, 59(1), 171-177.
- Yun, J., Kirsebom, H., Galaev, I. Y., & Mattiasson, B. (2009). Modeling of protein breakthrough performance in cryogel columns by taking into account the overall axial dispersion. *Journal of separation science*, 32(15-16), 2601-2607.
- Zhang, M., Zhang, Y., & Helleur, R. (2015). Selective adsorption of Ag<sup>+</sup> by ion-imprinted O-carboxymethyl chitosan beads grafted with thiourea-glutaraldehyde. *Chemical Engineering Journal*, 264, 56-65.
- Zhou, L., Liu, Z., Liu, J., & Huang, Q. (2010). Adsorption of Hg (II) from aqueous solution by ethylenediamine-modified magnetic crosslinking chitosan microspheres. *Desalination*, 258(1), 41-47.
- Zhou, W., Wang, J., Shen, B., Hou, W., & Zhang, Y. (2009). Biosorption of copper (II) and cadmium (II) by a novel exopolysaccharide secreted from deep-sea mesophilic bacterium. *Colloids and Surfaces B: Biointerfaces*, 72(2), 295-302.

## **Appendix**

Mao, CX., Zhang, Y., Syed, I.. (2015) Competitive Adsorption of Ag (I) and Cu (II) on Tripolyphosphate Crosslinked Chitosan Beads has been successfully accepted by the Journal of Applied Polymer Science.

